Morphological investigation of cellulose nanocrystals and nanocomposite applications

Wilson Pires Flauzino Neto

Communauté
UNIVERSITÉ Grenoble Alpes

Universidade Federal
de Uberlândia

THÈSE

Pour obtenir le grade de

DOCTEUR DE LA COMMUNAUTÉ UNIVERSITÉ GRENOBLE ALPES

préparée dans le cadre d'une cotutelle *entre la Communauté Université Grenoble Alpes* et *Universidade Federal de Uberlândia*

Spécialité : **Matériaux, Mécanique, Génie civil, Electrochimie**

Arrêté ministériel : le 6 janvier 2005 - 7 août 2006

Présentée par

Wilson PIRES FLAUZINO NETO

Thèse dirigée par **Alain DUFRESNE**
et codirigée par **Harumi OTAGURO**

préparée au sein des **Laboratoire de Génie des Procédés Papetiers** (Grenoble) et **Laboratório de Reciclagem de Polímeros** (Uberlândia)

dans **l'Écoles Doctorale Ingénierie – Matériaux, Mécanique, Environnement, Energétique, Procédés, Production (I-MEP2)**

Etude morphologique des nanocristaux de cellulose et application nanocomposites

Thèse soutenue publiquement le **26 Janvier 2017**,
devant le jury composé de:

Mme. Vivian CONSUELO REOLON SCHMIDT
Professeur, Universidade Federal de Uberlândia (Président du jury / Examinateur)
M. Daniel ALVES CERQUEIRA
Professeur, Universidade Federal do Triângulo Mineiro (Examinateur)
Mme. Alessandra DE ALMEIDA LUCAS
Professeur, Universidade Federal de São Carlos (Rapporteur)
M. Luís CARLOS DE MORAIS
Professeur, Universidade Federal do Triângulo Mineiro (Rapporteur)
M. Alain DUFRESNE
Professeur, Université Grenoble Alpes (Directeur de Thèse)
Mme. Harumi OTAGURO
Professeur, Universidade Federal de Uberlândia (Codirectrice de thèse)

“Conheça o mundo, mas nunca esqueça o quintal da sua casa”

(autor desconhecido)

“Real knowledge is to know the extent of one's ignorance”

(Confucius)

ACKNOWLEDGEMENTS

First and foremost, I would like to register my heartfelt gratitude and sincere appreciation to my thesis supervisor and co-supervisor: Prof. Dr. Alain Dufresne and Prof. Dr. Harumi Otaguro, for their patience, time, support and guidance throughout my doctoral studies. Their observations, advices and immense knowledge helped me to establish the overall direction of the research and to move forward with investigation in depth. Without their contribution, this endeavor would not have been accomplished.

Very special thanks go to Dr. Jean-Luc Putaux for his help, many insightful comments and discussions. I deeply appreciate your work efficiency and your valuable advices. It was a great pleasure and honor to work with him. Your expertise in science helped me a lot in many aspects from experimental part till the final revision of the papers.

I am grateful to all the professors, particularly Prof. Dr. Daniel Pasquini and Prof. Dr. Rosana Maria Nascimento de Assunção for introducing me to the exciting world of polymer chemistry. I am thankful to my dear friends and colleagues for the support and many memorable moments, work-related or not, during these years. I do not name them, but I am sure that they will recognize themselves in these words.

My respectful thanks to the members of the reading committee, for their time, critical comments and suggestions which have helped to improve this work. I also gratefully acknowledge to all funding agencies and research parts involved in this study: CAPES, FAPEMIG, CNPq, Universidade Federal de Uberlândia, LGP2, CNRS and Université Grenoble Alpes.

I would also like to convey my sincere gratitude to all people who have directly or indirectly helped me in completing this academic work. During the last years I have dedicated myself to the realization of this work, but it would not have been possible without those supports from many people.

My deepest thanks go to my family (my parents, sister, and nephews) for their support throughout my life. I am particularly indebted to my girlfriend for her incredible patience and love. I dedicate my thesis to my parents for their unconditional love and belief in me, this thesis is simply impossible without them. Thank you, I love you so very much! Last, but not least, I am truly grateful to God for all the blessings that have come to my family!

PREFACE

The present doctoral thesis is based on experimental data obtained mostly using the structure of two research units: the “Laboratório de Reciclagem de Polímeros” at “Universidade Federal de Uberlândia”, Brazil, and “Laboratoire Génie des Procédés Papetiers” at “Université Grenoble Alpes”, France. This study was performed from 2014 to 2017 within the joint doctoral program between Universidade Federal de Uberlândia and Université Grenoble Alpes established in the agreement for cotutelle of doctoral thesis signed by these two institutions.

This manuscript is organized in three chapters. Chapter I is the literature review. This section was designed to provide most of information required to understanding of context of the research work developed in the following chapters. Through the analysis and comparison of selected publications, this chapter covers topics such as: cellulose structure and its features, cellulose polymorphs, mercerization and regeneration process, cellulose nanocrystals, its production, properties and applications. Chapter II presents a comprehensive study of cellulose I and II nanocrystals prepared by sulfuric acid hydrolysis focusing basically on morphological and molecular structure. Chapter III is a research work on mechanical properties of natural rubber nanocomposites reinforced using high aspect ratio cellulose nanocrystals isolated from soy hulls, with emphasis on the mechanical, thermal and morphological properties of the nanocomposites obtained. This manuscript is the original work of the author.

Uberlândia, September 08th, 2016

Wilson Pires Flauzino Neto

SCIENTIFIC PUBLICATIONS

Some parts of this work (and additional research developed during this doctoral thesis) are available as scientific publications in the following formats:

Articles in Scientific Journals

[1] **Flauzino Neto, W. P.**, Putaux, J-L., Mariano, M., Ogawa, Y., Otaguro, H., Pasquini, D., & Dufresne, A. (2016). Comprehensive morphological and structural investigation of cellulose I and II nanocrystals prepared by sulfuric acid hydrolysis. *RSC Advances, 6*, 76017-76027.

[2] **Flauzino Neto, W. P.**, Mariano, M., da Silva, I. S. V., Silvério, H. A., Putaux, J-L., Otaguro, H., Pasquini, D., & Dufresne, A. (2016). Mechanical properties of natural rubber nanocomposites reinforced with high aspect ratio cellulose nanocrystals isolated from soy hulls. *Carbohydrate Polymers*, *153*, 143-152.

[3] da Silva, I. S. V.; **Flauzino Neto, W. P.**, Silvério, H. A., Pasquini, D., Andrade, M. Z., & Otaguro, H. (2015). Mechanical, thermal and barrier properties of pectin/cellulose nanocrystal nanocomposite films and their effect on the storability of strawberries (Fragaria ananassa). *Polymer Advanced Technologies*. doi: 10.1002/pat.3734

[4] Henrique, M. A., **Flauzino Neto, W. P.**, Silvério, H. A., Martins, D. F., Gurgel, L. V. A., Barud, H. da S., de Morais, L. C., & Pasquini, D. (2015). Kinetic study of the thermal decomposition of cellulose nanocrystals with different polymorphs, cellulose I and II, extracted from different sources and using different types of acids. *Industrial Crops and Products, 76*, 128-140.

[5] Guimarães, M., Botaro, V. R., Novack, K. M., **Flauzino Neto, W. P.**, Mendes, L. M., & Tonoli, G. H. D. (2015). Preparation of Cellulose Nanofibrils from Bamboo Pulp by Mechanical Defibrillation for Their Applications in Biodegradable Composites. *Journal of Nanoscience and Nanotechnology*, *15*, 6751-6768.

[6] Martins, D. F., de Souza, A. B., Henrique, M. A., Silvério, H. A., **Flauzino Neto, W. P.**, & Pasquini, D. (2015). The influence of the cellulose hydrolysis process on the

structure of cellulose nanocrystals extracted from capim mombaça (Panicum Maximum). *Industrial Crops and Products, 65*, 496-505.

[7] Silvério, H. A., **Flauzino Neto, W. P.**, Silva I. S. V., Rosa, J. R., Assuncão, R. M. N., Barud, H. S., Ribeiro, S. J. L., & Pasquini, D. (2014). Mechanical, Thermal, and Barrier Properties of Methylcellulose/Cellulose Nanocrystals Nanocomposites. *Polímeros, 24*, 683-688.

[8] Rosa, J. R., Silva I. S. V., Lima, C. S. M., **Flauzino Neto, W. P.**, Silvério, H. A., Santos, D. B., Barud, H. S., Ribeiro, S. J. L., & Pasquini, D. (2014). New biphasic mono-component composite material obtained by partial oxypropylation of bacterial cellulose. *Cellulose, 21,* 1361-1368.

[9] dos Santos, R. M., **Flauzino Neto, W. P.,** Silvério, H. A., Martins, D. F., Dantas, N. O., & Pasquini, D. (2013). Cellulose nanocrystals from pineapple leaf, a new approach for the reuse of this agro-waste. *Industrial Crops and Products*, *50,* 707-714.

[10] Silvério, H. A., **Flauzino Neto, W. P.**, & Pasquini, D. (2013). Effect of Incorporating Cellulose Nanocrystals from Corncob on the Tensile, Thermal and Barrier Properties of Poly(Vinyl Alcohol) Nanocomposites. *Journal of Nanomaterials, 2013*, 1-9.

[11] Henrique, M. A., Silvério, H. A., **Flauzino Neto, W. P.**, & Pasquini, D. (2013). Valorization of an agro-industrial waste, mango seed, by the extraction and characterization of its cellulose nanocrystals. *Journal of Environmental Management*, *121*, 202-209.

Refereed Conference Proceedings

Communications

[1] **Flauzino Neto, W. P.**, Mariano, M., Putaux, J-L., & Dufresne, A. Morphology of cellulose nanocrystals II recrystallized from sulfuric acid. *2016 nanoTAPPI International Conference*, June 2016, Grenoble (France).

[2] **Flauzino Neto, W. P.**, Silvério, H. A., da Silva, I. S. V., Henrique, M. A., & Pasquini,

D. Produção e caracterização de nanocompósitos de matriz de agarose reforçados com nanocristais de celulose extraídos de casca de soja. *XXVIII Encontro Regional da Sociedade Brasileira de Química*, November 2014, Rio de Janeiro (Brasil).

[3] Henrique, M. A., Silvério, H. A., **Flauzino Neto, W. P.**, & Pasquini, D. Produção e caracterização de nanocompósitos de matriz de agarose reforçados com nanocristais de celulose extraídos de casca de soja. *53° Congresso Brasileiro de Química*, October 2013, Rio de Janeiro (Brasil).

[4] Silvério, H. A., **Flauzino Neto, W. P.**, Pasquini, D. Efeito da incorporação de nanocristais de celulose de sabugo de milho nas propriedades de tração, barreira e térmica dos nanocompósitos de poli (álcool vinílico). *12° Congresso Brasileiro de Polímeros (CBPol)*, September 2013, Florianópolis (Brazil). ISSN 2176-0020.

O*ral communications*

[1] Production and characterization of new hybrid bio-based nanocrystals, from cellulose and chitosan. *International Conference on Bio-based Materials and Composites (ICBMC'14)*, May 2014, Montreal (Canada).

[2] Preparation and characterization of the nanocomposites of cellulose nanocrystals, isolated from soy hulls, and methylcellulose matrix. *International Conference on Bio-based Materials and Composites (ICBMC'14)*, May 2014, Montreal (Canada).

[3] Obtenção e caracterização de nanocristais de celulose a partir da folha de abacaxi. *12° Congresso Brasileiro de Polímeros (CBPol)*, September 2013, Florianópolis (Brazil). ISSN 2176-0020.

SUMMARY

PREFACE ii

ABBREVIATIONS AND SYMBOLS vii

ABSTRACT x

RÉSUMÉ xvii

CHAPTER I: Literature Review 1

CHAPTER II: Comprehensive morphological and structural investigation of cellulose I and II nanocrystals prepared by sulfuric acid hydrolysis 76

CHAPTER III: Mechanical properties of natural rubber nanocomposites reinforced with high aspect ratio cellulose nanocrystals isolated from soy hulls..... ..113

GENERAL CONCLUSIONS AND FUTURE PERSPECTIVES..... ..140

ABBREVIATIONS AND SYMBOLS

Abbreviations

AFM – atomic force microscopy

AGU – anhydroglucose unit

ATR – attenuated total reflection

a.u. – arbitrary units

Cel-I – cellulose I

Cel-II – cellulose II

CI – crystallinity index

CI^{XRD} – crystallinity index estimated from X-ray diffraction data

CI^{NMR} – crystallinity index estimated from ^{13}C nuclear magnetic resonance data

CNC – cellulose nanocrystal

CNC_{SH} – cellulose nanocrystals isolated from soy hulls

CN-I – cellulose nanocrystals corresponding to type I allomorph, produced from eucalyptus wood pulp using classical sulfuric acid hydrolysis

CP/MAS – cross polarization magic angle spinning

CS – cellulose synthase

CSC – cellulose synthase complex

D – diameter

DMA – dynamic mechanical analysis

DP – degree of polymerization

FTIR – Fourier-transform infrared spectroscopy

gg – gauche-gauche

gt – gauche-trans

L – length

LODP – level-off degree of polymerization

LDPE – low density polyethylene

L/D – aspect ratio

MCC – microcrystalline cellulose

MCN-II – cellulose nanocrystals corresponding to type II allomorph, produced by sulfuric acid hydrolysis of cellulose previously mercerized by alkaline treatment

MD – molecular dynamics

ML – middle lamella

MWP – mercerized wood pulp

NMR – nuclear magnetic resonance

NR – natural rubber

P – primary cell wall

PLA – Polylactic acid

POE – polyoxyethylene

PS – polystyrene

PVA – polyvinyl alcohol

RCN-II – cellulose nanocrystals corresponding to type II allomorph, produced by solubilization of cellulose in sulfuric acid and subsequent regeneration in water

RH – relative humidity

S – secondary cell wall

SEM – scanning electron microscopy

SUSY – sucrose synthase

S1 – outer layer of secondary cell wall

S2 – middle layer of secondary cell wall

S3 – inner layer of secondary cell wall

TAPPI – Technical Association of the Pulp and Paper Industry

TC – terminal complex

TEM – transmission electron microscopy

TEMPO – 2,2,6,6-Tetramethylpiperidine-1-oxyl

tg – trans-gauche

T_g – glass-rubber transition temperature

T_{onset} – onset degradation temperature

TGA – thermogravimetric analysis

UDP – uridine diphosphate

WAXS – Wide-angle X-ray scattering

WP – wood pulp

XRD – X-ray diffraction

Symbols

$\bar{\boldsymbol{D}}$ – average width

$\bar{\boldsymbol{L}}$ – average length

$\bar{H}$ – average thickness

$\bar{L}/\bar{D}$ – average aspect ratio

ζ – zeta-potential

$[\eta]$ – intrinsic viscosity

T_α – main relaxation temperature

E' – tensile storage modulus

E – Young's modulus

$E'_{25°C}$ – tensile storage modulus at 25°C

$E'_{25°CR}$ – relative rubbery storage tensile modulus at 25°C

δ – mechanical loss factor

σ_y – yield stress

ε_y – yields strain

σ_B – strength

ε_B – strain at break

$\overline{\mathbf{DP}_v}$ – viscosimetric average degree of polymerization

$\overline{\mathbf{DP}_n}$ – number-average degree of polymerization

G – Gibbs free energy

S – entropy

H – enthalpy

ABSTRACT

Since this thesis presents two independent studies on cellulose nanocrystals (CNCs), the abstract was divided in two sections referring to chapters II and III, respectively.

Comprehensive morphological and structural investigation of cellulose I and II nanocrystals prepared by sulfuric acid hydrolysis

Cellulose has several polymorphs. These polymorphs differ by crystal packing (*i.e.* unit cell parameters), polarity of the constituting chains and hydrogen bond patterns established between them. Most of cellulose polymorphs result from chemical treatments of the native polymorph, the so-called cellulose I (Cel-I) (Wada *et al.*, 2008). In Cel-I, the chains are parallel and can be packed into two allomorphs, namely Iα and Iβ. Among the cellulose polymorphs, cellulose II (Cel-II), in which the chains are antiparallel, can be prepared from Cel-I by two distinct processes: Mercerization or Regeneration. Mercerization is an essentially solid-state process during which cellulose fibers are swollen in concentrated alkali media and recrystallized into cellulose II upon washing and drying (removal of the swelling agent). Unlike the mercerization process, in process known as regeneration, cellulose is first dissolved in an appropriated solvent and subsequent reprecipitated by adding a non-solvent, leading the chains to recrystallize into into Cel-II polymorph. The Cel-I to Cel-II transition is irreversible, which suggests that Cel-II is thermodynamically more stable (Habibi *et al.*, 2010).

Cell-II is the second most extensively studied polymorph due to its technical relevance. Nevertheless, so far, most of investigations involving Cel-II have focused on fibers and only a few recent studies have been carried out on CNCs. Cel-II nanocrystals have been prepared either by acid hydrolysis of mercerized fibers (Hirota *et al.*, 2012; Kim *et al.*, 2006; Yue *et al.*, 2012), mercerization of Cel-I CNCs (Jin *et al.*, 2016), or after recrystallization of fractions of short cellulose chains in solution (Dhar *et al.*, 2015; Hirota *et al.*, 2012; Hu *et al.*, 2014; Sèbe *et al.*, 2012). However, while these studies have generally combined the data from several imaging, diffraction and spectroscopic techniques, a complete structural picture of the nanocrystals has not been reported so far.

In this context, the purpose of the research work presented in chapter II was to produce, characterize and compare CNCs obtained from eucalyptus wood pulp using three different methods: i) classical sulfuric acid hydrolysis (CN-I), ii) acid hydrolysis of cellulose previously mercerized by alkaline treatment (MCN-II), and iii) solubilization of

cellulose in sulfuric acid and subsequent recrystallization in water (RCN-II). The morphology, crystal structure, crystallinity index, surface charge and degree of polymerization of these nanocrystals were characterized by complementary techniques, namely elemental analysis, zetametry, viscometry, transmission electron microscopy (TEM), atomic force microscopy (AFM), X-ray diffraction (XRD), Fourier-transform infrared and solid-state nuclear magnetic resonance spectroscopies (FTIR and NMR, respectively).

The three types of prepared CNC exhibit different morphologies and crystalline structures. When the acid hydrolysis conditions are set-up in such a way that the crystalline domains in the initial wood pulp and mercerized cellulose (WP and MWP, respectively) are preserved (60 wt% H_2SO_4, 45°C, 50 min), the resulting nanocrystals retain the fibrillar nature of the parent fibers (*i.e.*, the chain axis is parallel to the long axis of the acicular particles) and their initial allomorphic type (I for WP and II for the MWP). In both cases, the particles are mostly composed of a few laterally-bound elementary crystallites, in agreement with what was shown for cotton CNCs by Elazzouzi-Hafraoui *et al.* (2008). The unit nanocrystals in CNCs from mercerized cellulose (MCN-II) are shorter but broader than those prepared from cellulose I fibers (CN-I). If harsher conditions are used (64 wt% H_2SO_4, 40°C, 20 min), resulting in the depolymerisation and dissolution of native cellulose, the short chains (with degree of polymerization DP ≈ 17) recrystallize into Cel-II ribbons upon regeneration in water at room temperature. In these somewhat tortuous ribbons, the chain axis would lie perpendicular to the long axis of the nanocrystal and parallel to its basal plane. In addition, these nanoribbons are very similar in shape and molecular orientation to mannan II nanocrystals prepared by recrystallization of mannan (Heux *et al.*, 2005), a linear polymer of *β*-(1,4)-D-mannosyl residues, suggesting that this mode of crystallization may be a feature of short-chain linear *β*-(1,4)-linked polysaccharides.

Although similar ribbons of recrystallized cellulose II have been reported by other authors, to our knowledge, it is the first time that a detailed morphological and structural description is proposed in terms of particle morphology, crystal structure and chain orientation. By comparison with the fibrillar nanocrystals prepared by acid hydrolysis of native or mercerized cellulose fibers, the unique molecular and crystal structure of the nanoribbons imply that a higher number of reducing chain ends are located at the particle surface, which may be important for subsequent chemical modification and specific potential applications such as biosensing and bioimaging agents. Therefore this study

offers scope to a better understanding of crystalline structure and morphology of CNC obtained by regeneration process with sulfuric acid.

REFERENCES

Dhar, P., Tarafder, D., Kumar, A., & Katiyar, V. (2015). Effect of cellulose nanocrystal polymorphs on mechanical, barrier and thermal properties of poly(lactic acid) based bionanocomposites. *Royal Society of Chemistry Advances, 5*, 60426–60440.

Elazzouzi-Hafraoui, S., Nishiyama, Y., Putaux, J-L., Heux, L., Dubreuil, F., & Rochas, C. (2008). The shape and size distribution of crystalline nanoparticles prepared by acid hydrolysis of native cellulose. *Biomacromolecules, 9*, 57-65.

Habibi, Y., Lucia, L. A., & Rojas, O. J. (2010). Cellulose nanocrystals: chemistry, self-assembly and applications. *Chemical Reviews, 110*, 3479–3500.

Heux, L., Hägglund, P., Putaux, J-L., & Chanzy, H. (2005). Structural aspects in semi-crystalline samples from the mannan II family. *Biomacromolecules, 6*, 324–332.

Hirota, M., Tamura, N., Saito, T., & Isogai, A. (2012). Cellulose II nanoelements prepared from fully mercerized, partially mercerized and regenerated celluloses by 4-acetamido-TEMPO/NaClO/$NaClO_2$ oxidation. *Cellulose, 19*, 435–442.

Hu, T. Q., Hashaikeh, R., & Berry, R. N. (2014). Isolation of a novel, crystalline cellulose material from the spent liquor of cellulose nanocrystals (CNCs). *Cellulose, 21*, 3217–3229.

Jin, E., Guo, J., Yang, F., Zhu, Y., Song, J., Jin, Y., & Rojas, O. J. (2016). On the polymorphic and morphological changes of cellulose nanocrystals (CNC-I) upon mercerization and conversion to CNC-II. *Carbohydrate Polymers, 143*, 327–335.

Kim, N., Imai, T., Wada, M., & Sugiyama, J. (2006). Molecular directionality in cellulose polymorphs. *Biomacromolecules, 7*, 274–280.

Sèbe G., Ham-Pichavant, F., Ibarboure, E., Koffi, A. L. C., & Tingaut, P. (2012). Supramolecular structure characterization of cellulose II nanowhiskers produced by acid hydrolysis of cellulose I substrates. *Biomacromolecules, 13*, 570–578.

Wada, M., Nishiyama, Y., Chanzy, H., Forsyth, T., & Langan, P. (2008). The structure of celluloses. *Powder Diffraction, 23*, 92–95.

Yue, Y., Zhou, C., French, A. D., Xia, G., Han, G., Wang, Q., & Wu, Q. (2012). Comparative properties of cellulose nano-crystals from native and mercerized cotton fibers. *Cellulose, 19*, 1173–1187.

Mechanical properties of natural rubber nanocomposites reinforced with high aspect ratio cellulose nanocrystals isolated from soy hulls

At present, the most promising application of CNCs is as reinforcement material in the field of polymer nanocomposites.The incorporation of CNCs in polymer matrices generally leads to polymer-based nanocomposite materials with higher mechanical and barrier properties than the neat polymer or conventional composites. Among various factors that influence the efficiency of the reinforcing effect of CNCs, their intrinsic characteristics, including crystallinity and aspect ratio, play a key role (Dufresne, 2012; Favier et al., 1995; Mariano et al., 2014). It is also well-known that these characteristics depend on the source of the original cellulose, on the extraction method and its conditions (including pretreatment). However, it is widely accepted that the raw starting material is the most important factor (Beck-Candanedo et al., 2005; Dufresne, 2012; Elazzouzi-Hafraoui et al., 2008). The reinforcement capability of CNCs is therefore directly linked to the source of cellulose as well as its biosynthesis. Thus, the optimization of the extraction procedure and further characterization of CNCs from different sources of cellulose are crucial for an efficient exploitation of these sources, allowing the selection of the appropriate source (*i.e.* with targeted morphology) to suit specific end user applications (Brinchi et al., 2013).

Natural rubber (NR) is a perfect polymer matrix to be used as a model system to study the effect of filler reinforcement, owing to its high flexibility and low stiffness. Its properties can be tailored by the addition of reinforcing fillers of various surface chemistries and aggregate size/aspect ratios to suit the targeted application. CNCs extracted from different sources have already been studied as nanoreinforcement in NR-based nanocomposites, including CNCs isolated from capim dourado (Siqueira et al., 2010), rachis of palm date tree (Bendahou et al., 2009), sugarcane bagasse (Pasquini et al., 2010; Bras et al., 2010), sisal (Siqueira et al., 2011), and bamboo (Visakh et al., 2012).

So far, little results have been reported in the literature on the isolation of CNCs from soy hulls or their use in nanocomposites (Flauzino Neto et al., 2013, Silvério et al., 2014). In this study, CNCs were isolated from soy hulls by sulfuric acid hydrolysis treatment. The resulting CNCs, referred to as CNC_{SH} in the following, were characterized using transmission electron microscopy (TEM), atomic force microscopy (AFM), X-ray diffraction (XRD), wide-angle X-ray scattering (WAXS). These CNC_{SH} were used as a reinforcing phase in a NR matrix to prepare nanocomposite films by casting/evaporation at 1, 2.5 and 5 wt% (dry basis) loading levels. The effect of CNC_{SH} on the structure, as

well as thermal and mechanical properties of NR, was investigated by means of scanning electron microscopy (SEM), Fourier-transform infrared spectroscopy (FTIR), dynamic mechanical analysis (DMA), tensile tests and thermogravimetric analysis (TGA).

For the acid hydrolysis treatment, were chose milder conditions compared to those described in Flauzino Neto et al. (2013) in order to avoid as much as possible the hydrolysis of crystalline cellulose domains. The CNC_{SH} was found to have a type I crystal structure, high crystallinity (crystallinity index ≈ 80%), large specific surface area (estimated to be 747 $m^2 \cdot g^{-1}$ from geometrical considerations) and high aspect ratio (around 100). This aspect ratio is the largest ever reported in the literature for a plant cellulose source. Futhermore, from microscopic observations it is clearly seen that CNC_{SH} does not consist of partially hydrolyzed microfibril since it displays the classical rod-like morphology of CNC. Thus, soy hull was found to be an interesting source of raw material for the production of CNC, due to the characteristics of the obtained nanocrystals associated with low lignin content and wide availability of this agro-industrial residue. In the meantime, the reuse of this agro-industrial residue goes towards sustainable development and environment-friendly materials. To tailor the dimensions of CNC and take full advantage of this source, special care needs to be paid to the extraction process and its conditions. A milder acid hydrolysis is preferable to improve the extraction yield, preserve the crystallinity of native cellulose and obtain high aspect ratio CNC.

As expected, a high reinforcing effect is observed even at low filler contents when using this nanofiller (CNC_{SH}) to prepare nanocomposites with a natural rubber (NR) matrix by casting/evaporation. For instance, by adding only 2.5 wt% CNC, the storage tensile modulus at 25°C of the nanocomposite was about 21 times higher than that of the unfilled NR matrix. This reinforcing effect was higher than the one observed for CNCs extracted from other sources. It may be assigned not only to the high aspect ratio of these CNCs but also to the stiffness of the percolating nanoparticle network formed within the polymer matrix. Moreover, the sedimentation of CNCs during the film processing by casting/evaporation was found to take place and play a crucial role on the mechanical properties. Thus, both the high aspect ratio of the CNC and sedimentation due to the processing technique are involved in the good mechanical results obtained. Indeed, if sedimentation occurs, then a multilayered film results and the CNC content in the lowest layers is higher than the average CNC content. It means that CNC mechanical percolation can occur in the lowest layers for an average CNC content which is lower than the percolation threshold. Hence, the system can be considered as constituted of parallel

layers in the direction of the mechanical solicitation (tensile mode), and the CNC-rich layers can support a higher stress leading to a higher modulus value. Moreover, if high aspect ratio CNC is used, then percolation can occur in the lowest layers for lower average CNC contents. An important contribution of this work is to highlight the importance of the sedimentation of CNC during the evaporation step on the mechanical properties of the nanocomposites which is rarely mentioned in the literature.

REFERENCES

Beck-Candanedo, S., Roman, M., & Gray, D. G. (2005). Effect of reaction conditions on the properties and behavior of wood cellulose nanocrystal suspensions *Biomacromolecules, 6*, 1048-1054.

Bendahou, A., Habibi, Y., Kaddami, H., & Dufresne, A. (2009). Physico-chemical characterization of palm from Phoenix dactylifera L., preparation of cellulose whiskers and natural rubber-based nanocomposites. *Journal of Biobased Materials and Bioenergy*, *3*, 81-90.

Bras, J., Hassan, M. L., Bruzesse, C., Hassan, E. A., El-Wakil, N. A., & Dufresne, A. (2010). Mechanical, barrier, and biodegradability properties of bagasse cellulose whiskers reinforced natural rubber nanocomposites. *Industrial Crops and Products*, *32*, 627-633.

Brinchi, L., Cotana, F., Fortunati, E., & Kenny, J. M. (2013). Production of nanocrystalline cellulose from lignocellulosic biomass: Technology and applications. *Carbohydrate Polymers*, *94*, 154-169.

Dufresne, A. (2012). *Nanocellulose: From nature to high-performance tailored materials*. de Gruyter, Berlin/Boston.

Elazzouzi-Hafraoui, S., Nishiyama, Y., Putaux, J-L., Heux, L., Dubreuil, F., & Rochas, C. (2008). The shape and size distribution of crystalline nanoparticles prepared by acid hydrolysis of native cellulose. *Biomacromolecules, 9*, 57-65.

Favier, V., Chanzy, H., & Cavaillé, J.-Y. (1995). Polymer nanocomposites reinforced by cellulose whiskers. *Macromolecules, 28*, 6365-6367.

Flauzino Neto, W. P., Silvério, H. A., Dantas, N. O., & Pasquini, D. (2013). Extraction and characterization of cellulose nanocrystals from agro-industrial residue-soy hulls. *Industrial Crops and Products, 42*, 480-488.

Mariano, M., El Kissi, N., & Dufresne, A. (2014). Cellulose nanocrystals and related nanocomposites: Review of some properties and challenges. *Journal of Polymer Science B, 52*, 791-806.

Pasquini, D., Teixeira, E. M., Curvelo, A. A. S., Belgacem, M. N., & Dufresne, A. (2010). Extraction of starch nanocrystals and cellulose whiskers from cassava bagasse and their applications as reinforcing agent in natural rubber. *Industrial Crops and Products*, *32*, 486-490.

Siqueira, G., Abdillahi, H., Bras, J., & Dufresne, A. (2010). High reinforcing capability cellulose nanocrystals extracted from *Syngonanthus nitens* (Capim dourado). *Cellulose*, *17*, 289-298.

Siqueira, G., Tapin-Lingua, S., Bras, J., da Silva Perez, D., & Dufresne, A. (2011). Mechanical properties of natural rubber nanocomposites reinforced with cellulosic nanoparticles obtained from enzymatic and acid hydrolysis of sisal fibers. *Cellulose*, *18*, 57-65.

Visakh, P. M., Thomas, S., Oksman, K., & Mathew, A. P. (2012). Crosslinked natural rubber nanocomposites reinforced with cellulose whiskers isolated from bamboo waste: Processing and mechanical/thermal properties. *Composites Part A, 43*, 735-741.

RÉSUMÉ

Puisque cette thèse présente deux études indépendantes sur les nanocristaux de cellulose (CNC), le résumé a été divisé en deux sections qui font référence aux chapitres II et III, respectivement.

Investigation morphologique et structurelle des nanocristaux de cellulose I et II préparés par hydrolyse à l'acide sulfurique

La cellulose a plusieurs polymorphes. Ces polymorphes diffèrent l'un de l'autre par l'arrangement cristallin (c'est-à-dire les paramètres de la maille unitaire), la polarité des chaînes et les types de lisons d'hydrogène entre elles. La plupart des polymorphes de la cellulose résultent de traitements chimiques appliqués au polymorphe natif, la cellulose I (Cell-I) (Wada *et al.*, 2008). Dans la Cell-I, les chaînes sont parallèles et peuvent être divisées en deux allomorphes, à savoir Iα et Iβ. Parmi les polymorphes cellulosiques, la cellulose II (Cell-II), dans laquelle les chaînes sont antiparallèles, peut être préparée à partir de Cell-I par deux processus distincts: mercerisation ou régénération. La mercerisation est un processus qui se déroule essentiellement à l'état solide dans lequel les fibres de cellulose sont gonflées dans un milieu alcalin concentré et recristallisées en cellulose II lors du lavage et du séchage (élimination de l'agent gonflant). Contrairement au processus de mercerisation, dans la régénération, la cellulose est tout d'abord dissoute dans un solvant approprié et ensuite précipitée par addition d'un non-solvant, ce qui provoque la recristallisation des chaînes dans le polymorphe Cell-II. La transition de Cell-I à Cell-II est irréversible, ce qui suggère que la Cell-II est thermodynamiquement plus stable (Habibi *et al.*, 2010).

La Cell-II est le second polymorphe le plus étudié en raison de sa pertinence technique. Néanmoins, la plupart des études impliquant la Cell-II jusqu'à présent se concentrent sur les fibres et seules quelques études récentes ont été réalisées sur les nanocristaux. Les nanocristaux Cell-II ont été préparés soit par hydrolyse acide de fibres mercerisées (Hirota *et al.*, 2012; Kim *et al.*, 2006; Yue *et al.*, 2012), soit mercerisation de CNC de Cell-I (Jin *et al.*, 2016), ou après recristallisation de fractions de chaînes courtes de cellulose en solution (Dhar *et al.*, 2015; Hirota *et al.*, 2012; Hu *et al.*, 2014; Sèbe *et al.*, 2012). Ces études ont combiné les données de plusieurs techniques d'imagerie, de diffraction et de spectroscopie. Cependant, une image structurelle complète des nanocristaux n'a pas encore été rapportée.

Dans ce contexte, le but du travail de recherche présenté dans le chapitre II était de produire, de caractériser et de comparer les CNC obtenus à partir de la pâte de bois d'eucalyptus en utilisant trois méthodes différentes: i) l'hydrolyse classique à l'acide sulfurique (CN-I), ii) l'hydrolyse acide de la cellulose précédemment mercerisée par traitement alcalin (MCN-II), et iii) la solubilisation de la cellulose dans l'acide sulfurique et la recristallisation subséquente dans l'eau (RCN-II). La morphologie, la structure cristalline, l'indice de cristallinité, la charge superficielle et le degré de polymérisation de ces nanocristaux ont été caractérisés par des techniques complémentaires, à savoir: l'analyse élémentaire, la zétamétrie, la viscométrie, la microscopie électronique en transmission (TEM), la microscopie à force atomique (AFM), la diffraction des rayons X (XRD), la spectroscopie infrarouge à transformée de Fourier et la spectroscopie de résonance magnétique nucléaire à l'état solide (FTIR et NMR, respectivement).

Les trois types de CNC préparés présentent des morphologies et des structures cristallines différentes. Lorsque les conditions d'hydrolyse acide sont mises en place de telle sorte que les domaines cristallins dans la pâte de bois initial et la cellulose mercerisée (WP et MWP, respectivement) sont préservés (60 wt% H_2SO_4, 45°C, 50 min), les nanocristaux résultants conservent la nature fibrillaire des fibres d'origine (c'est-à-dire que l'axe de la chaîne est parallèle au grand axe des particules aciculaires) et leur type allomorphe initial (I pour WP et II pour la MWP). Dans les deux cas, les particules sont principalement composées de quelques cristallites élémentaires liées latéralement, en accord avec ce qui a été montré pour les CNC de coton par Elazzouzi-Hafraoui *et al*. (2008). Les nanocristaux unitaires dans les CNC préparés à partir de cellulose mercerisée (MCN-II) sont plus courts, mais plus larges que ceux préparés à partir des fibres de cellulose I (CN-I). Si des conditions plus sévères sont considérées (64 wt% H_2SO_4, 40°C, 20 min), ce qui entraîne la dépolymérisation et la dissolution de la cellulose native, les chaînes courtes (avec un degré de polymérisation DP ≈ 17) recristallisent en rubans de Cell-II lors de la régénération dans l'eau à température ambiante. Dans ces rubans tortueux, l'axe de la chaîne serait perpendiculaire au grand axe du nanocristal et parallèle à son plan basal. De plus, ces nano-rubans ont une forme et une orientation moléculaire très similaires aux nanocristaux de mannan II préparés par recristallisation de mannan (Heux *et al*., 2005), un polymère linéaire de résidus β-(1,4)-D-mannosyl, ce qui suggère que ce mode de cristallisation peut être une caractéristique des polysaccharides linéaires à chaîne courte et à liaison β-(1,4).

Bien que des rubans de cellulose recristallisés II similaires ont été rapportés par d'autres auteurs, à notre connaissance, c'est la première fois qu'une description morphologique et structurelle détaillée est proposée en termes de morphologie des particules, de structure des cristaux et d'orientation des chaînes. Par comparaison avec les nanocristaux fibrillaires préparés par hydrolyse acide des fibres de cellulose native ou mercerisée, la structure moléculaire et cristalline unique des nano-rubans implique qu'un nombre plus élevé d'extrémités de chaîne réductrice sont situées à la surface des particules, ce qui peut être important pour des modifications chimiques subséquentes et pour de potentielles applications spécifiques telles que la biodétection et la bio-imagerie. Donc, cette étude permet de mieux comprendre la structure cristalline et la morphologie de la CNC obtenue par régénération à l'acide sulfurique.

RÉFÉRENCES

Dhar, P., Tarafder, D., Kumar, A., & Katiyar, V. (2015). Effect of cellulose nanocrystal polymorphs on mechanical, barrier and thermal properties of poly(lactic acid) based bionanocomposites. *Royal Society of Chemistry Advances, 5*, 60426–60440.

Elazzouzi-Hafraoui, S., Nishiyama, Y., Putaux, J-L., Heux, L., Dubreuil, F., & Rochas, C. (2008). The shape and size distribution of crystalline nanoparticles prepared by acid hydrolysis of native cellulose. *Biomacromolecules, 9*, 57-65.

Habibi, Y., Lucia, L. A., & Rojas, O. J. (2010). Cellulose nanocrystals: chemistry, self-assembly and applications. *Chemical Reviews, 110*, 3479–3500.

Heux, L., Hägglund, P., Putaux, J-L., & Chanzy, H. (2005). Structural aspects in semi-crystalline samples from the mannan II family. *Biomacromolecules, 6*, 324–332.

Hirota, M., Tamura, N., Saito, T., & Isogai, A. (2012). Cellulose II nanoelements prepared from fully mercerized, partially mercerized and regenerated celluloses by 4-acetamido-TEMPO/NaClO/$NaClO_2$ oxidation. *Cellulose, 19*, 435–442.

Hu, T. Q., Hashaikeh, R., & Berry, R. N. (2014). Isolation of a novel, crystalline cellulose material from the spent liquor of cellulose nanocrystals (CNCs). *Cellulose, 21*, 3217–3229.

Jin, E., Guo, J., Yang, F., Zhu, Y., Song, J., Jin, Y., & Rojas, O. J. (2016). On the polymorphic and morphological changes of cellulose nanocrystals (CNC-I) upon mercerization and conversion to CNC-II. *Carbohydrate Polymers, 143*, 327–335.

Kim, N., Imai, T., Wada, M., & Sugiyama, J. (2006). Molecular directionality in cellulose polymorphs. *Biomacromolecules, 7*, 274–280.

Sèbe G., Ham-Pichavant, F., Ibarboure, E., Koffi, A. L. C., & Tingaut, P. (2012). Supramolecular structure characterization of cellulose II nanowhiskers produced by acid hydrolysis of cellulose I substrates. *Biomacromolecules, 13*, 570–578.

Wada, M., Nishiyama, Y., Chanzy, H., Forsyth, T., & Langan, P. (2008). The structure of celluloses. *Powder Diffraction, 23*, 92–95.

Yue, Y., Zhou, C., French, A. D., Xia, G., Han, G., Wang, Q., & Wu, Q. (2012). Comparative properties of cellulose nano-crystals from native and mercerized cotton fibers. *Cellulose, 19*, 1173–1187.

Propriétés mécaniques de nanocomposites de caoutchouc naturel renforcé avec des nanocristaux de cellulose à facteur de forme élevé extraits de la coque de soja

Actuellement, l'application la plus prometteuse des CNCs est en tant que matériau de renfort dans le domaine des nanocomposites polymères. L'incorporation de CNCs dans une matrice polymère génère généralement des matériaux nanocomposites ayant des propriétés mécaniques et barrières plus élevées que le polymère pur ou les composites classiques. Parmi les différents facteurs qui influencent l'efficacité de l'effet de renfort des CNCs, leurs caractéristiques intrinsèques, y compris la cristallinité et le facteur de forme, jouent un rôle fondamental (Dufresne, 2012; Favier *et al*., 1995; Mariano *et al*., 2014). Il est bien connu que ces caractéristiques dépendent de la source de la cellulose d'origine, de la méthode d'extraction et de ses conditions (y compris le prétraitement). Cependant, il est largement admis que le matériau brut de départ est le facteur le plus important (Beck-Candanedo *et al*., 2005; Dufresne, 2012; Elazzouzi-Hafraoui *et al*., 2008). La capacité de renfort des CNC est donc directement liée à la source de cellulose ainsi qu'à sa biosynthèse. Par conséquent, l'optimisation de la procédure d'extraction et la caractérisation de CNCs de différentes sources de cellulose sont cruciales pour une exploitation efficace de ces sources, permettant une sélection de la source appropriée (c'est-à-dire avec une morphologie ciblée) pour s'adapter à des applications spécifiques (Brinchi *et al*., 2013).

Le caoutchouc naturel (NR) est une matrice polymère parfaite pouvant être utilisée comme système modèle pour étudier l'effet de renfort, en raison de sa grande flexibilité et de sa faible rigidité. Ses propriétés peuvent être ajustées en ajoutant des charges de renfort de différentes chimies de surface et de différentes taille/facteur de forme des agrégats en fonction de l'application ciblée. Des CNCs extraits de différentes sources ont déjà été étudiés en tant que nano-renfort dans des nanocomposites à base de

NR, y compris des CNCs extraits de capim dourado (Siqueira *et al*., 2010), du rachis de palmier dattier (Bendahou *et al*., 2009), de la bagasse de canne à sucre (Pasquini *et al*., 2010; Bras *et al*., 2010), du sisal (Siqueira *et al*., 2011), et du bambou (Visakh *et al*., 2012).

Jusqu'à présent, peu de résultats ont été rapportés dans la littérature sur l'extraction de CNC à partir de la coque de soja ou leur utilisation dans des nanocomposites (Flauzino Neto *et al*., 2013, Silvério *et al*., 2014). Dans cette étude, les CNCs ont été isolés des coques de soja à partir d'un traitement par hydrolyse avec de l'acide sulfurique. Les CNCs résultants, désignés CNC_{SH} par la suite, ont été caractérisés par microscopie électronique en transmission (TEM), par microscopie à force atomique (AFM), par diffraction des rayons X (XRD) et par diffusion des rayons X aux grands angles (WAXS). Ces CNC_{SH} ont été utilisés comme phase de renfort dans une matrice NR par casting/évaporation à différents taux de charge, à savoir 1, 2.5 et 5% en poids (base sèche). Les effets des CNC_{SH} sur la structure ainsi que sur les propriétés thermiques et mécaniques du NR ont été étudiés en utilisant la microscopie électronique à balayage (SEM), la spectroscopie infrarouge à transformée de Fourier (FTIR), l'analyse mécanique dynamique (DMA), les essais de traction et l'analyse thermogravimétrique (TGA). Pour le traitement par hydrolyse acide, nous avons choisi des conditions plus douces par rapport à celles décrites par Flauzino Neto *et al*. (2013) afin d'éviter autant que possible l'hydrolyse des domaines cellulosiques cristallins. Il a été constaté que les CNC_{SH} ont une structure cristalline de type I, une haute cristallinité (indice de cristallinité ≈ 80%), une grande surface spécifique (estimée à 747 $m^2 \cdot g^{-1}$ par des considérations géométriques) et un facteur de forme élevé (environ 100). Ce facteur de forme est le plus important rapporté dans la littérature pour une source de cellulose végétale. De plus à partir des observations microscopiques, il est clair que le CNC_{SH} ne se compose pas de microfibrilles partiellement hydrolysées car il présente la morphologie classique du CNC (en bâtonnet). Ainsi, il a été constaté que la coque de soja est une source intéressante de matière première pour la production de CNC, notamment en raison des caractéristiques des nanocristaux obtenus associées à une faible quantité de lignine et une large disponibilité de ce résidu agro-industriel. Dans l'intervalle, la réutilisation de ce résidu agro-industriel va vers le développement durable et des matériaux respectueux de l'environnement. Toutefois, pour adapter les dimensions du CNC et profiter pleinement de cette source, une attention particulière doit être accordée à son processus d'extraction. Une hydrolyse acide plus douce est préférable pour

améliorer le rendement d'extraction, préserver la cristallinité de la cellulose native et obtenir un CNC avec rapport d'aspect élevé.

Comme on pouivait s'y attendre, un effet de renfort élevé est observé même pour de faibles taux de charge lors de l'utilisation de cette nanocharge (CNC_{SH}) pour préparer des nanocomposites avec une matrice de caoutchouc naturel (NR) par casting/évaporation. Par exemple, en ajoutant seulement 2,5% en poids de CNC, le module de conservation en traction du nanocomposite à 25°C est environ 21 fois plus élevé que celui de la matrice NR non chargée. Cet effet de renfort est supérieur à celui observé pour les CNCs extraits d'autres sources. Il peut être attribué non seulement au facteur de forme élevé de ces CNCs, mais aussi à la rigidité du réseau percolant de nanoparticules formé au sein de la matrice polymère. De plus, il a été constaté que la sédimentation des CNC pendant la mise en œuvre du film nanocomposite par casting/évaporation joue un rôle crucial sur les propriétés mécaniques. Donc, le facteur de forme élevé du CNC ainsi que sa sédimentation en raison de la technique de mise en œuvre sont impliqués dans les bons résultats mécaniques obtenus. En effet, si une sédimentation se produit, un film avec plusieurs couches est produit dans lequel la quantité de CNC dans les couches inférieures est supérieure à la quantité moyenne de CNC. Cela signifie que la percolation mécanique des CNCs peut se produire dans les couches les plus basses pour un taux moyen de CNC, qui est inférieure au seuil de percolation. Par conséquent, le système peut être considéré comme constitué de couches parallèles dans la direction de la sollicitation mécanique (mode de traction), et les couches riches en CNC peuvent supporter une contrainte mécanique plus élevée, ce qui donne une valeur de module plus élevée. De plus, si des CNCs à facteur de forme élevé sont utilisés, la percolation peut se produire dans les couches les plus basses pour un taux moyen inférieur de CNC. Une contribution importante de ce travail est de mettre en évidence l'importance de la sédimentation des CNCs, pendant l'étape d'évaporation sur les propriétés mécaniques des nanocomposites, ce qui est rarement mentionné dans la littérature.

RÉFÉRENCES

Beck-Candanedo, S., Roman, M., & Gray, D. G. (2005). Effect of reaction conditions on the properties and behavior of wood cellulose nanocrystal suspensions *Biomacromolecules, 6*, 1048-1054.

Bendahou, A., Habibi, Y., Kaddami, H., & Dufresne, A. (2009). Physico-chemical characterization of palm from Phoenix dactylifera L., preparation of cellulose whiskers and natural rubber-based nanocomposites. *Journal of Biobased Materials and Bioenergy*, *3*, 81-90.

Bras, J., Hassan, M. L., Bruzesse, C., Hassan, E. A., El-Wakil, N. A., & Dufresne, A. (2010). Mechanical, barrier, and biodegradability properties of bagasse cellulose whiskers reinforced natural rubber nanocomposites. *Industrial Crops and Products*, *32*, 627-633.

Brinchi, L., Cotana, F., Fortunati, E., & Kenny, J. M. (2013). Production of nanocrystalline cellulose from lignocellulosic biomass: Technology and applications. *Carbohydrate Polymers*, *94*, 154-169.

Dufresne, A. (2012). *Nanocellulose: From nature to high-performance tailored materials*. de Gruyter, Berlin/Boston.

Elazzouzi-Hafraoui, S., Nishiyama, Y., Putaux, J-L., Heux, L., Dubreuil, F., & Rochas, C. (2008). The shape and size distribution of crystalline nanoparticles prepared by acid hydrolysis of native cellulose. *Biomacromolecules*, *9*, 57-65.

Favier, V., Chanzy, H., & Cavaillé, J.-Y. (1995). Polymer nanocomposites reinforced by cellulose whiskers. *Macromolecules*, *28*, 6365-6367.

Flauzino Neto, W. P., Silvério, H. A., Dantas, N. O., & Pasquini, D. (2013). Extraction and characterization of cellulose nanocrystals from agro-industrial residue-soy hulls. *Industrial Crops and Products, 42*, 480-488.

Mariano, M., El Kissi, N., & Dufresne, A. (2014). Cellulose nanocrystals and related nanocomposites: Review of some properties and challenges. *Journal of Polymer Science B*, *52*, 791-806.

Pasquini, D., Teixeira, E. M., Curvelo, A. A. S., Belgacem, M. N., & Dufresne, A. (2010). Extraction of starch nanocrystals and cellulose whiskers from cassava bagasse and their applications as reinforcing agent in natural rubber. *Industrial Crops and Products*, *32*, 486-490.

Siqueira, G., Abdillahi, H., Bras, J., & Dufresne, A. (2010). High reinforcing capability cellulose nanocrystals extracted from *Syngonanthus nitens* (Capim dourado). *Cellulose*, *17*, 289-298.

Siqueira, G., Tapin-Lingua, S., Bras, J., da Silva Perez, D., & Dufresne, A. (2011). Mechanical properties of natural rubber nanocomposites reinforced with cellulosic

nanoparticles obtained from enzymatic and acid hydrolysis of sisal fibers. *Cellulose, 18*, 57-65.

Visakh, P. M., Thomas, S., Oksman, K., & Mathew, A. P. (2012). Crosslinked natural rubber nanocomposites reinforced with cellulose whiskers isolated from bamboo waste: Processing and mechanical/thermal properties. *Composites Part A, 43*, 735-741.

CHAPTER I

Literature Review

CONTENT CHAPTER I

1. CELLULOSE, AN IMPORTANT SUBSTANCE 3

2. CELLULOSE STRUCTURE 4

2.1. Molecular features of cellulose 6

2.2. Degree of polymerization of cellulose 10

2.3. Cellulose biosynthesis and cellulose microfibril formation 10

2.4. Cellulose microfibrils and hierarchical organization of plant fibers 16

3. SEMICRYSTALLINE NATURE OF CELLULOSE 20

3.1. Cellulose crystal structure and cellulose Polymorphs 25

3.2. Mercerization and regeneration processes 32

3.3. Technical relevance of cellulose polymorph II 38

3.4. Crystall Orientation and folded-chain structure of cellulose II 39

4. CELLULOSE NANOCRYSTALS: PROPERTIES, PRODUCTION AND APPLICATIONS 41

4.1. Isolation of CNC from cellulose source material 43

4.2. Influence of cellulose source and isolation process on CNC properties 45

4.3. Acid hydrolysis 46

4.4. Degree of polymerization 48

4.5. Specific surface area 48

4.6. Excellent mechanical properties 50

4.7. Crystallinity 51

4.8. Aspect ratio 51

4.9. Challenges on commercial CNC production 52

4.10. Toxicology assessment and biodegradability 52

4.11. Durability of CNC based products 53

4.12. Cellulose nanocomposites based on cellulose nanocrystals 53

4.13. Mechanical properties of CNC/polymer nanocomposites and percolation theory 55

5. REFERENCES 61

1. CELLULOSE, AN IMPORTANT SUBSTANCE

Cellulose is the major component of the plant biomass. Since it is made by all true plants (Kingdom *Plantae*), from the current point of view, cellulose is considered the most abundant naturally occurring organic compound on Earth. Cellulose metabolism is an important part of the biosphere's carbon cycle. This carbohydrate is found primarily in plant cell walls, where its main function is to provide structural support and protection to the cells. It can be also found in several other types of organisms such as bacteria, fungi, animal tunicates and even amoeba, although the content of cellulose in these species is negligible when compared with plants (Chen, 2014; Dufresne, 2012). Cellulose is continually produced by different living species every day in the biosphere, providing a total annual production around $1.5 \cdot 10^{12}$ tons (Klemm *et al.*, 2005). Thereby, cellulose is a renewable (naturally replenished) resource widely available all over the world. Further, it is biodegradable, returning to the natural carbon cycle by simple rotting, and non-toxic to living organisms, including humans.

Cellulose has always played an important role in the life of man, from prehistoric to present time, and its applications could even represent a landmark in the understanding of human evolution. Natural cellulose-based materials, such as wood, have been utilized to many purposes for thousands of years, *e.g.*, as source of heat for warming, cooking and industrial production; as engineering materials for buildings, bridges, ships, furniture, utensils *etc*. In its almost pure form, such as cotton and flax fibers, cellulose has also been used since a long time ago, as clothing and writing material going back to the time of Egyptian pharaohs (Kamide, 2005; Pérez & Mazeau, 2004). The first industrial scale product based on cellulose was created from nitrocellulose and camphor by the Hyatt Manufacturing Company in 1870, corresponding to the first thermoplastic polymer material under the trade name of celluloid (Klemm *et al.*, 2005).

Currently, cellulose has a great economic importance, because it is used as feedstock in numerous industries and gives rise to a broad spectrum of products and materials, ranging from packaging to biomedical field. The paper and cardboard industries are the largest consumers of cellulose. Only a small amount of cellulose used is used to produce textile fibers, films and a larger number of cellulose derivatives, such as cellulose ethers and esters (Dufresne, 2012; Klemm *et al.*, 2005; Moon *et al.*, 2011; Varshney & Naithani, 2011). For instance, carboxymethylcellulose is a cellulose derivative utilized in foodstuffs, pharmaceuticals, cosmetics, detergents, paints, coatings, adhesives and plastics *etc*.

Although cellulose can be derived from a broad variety of sources (such as: cotton, jute, flax, ramie, sisal, bagasse, bamboo *etc*), wood is presently the most important raw material for commercial production of cellulose (Siró & Plackett, 2010).

When it comes to sustainable raw materials for future demands on energy, chemicals and materials, cellulose definitely has great importance on account of its abundance and renewability, but still today is underutilized. For this reason, intensive research efforts have been devoted to seeking efficient processing technologies for conversion of this biomass into multiple value-added bioproducts. Therefore, cellulose is a promising versatile resource with potential to decrease the dependence on pretroleum-based products and at the same time attends the increasing need for environmentally friendly, biocompatible products and carbon-neutral (Cherubini, 2010; Olsson & Westman, 2013). Nevertheless, numerous technical challenges must be overcome to enable the efficient and profitable utilization of cellulose for the production of energy, chemicals and materials.

2. CELLULOSE STRUCTURE

Cellulose has been used for centuries in highly diverse applications, however its chemical composition, structure and morphology remained very long ignored. Though the early work of Braconnot concerning the acid hydrolysis of the substance constituting plant cell walls goes back to the beginning of the 19th century (Braconnot, 1819), it was the French chemist Anselme Payen (1795–1871) who established that the main constituent of all plant cells has a unique chemical structure (Payen, 1838) and coined the word "cellulose" (*Latin*: rich in small cells) for the first time in 1838. In his studies, Payen described that when various plant tissues were treated with acid-ammonia treatment, followed by subsequent extraction in water, alcohol and ether a constant fibrous material was formed. He deduced the molecular formula to be $C_6H_{10}O_5$ by elemental analysis, and observed the isomerism with starch (Klemm *et al.*, 2005; Pérez & Mazeau 2004).

It is only later, due to the pioneering works of the German chemist Hermann Staudinger (1881-1965) at the beginning of the 20th century that the macromolecular nature of cellulose was recognized. Through acetylation and deacetylation of cellulose, he suggested that its structure does not merely consist of an aggregation of *D*-glucose units. Rather, the glucose units were found to be linked to each other covalently to form long molecular chains. This, along with Staudinger's research with other chain molecules (*e.g.* natural rubber), marked the discovery of the polymeric state of molecules and

represents the origin of polymer science. Staudinger's research on macromolecules was acknowledged by the award of the Nobel Prize in Chemistry in 1953 (Klemm *et al.*, 2005; Mülhaupt, 2004; Pérez & Mazeau 2004; Staudinger, 1920, 1926).

Despite the degree to which cellulose has been investigated, its molecular structural features have not been identified with absolute clarity and new information appeared in the literature constantly by employing technological advances alongside conventional analytical tools. Thus, the progress of knowledge on cellulose is closely linked to the evolution of characterization techniques, such as X-ray diffraction, neutron scattering, electron microscopy, ^{13}C solid state nuclear magnetic resonance *etc* (Dufresne, 2012; O'Sullivan, 1997). Several reviews and books have already been published reporting the state of knowledge of this fascinating polymer (Fengel & Wegener 1989; Gardner & Blackwell, 1974; Habibi *et al.*, 2010; Hon, 1994; Kamide, 2005; Klemm *et al.*, 2005; Kovalenko, 2010; O'Sullivan, 1997).

Cellulose displays unusual physical and chemical properties arising from its structural architecture, such as:

i) Highly hydrophilic nature. However, it is insoluble in water and in most conventional organic solvents. Even such a short oligosaccharide as celloheptose is virtually insoluble. This does not mean that cellulose interacts poorly with water - a cellulose surface is very hydrophilic, *e.g.* cotton fibers can absorb 10 times its own weight of water (Monica *et al.*, 2009).

ii) Good thermal stability. But it decomposes prior to the onset of melting, *i.e.* it is a non-thermoplastic material.

iii) Resistant to chemicals attack. Cellulose is relatively resistant to chemical derivatization, and added groups are seldom evenly distributed. Nevertheless, there is a large industry based on derivatization of cellulose, as previously mentioned.

iv) Good mechanical properties. Cellulose form fibers with high tensile strength and stiffness, which makes the cellulose fibers useful *e.g.* as reinforcing element in polymeric composites.

v) Low density and thermal conductivity. *Etc.*

Therefore, in order to understand properly the macroscopic properties of cellulose it is essential to acquire knowledge of its structural architecture from the atomic scale, all the way up to the macro scale. In that case, the cellulose biosynthesis, its supramolecular

structures and hierarchical organization inside the cell wall must be considered. Besides this, it is important to examine how interactions at and between the various levels of structure have important and often quite specific influences.

2.1. Molecular features of cellulose

Cellulose is a semicrystalline long chain linear homopolymer, consisting of *β-D*-glucopyranose (glucose) molecules covalently linked through acetal functions formed by *β*-(1,4)-glycosidic bonds (Figure 1), *i.e.* *β*-type glycosidic bond between the hemiacetal group of anomeric carbon atom C1 of one *D*-glucose and the hydroxyl group at C4 of the adjacent molecule. This glycosidic bond has a strength on the order of ~360 kJ/mol. Since a molecule of water is lost when an alcohol and a hemiacetal react to form an acetal linkage, each glucose molecule in cellulose is referred to as anhydroglucose unit (AGU). The AGUs are joined to one another in head-to-tail orientation and the C–O–C angle between two AGU rings is ~116°. To accommodate the preferred bond angles of this acetal oxygen bridges formed by *β* 1→4 links, each AGU ring is rotated 180° in the plane with respect to its neighbor. In this manner, two adjacent AGU rings define the repeating structural unit of cellulose polymer, known as **cellobiose**. However, the chain length of cellulose is expressed in the number of constituent AGUs (degree of polymerization, DP), and hence, the chemical formula of cellulose is $(C_6H_{10}O_5)_n$.

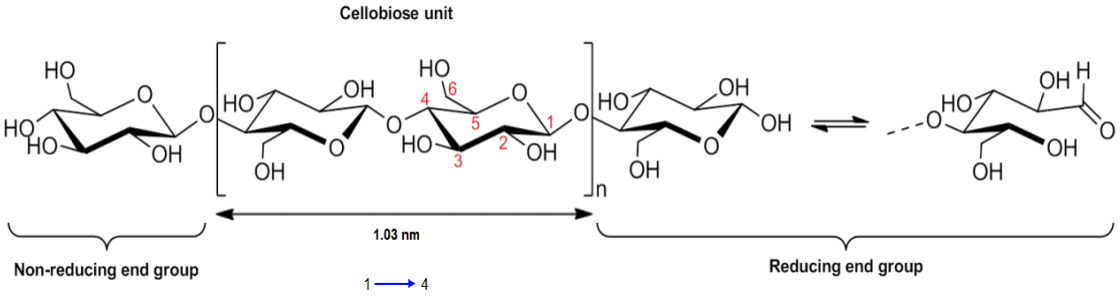

Figure 1 – Structure of cellulose molecule, representing the cellubiose unit as the repeating structural unit having a periodicity of ~1.03 nm and showing the quite different terminal groups non-reducing end (left) and reducing end (right). The numbering system for carbon atoms in anhydroglucose unit is also indicated in red; and the directionality of the 1→4 linkage is indicated by the blue arrow.

Taking the cellobiose as the basic unit, cellulose can be considered as an isotactic polymer of cellobiose. Each of the AGU ring contains three hydroxyl groups. The hydroxyl group at the C6 position is a primary alcohol, while the hydroxyl groups at the C2 and C3 positions are secondary alcohols. These hydroxyl groups are all accessible

sites for chemical reactions. Unlike simple alcohols, however, the reactivity of these hydroxyl groups are usually controlled more by steric factors and molecular interactions than would be expected on the basis of the inherent reactivity of the different hydroxyl groups. The cellulose molecule has a directional chemical asymmetry with respect to the termini of its chain axis: one end is a hemiacetal which is in equilibrium with the aldehyde structure (*i.e.* the reducing end); and the other end has a pendant hydroxyl group, the nominal non-reducing end (Dufresne, 2012; Habibi *et al.*, 2010; Klemm *et al.*, 2005; Pérez & Mazeau 2004).

The *β* configuration allows cellulose to form long, straight, "fully extended" chains, *i.e.* molecular chains are stretched out in a straight line, in the opposite to the 1→4 glucan of *α* -anomers, amylose, which is hexicalled shaped. All *β-D*-glucopyranose rings adopt a $^4C_1$ chair conformation, the lowest free energy conformation of the molecule, in which, the glycosidic bonds and the ring substituents are all positioned in the ring plane (equatorial), while the hydrogen atoms are in the vertical position (axial) (Kovalenko, 2010; Pérez & Mazeau 2004; Varshney & Naithani, 2011). This way, as represented in Figure 2, the cellulose molecule takes the form of a flat ribbon with hydroxyl groups protruding laterally along the extended chain and, as a consequence, these hydroxyl groups are readily available for hydrogen bonding, either within the same cellulose chain (intramolecular) or between different chains (intermolecular).

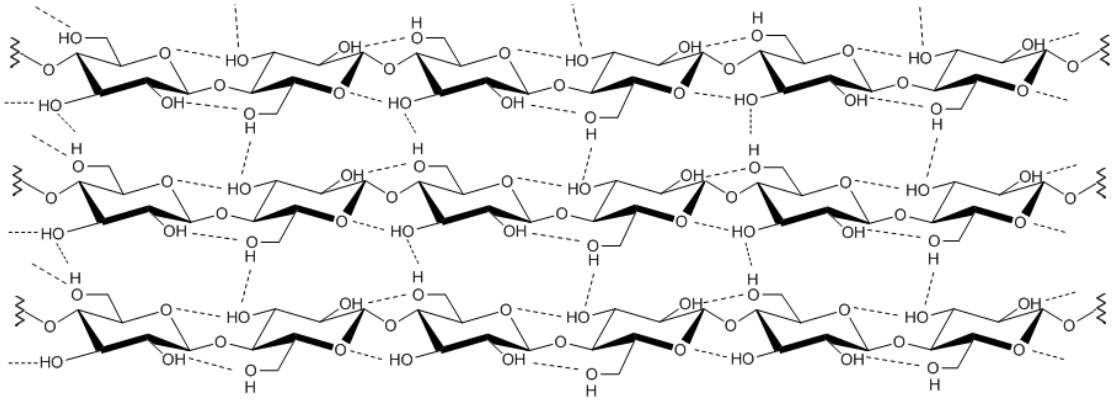

Figure 2 – Schematic drawing of the intra- and intermolecular hydrogen bonding network in cellulose. It is important pointing out that the detailed features of hydrogen-bond pattern is still an ongoing subject for discussion.

The presence of intramolecular hydrogen bonds is of high relevance with regard to single-chain conformation of cellulose, since they hinder the free rotation of the rings along their linking glycoside bonds resulting in the stiffening of the cellulose chain. These

intramolecular hydrogen bonds between adjacent AGU rings stabilize the glycosidic linkage insomuch that the rigidity and the linear integrity of the polymer chain are enhanced. The intermolecular hydrogen bonds, in turn, are thought to be mostly responsible to interchain cohesion, and thus, also to the aggregation state of cellulose (from sheet-like to fibrillar aggregates), also known as supramolecular structure (Djahedi *et al.*, 2016; Dufresne, 2012; Habibi *et al.*, 2010; Varshney & Naithani, 2011).

Therefore, this very complex and strong hydrogen bonding network present in cellulose is extremely important for the particular characteristics of cellulose, such as reactivity, solubility, thermal stability and mechanical properties. For instance, it affects: (i) the reactivity of the hydroxyl groups, particularly of the C3 hydroxyl group, which hydrogen binds strongly to the endocyclic oxygen of the adjoining AGU unit in the same chain; (ii) the solubility, *a priori*, the high number of hydroxyl groups in a molecule should lead to a large solubility in water, but cellulose is insoluble in water and in most conventional solvents, since to solubilize it the solvent-solute attraction must be stronger than the high intermolecular attractive forces which hold the cellulose molecules together; (iii) the thermal stability, since high energy in the form of heat is required to overcome the high cohesive energy between the cellulose molecules, it explains why cellulose does not possess a liquid state (it decomposes prior to the onset of melting), this means that the total bonding force between the cellulose molecules is stronger than their covalent intramolecular bonds; (iv) mechanical properties, the intra and inter-chain hydrogen bonding system imparts to cellulose fibrils a relatively high axial stiffness and good strength.

Another important feature arising from the flat ribbon-like shape of cellulose molecule and the positioning of its hydroxyl groups and hydrogen atoms in the pyranose ring (OH groups are equatorial, while the H atoms are oriented axially to the ring plane) is the formation of sites with markedly distinct polarities: the hydrophilic sites parallel to the ring plane and the hydrophobic sites perpendicular to the ring (Jarvis, 2003; Li & Renneckar 2011; Medronho & Lindman, 2014; Yamane *et al.*, 2006). This feature is depicted in Figure 3, and is expected to considerably influence both the microscopic (*e.g.* interactions) and macroscopic properties (*e.g.* solubility) of cellulose.

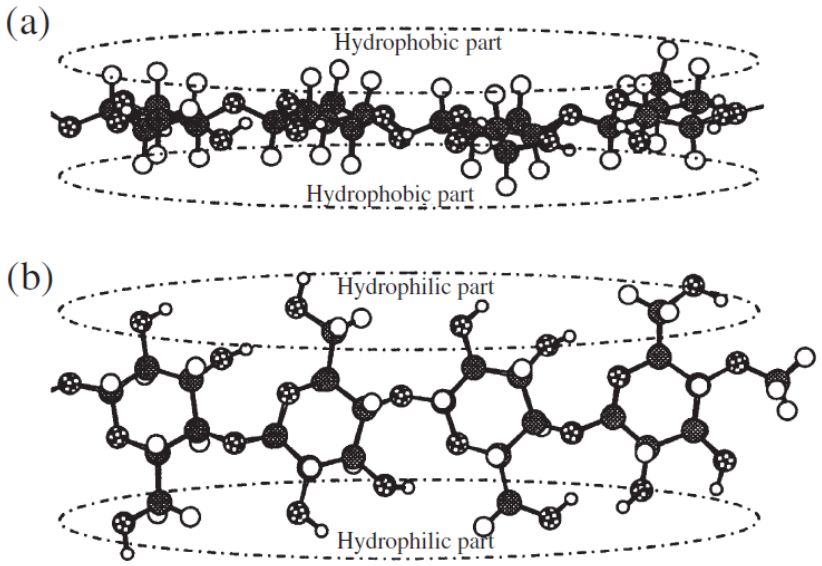

Figure 3 – Hydrophilic and hydrophobic parts of cellulose molecule. (a) Hydrophobic sites of cellulose molecule in side view of glucopyranose ring plane showing the hydrogen atoms of C–H bonds on the axial positions of the rings, (b) hydrophilic sites of cellulose molecule in top view of glucopyranose ring plane showing the hydroxyl groups located on the equatorial positions of the rings (Yamane *et al.*, 2006).

The rotational conformation of the hydroxymethyl group can be altered, as shown in Figure 4, and this will have a profound impact on the hydrogen bonding pattern (Nishiyama *et al.*, 2002). There are three possible low energy orientations for this substituent to the pyranose ring, defined by two letters (*gt*, *gg* and *tg*) referring to the *trans* and *gauche* states of the dihedral angles O6–C6–C5–O5 and O6–C6–C5–C4, respectively. For example, if O6–C6 is *gauche* to C5–O5 and *trans* to C5–C4, then the conformation is called *gt*. The reason for the difference in stability between these three staggered conformers is the relative proximity of the oxygen and carbon substituents (Habibi *et al.*, 2010; O'Sullivan, 1997).

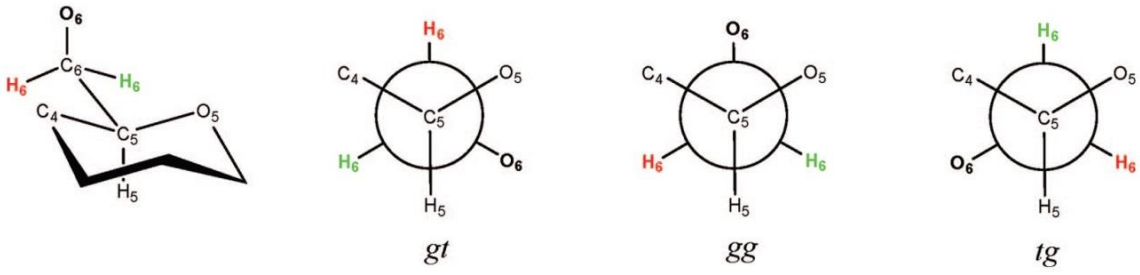

Figure 4 – The three most probable rotational positions of the hydroxymethyl group defined by ascertaining the placement of the O6-C6 bond with respect to the C5-O5 and C5-C4 bonds. In this figure *g* and *t* are abbreviations of *gauche* (60°) and *trans* (180°), respectively, indicating qualitatively the value of a dihedral angle (Habibi *et al.*, 2010).

2.2. Degree of polymerization of cellulose

The size of the cellulose molecule, indicated by the degree of polymerization (DP) or molecular weight (MW), has a great influence on the mechanical, solution, biological, and physiological properties of cellulose. It is believed that a β (1→4) linked glucan with DP around 20–30 can offer all properties of cellulose (Dufresne, 2012; Klemm *et al.*, 2005; Kobayashi *et al.*, 2001). Values of DP ranging from hundreds and several tens of thousands have been reported. The DP is heavily dependent on the source of the original cellulose (*e.g.*, 10 000 in native wood, 15 000 in cotton, 44 000 in *Valonia*), and in less degree on the isolation and purification methods (*e.g.*, 250 – 500 in regenerated cellulose and 1000 in bleached kraft pulp). The combination of procedures required to isolate and purify cellulose inevitably causes some degradation during analysis resulting in chains scission. The values of DP obtained are therefore minimal and depend on the method used to determine it. For the same reasons, the distribution of chain lengths of cellulose is not well established. Nonetheless, some authors suggest that the molecular mass distribution must be homogeneous for cellulose of a given source (Dufresne, 2012; Fengel & Wegener 1989; Habibi *et al.*, 2010; Klemm *et al.*, 2005; Varshney & Naithani, 2011).

In its commonly used form, isolated cellulose is always a polydisperse polymer, *viz.*, like nearly all polymers it is a mixture of molecules that have the same basic composition but differ in the chain length. Thereby, the molecular mass and the DP of cellulose can only be considered as average values. Since celulose often has a high DP, the fibrils are quite long. For example, given a glucose unit as 0.515 nm long, for DP value of 10 000, the cellulose molecules may have average length around 5 μm by considering stretched chains.

2.3. Cellulose biosynthesis and cellulose microfibril formation

In nature, cellulose does not occur as an isolated molecule, but it is found as assemblies of individual chains forming a fiber-like structure. This is because cellulose is polymerized as individual molecules, which undergo spinning and crystallization in a hierarchical order at the site of biosynthesis resulting in fibrillar supramolecular structures (Habibi *et al.*, 2010). That way, the biosynthesis of cellulose can be described as a complex sequential multistep phenomenon, involving coupled processes (i) the enzymatic polymerization of individual β-(1,4)-*D*-glucopyranose chains from glucose monomers, and (ii) the assemble of these glucan chains, through spinning and crystallization, to form fibrillar supramolecular structures (Dufresne, 2012).

Cellulose biosynthesis process takes place at plasma membrane-bound enzyme system in the cell wall, known as cellulose synthase complexes (CSCs). The CSCs have functional specialization roles in gene expression, regulation and catalytic functions (Festucci-buselli *et al.*, 2007). The model proposed by Delmer and Amor (Delmer & Amor, 1995) represents the CSC through the cytoplasmic membrane within the plant cell (Figure 5). This hypothetical model describes the growth of glycosidic chains and the catalytic role of the main enzymes. According to this model, the polymerization of glucose is provided by an enzyme system whose main family is named *cellulose synthase* (CS), which cannot function without the presence of another class of enzymes called *sucrose synthase* (SUSY). SUSY hydrolyzes sucrose to fructose by creating a UDP-glucose (uridine diphosphate-glucose) unit and it is within the CS that the UDP-glucose unit initiates the polymerization process by loss of the UDP (uridine diphosphate) unit and dimerization of glucose. Afther that, the growing chains are secreted via a pore (CSC subunit) and the crystallization event is brought about by a protein, the top subunit, which should facilitate alignment of the chains to promote precise crystallization into metastable cellulose I.

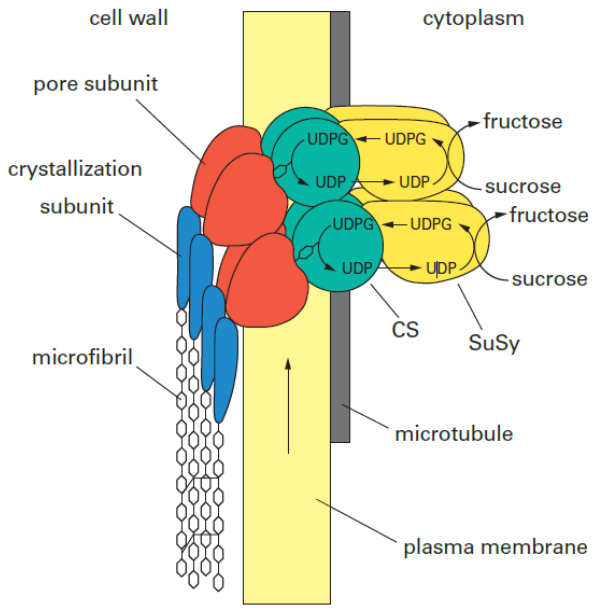

Figure 5 – The Hypothetical Model of a Cellulose Synthase Complex in the Plasma Membrane (Delmer & Amor, 1995). A microfibril is synthesized via a multisubunit complex, with one unit of the complex responsible for the polymerization, secretion, and alignment of each glucan chain. For simplicity, the number of such units shown here in the complex and the number of chains formed are less than that expected in nature. This model should be considered purely speculative and is a composite derived from studies done with a variety of organisms, including bacteria, algae, and higher plants.

CSCs are often called the terminal complexes (TCs), due to their association with one end of microfibrils (collections of celulose chains) (Li *et al.*, 2014; O'Sullivan, 1997). By microdiffraction investigation of nascent bacterial cellulose microfibrils Koyama *et al.* (1997) showed that the reducing end of the growing cellulose chains points away from the bacterium, providing evidence that polymerization takes place at the non-reducing end of the growing cellulose chains. Thus the non-reducing end is tightly associated with the catalytic region of TCs. TCs are made up of many identical subunits organized into specific geometrical arrangement, in which each subunit contains multiple catalytic sites for glucan chain polymerization (Moon *et al.*, 2011). Although significant progress has been made in understanding the structure and regulation of CSCs, many fundamental aspects remain to be addressed (Li *et al.*, 2014).

Multiple glucan chains are processively polymerized by the TCs and immediately assemble to form the supramolecular structures with parallel arrangement of glucan chains. This requires that the newly synthesized glucan chains (*i.e.* the growing chains within the TCs) align in a parallel way to each other and pack into a specific crystalline arrangement (cellulose I), otherwise they would fold into the more thermodynamically stable cellulose II or simply exist as non-crystalline cellulose. Hence, although polymerization and crystallization are separate events, it is believed that crystallization follows very closely the polymerization in a way that allows the enzyme complex to govern the crystalline form of the microfibril (Li *et al.*, 2014; O'Sullivan, 1997; Saxena & Brown, 2005).

Cousins & Brown (1995) have proposed a general four-stage model to describe the microfibril formation from glucose monomers (Figure 6). The first stage is the enzymatic polymerization of glucan chains from glucose monomers (Figure 6, step 1). Just after the extrusion of the glucan chains from the enzyme's catalytic site in TCs subunit, the second stage consists in the self-assembly of the chains via van der Waals forces which act perperdicularly to the main planes of the glucopyranose rings to produce a ''minisheet'' of cellulose chains parallely stacked (Figure 6, step 2). In the next step, as the "minisheets" pass from the interior of the enzyme complex subunit to the true exterior of the cell, these cellulose "minisheets" are held together side-by-side through hydrogen bonds to form elementary fibrils, also known as nanofibrils, where highly ordered regions (the crystallites) alternate with less organized ones (amorphous regions) (Figure 6, step 3). In the last stage the elementary fibrils from different TC subunits join together into

either micro or macrofibrils (Figure 6, step 4), depending on the organism (Dufresne, 2012; Moon *et al.* 2011; Cousins & Brown, 1995; Saxena & Brown, 2005).

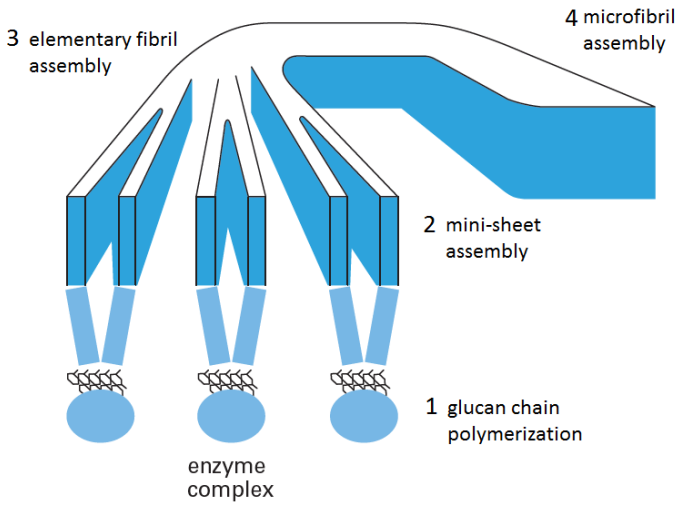

Figure 6 – A general proposed model for the stages of microfibril formation during celulose biosynthesis: (1) glucose monomers are polymerized enzymatically from catalytic sites in the enzyme complex subunits to form glucan chains; (2) the glucan chains associate via van der Waals forces to form mini-sheets; (3) minisheets associate and hydrogen bond to form elementary fibrils; (4) several minicrystals then associate to form a microfibril. Figure adapted from Cousins & Brown (1995).

The geometrical configuration and the number of catalytic sites of the subunits within the TC, both of which vary between organisms (Figure 7), dictate the aggregation process, and thus the resulting supramolecular cellulose structure.

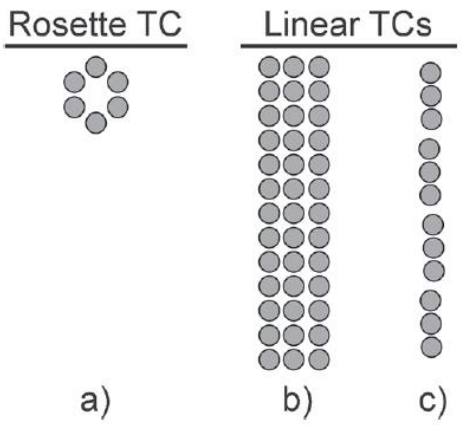

Figure 7 – Schematics of rosette and linear TCs, for (a) wood (6 chains/subunit), (b) green algae (Valonia) (10–12 chains/subunit), and (c) bacterial (Acetobacter) (16 chains/subunit). Each dark circle represents a single subunit. Adapted from Moon *et al.* (2011).

So, the cellulose biosynthesis is highly specific to the organism producing the cellulose. For example, in trees and plants the TC is proposed to be organized of 6 identical subunits in hexagonal symmetry, known as rosette structure, with each subunit composed of 6 catalytic sites for cellulose chain polymerization, so each TC subunit produces a linear "minisheet" of 6 cellulose chains. From a single TC, the assembly of 6 "minisheets" results in cellulose elementary fibril with 36 cellulose chains, a square cross-section ~3–5 nm in size and contains both crystalline and amorphous regions (Moon *et al.* 2011). These elementary fibrils or nanofibrils are guessed to be the basic building block of cellulose. Then multiple elementary fibrils are brought together into larger units called microfibrils with a diameter of ~20-30 nm and length of several micrometers (many times larger than the cross-section).

Figure 8 shows schematically these different stages of the formation of a wood microfibril. In wood, there are non-cellulosic constituents that are in close contact with cellulose in cell wall and they are thought to be involved in the bundling of cellulose microfibrils (Figure 8). Unlike cellulose, neither of these non-cellulosic constituents is manufactured directly in the cell wall, but both follow the more traditional intracellular synthesis followed by secretion. So, the inter-fibril space within a microfibril (*viz.* the space between the elementary fibrils or bundles of elementary fibrils within a microfibril) is filled with different proportions and kind of hemicelluloses, while the microfibril is wrapped with lignin. Thus, microfibril is essentially a natural composite material consisting of elementary fibrils embedded in a matrix of other cell wall compounds, mostly hemicelluloses and lignin (Chen, 2014; Ding *et al.*, 2014; Nishiyama, 2009).

It is worth mentioning that each microfibril in wood may contain multiple elementary fibrils, plus variable amounts and kinds of non-cellulosic matrix; hence the microfibrils can appear dramatically different in size and composition according to: cell wall, cell type, celulose-producing specie, state of cell differentiation of the plant *etc*.

Owing to this inhomogeneous nature, the small size (which represent a real challenge to the limited resolution of the characterization techniques used), the close relationship with other cell wall constituents and the tendency to tightly associate with each other in the cell wall the exact features of wood microfibril are still poorly understood (or has not been up to now fully elucidated), though wood represents the largest source of celulose (Ding *et al.*, 2014; Nishiyama 2009).

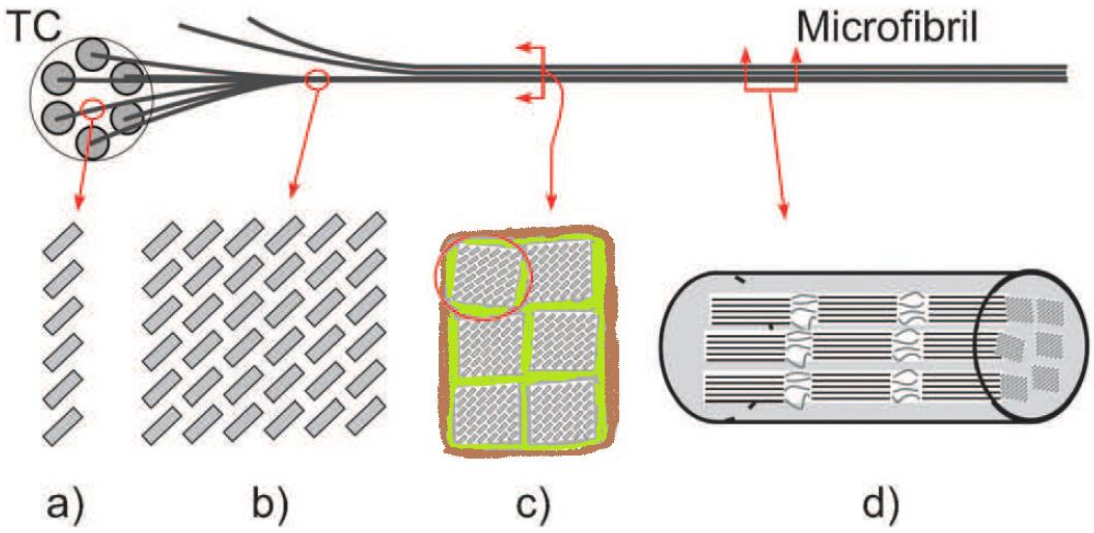

Figure 8 – Schematic of the different levels of the formation of a wood microfibril (adapted from Moon *et al.* 2011). (a) minisheet cross-section believed to form from a single subunit, in which van der Waals forces hold the cellulose chains together. Each grey box represents a cellulose chain looking down the chain-axis. (b) elementary fibril cross-section, the assembly of 6 minisheets into a cellulose crystal I lattice of ~3–5 nm dimensions. The consolidation of multiple elementary fibrils (the basic building block of cellulose) forms a microfibril, (c) microfibril cross-section composed of 6 elementary fibrils (according to the modified Frey-Wysling model) embedded in a matrix of other cell wall compounds, mostly hemicellulose and lignin (representend in green and brown, respectively), (d) microfibril lateral section showing the series configuration of crystalline and amorphous regions of elementary fibrils.

In view of the inequality in size, many terminologies including elementary fibril, protofibril, nanofibril, fibril, microfibril, mini-crystal, microfibril bundle, macrofibril, have been used to describe the fibrillar celulose entities. Sometimes it generates confusion, because different authors use the term in different ways. There are diverse models and structural concepts for fibrillar structure of cellulose based on different observation and scientific environments, some of them facing counter evidence but still persisting in the literature. Thus, there appears to be no agreement as to the size and nature of microfibrils, perhaps due to a dependence of cellulose structure on the sample source (Nishiyama 2009; O'Sullivan, 1997). These models differ mainly in the description of the organization and the distribution of the amorphous or less ordered regions within the microfibril. After many years of controversy, it is common practice to acknowledge that the amorphous regions are distributed as chain dislocations on segments along the elementary fibril where the microfibrils are distorted by internal strain in the fiber and proceed to tilt and twist (Habibi *et al.*, 2010).

Although the catalytic domains of celulose synthases are conserved for all cellulose-synthesizing organisms, the drastic differences in both the lifestyle of the organisms and the structure of the cellulose that they produce suggest that the regulatory proteins and the underlying mechanisms for celulose synthesis may have evolved independently (Li *et al.*, 2014).

The simplicity in the chemical structure of cellulose belies the complexities that are associated with the synthesis and assembly of this polysaccharide. Detailed descriptions of cellulose biosynthesis can be found in Festucci-buselli *et al.* (2007), Li *et al.* (2014) and Saxena & Brown (2005). Despite the recent advances using a combination of molecular genetics, live cell imaging, and spectroscopic tools, many aspects of the celulose biosynthesis are still not well understood (conjectural). Thus, there is problaby no biochemical pathway in plants that is both so important and so poorly understood at the molecular level as cellulose biosynthesis.

2.4. Cellulose microfibrils and hierarchical organization of plant fibers

Fiber is a generic term referring to material that has a length (that is long axis) many times greater than its diameter (most often 100 times greater in length than in diameter). For these materials the ratio between the length (L) and the diameter (D) (*i.e.* fiber length divided by diameter), known as aspect ratio (L/D), is normally greater than 100. They are usually circular or nearly circular and are significantly stronger in the longer direction. Due to the strength and stiffness of fibers, they are the predominantly used reinforcements for advanced composites (Campbell, 2010).

The fibers are classified according to their origin, which can be natural, artificial or synthetic. Specifically, the natural fibers can be divided into three groups: plant fibers, animal fibers and mineral fibers. Plant fibers are examples of complex systems developed by nature. Owing to their roles in the biological universe and to industrial applications, plant fibers are biodegradable materials of great importance today. Due to their unique structure the plant fibers can be considered as naturally occurring composites, in which the semicrystalline cellulose microfibrils act as reinforcing elements to a relatively amorphous matrix mostly made up of lignin and hemicellulose. While the matrix (lignin and hemicellulose) acts as a natural barrier to microbial degradation and serves as mechanical protection, the cellulose microfibrils have the function to provide rigidity and structural stability to the cell wall of the fibers (Célino *et al.*, 2013; John & Thomas, 2008; Silva *et al.*, 2009a). Plant fibers consist therefore of cellulose microfibrils aggregate.

The plant fibers are essentially composed of cellulose, hemicelluloses (or polyoses) and lignin. So, plant fibers are often called lignocellulosic fibers. However, besides these components, plant fibers also contain pectins, extractives, waxes and minerals *etc*. The proportion of plant fiber constituents depends on parameters like botanical origin, maturation time, climatic conditions, age of the plant *etc* (Célino *et al.*, 2013; John & Thomas, 2008; Silva *et al.*, 2009a).

Hemicelluloses are not a form of cellulose, but are short chain, amorphous polysaccharides with 500–3000 monomer units with acidic groups. They include xyloglucans, xylans, glucomannans and galactoglucomannans. Their composition and structure are reviewed in Ebringerova *et al.* (2005). Lignin is an amorphous, complex phenolic macromolecule; the biosynthesis and structure of lignin are discussed in detail by Boerjan *et al.* (2003). Pectins are a group of polysaccharides rich in galacturonic acid units; for review on their composition and structure, see Brejnholt (2010).

From a structural point of view, plant fibers are multicellular in nature and consist of bundles of elongated mostly cylindrical honeycomb cells which have different sizes, shapes and arrangements depending on the source of the plant fiber (Dufresne, 2012). Fibers may occur in almost any part of a plant: stems, leaves, fruits, seeds, *etc*. Their primary function is to provide mechanical support to the plants, although fibers in some species also participate in water transport.

As can be seen in Figure 9, the cell wall in a fiber is not a homogenous membrane. In general, the wall of each individual cell is divided in primary wall (P) and secondary wall (S). Primary and secondary walls differ in the arrangement of the cellulose microfibrils. The former is the thin outer layer of the cell, is less ordered and essentially composed of cellulose microfibrils running in all directions (randomly orientated) within the plane of the wall. In the secondary cell wall, which represents about 90% of the total thickness of the cell wall, the cellulose chains are grouped in microfibrils which are parallel, giving a more densely packed arrangement, and are aligned more or less with the fiber axis. Depending on the cellulose-producing organism these microfibrils are often further associated in bundles or macrofibrils. These two “types” of cell wall also differ in function and in composition. Primary walls surround growing and dividing plant cells. These walls provide mechanical strength but must also expand to allow the cell to grow and divide. The much thicker and stronger secondary wall, which accounts for most of the carbohydrate in biomass, is deposited once the cell has ceased to grow. The cell starts producing the secondary cell wall after the primary cell wall is complete and the cell has

stopped expanding (Monica *et al.*, 2009; O'Sullivan, 1997; Ramos, 2003, Silva *et al.*, 2009a).

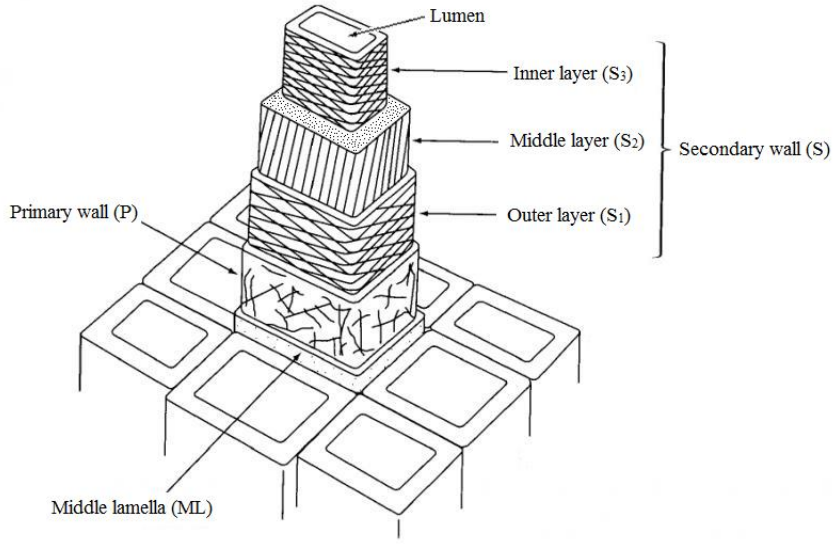

Figure 9 – Ilustration of the plant cell wall made up primary layer and secondary layers (S1, S2 and S3), with the volume fraction and orientation of cellulose microfibrils varying in each layer. Neighbouring cells are attached to each other by the middle lamella. Adapted from Dinwoodie (1975).

The secondary wall can be subdivided into three distinct layers: inner layer (S3), middle layer (S2), and outer layer (S1) (Figure 9). These different layers have differences in composition, thickness, structure, microfibrillar angle (the angle between the fiber axis and the cellulose microfibrils), and so on. The central middle layer (S2) may contribute as much as 70–80% of the total cell wall. This thickest layer contains the main quantity of cellulose and thus the fiber properties certainly are largely governed by the feature of this layer, including the mechanical properties of the fiber. Within this layer the microfibrils are aligned parallel and packed densely in a flat helix. The middle lamella (ML) is the region between the cells and due to its high content of lignin the ML binds the neighboring cells, like a cementing agent or adhesive. The cells surround a central cavity called lumen. (Célino *et al.*, 2013; Dufresne, 2012; Monica *et al.*, 2009; Ramos, 2003, Silva *et al.*, 2009a).

The structure, microfibrillar angle, cell dimensions, defects, and the chemical composition of fibers are the most important variables that determine the overall properties of the fibers. Generally, the tensile strength and the Young's modulus of the fiber increase with increasing cellulose content. The microfibrillar angle determines the stiffness of the fibers. Plant fibers are more ductile if the microfibrils have a spiral

orientation to the fiber axis. If the microfibrils are oriented parallel to the fiber axis, the fibers will be rigid, inflexible and have high tensile strength. Lastly, the properties of natural fibers vary largely depending on the processing method used to break down the lignocellulosic material to the fiber level. The world-wide most important plant fibers used today are: sugarcane bagasse, bamboo, cotton, flax, jute, curaua, sisal and wood fibers (Thomas & Pothan, 2008).

Therefore, in nature, cellulose occurs as a slender rod-like or threadlike entity, formed during biosyntesis. This entity is called the microfibril (collection of cellulose chains) and it forms the basic structural unit of the plant cell wall. Each microfibril can be considered as a string of cellulose crystallites, linked along the chain axis by amorphous domains. They are biosynthesized by enzymes and deposited in a continuous fashion. Their structure consists of a predominantly crystalline cellulose core. This is covered with a sheath of paracrystalline polyglucosan material surrounded by hemicelluloses (Dufresne, 2012). Figure 10 represents the hierarchical organization of cellulose molecules in the cell wall in the form of microfibrils within the wood fibers.

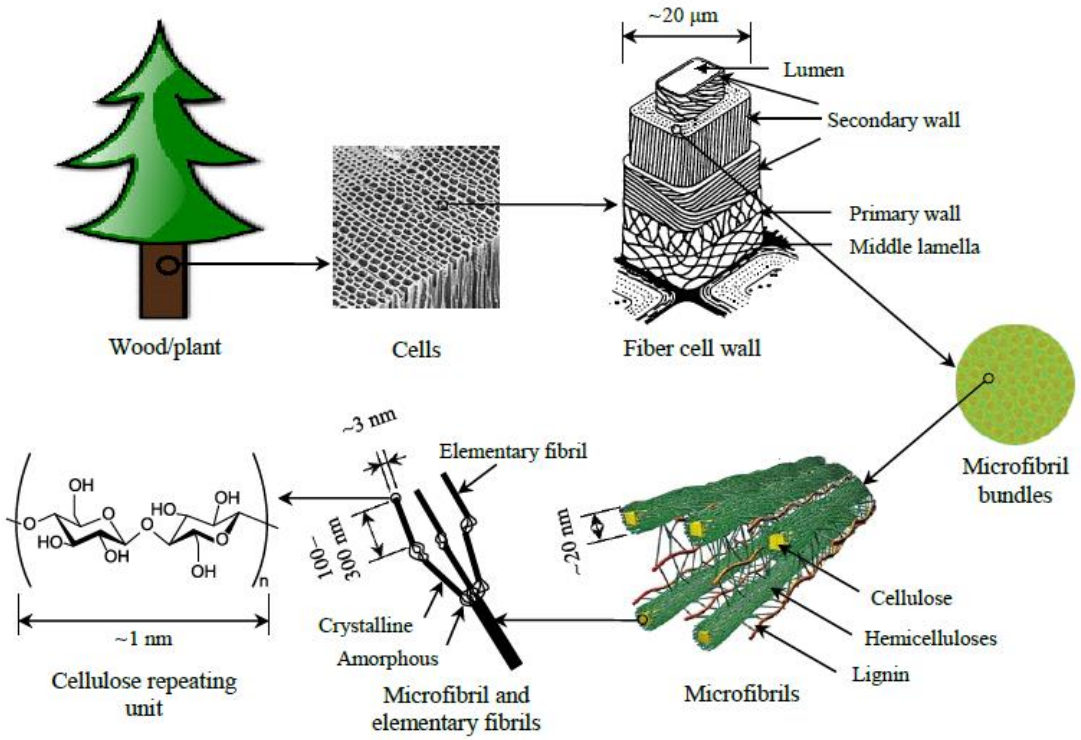

Figure 10 – Schematic diagram for the hieralchical structure: from tree to cellulose (adpted from Fengel &Wegener 1989; and Ritter 2008).

3. SEMICRYSTALLINE NATURE OF CELLULOSE

As might be expected, the many hydroxyl groups readily available for hydrogen bonding associated to "extended" chain structure of cellulose macromolecule causes the chains, or part of them, to become sufficiently aligned parallel to each other forming a compact packing that gives rise to three-dimensional highly ordered structures (crytal-like) of long-range, *viz.* order extending to distances of hundreds or thousands of times the molecular size of the repeating unit. However, seeing that the chains are usually longer than these crystalline regions, they are thought to pass through several different crystalline regions which have less-ordered areas in between them. These less-ordered regions are also frequently referred to as amorphous or non-crystalline regions. Unlike the crystalline region, the cellulose chains in the amorphous region are arranged irregularly and loosely, so the distance between molecules is larger. The amorphous state is thus characterized by an absence of long-range ordering and greater orientation disorder of cellulose chains. Accordingly, cellulose microfibrils are said to be semicrystalline materials, because ordered regions characterized by a long-range regular spatial arrangement coexist with disordered regions typical of the amorphous state.

It must be emphasized that polymers are often referred to as crystalline, but, unlike ionic crystals and metals, in crystals of polymers, the arrangement of atoms is not perfectly regular as in ideal crystals and considerable disorder can be included. On one hand, this may be due to the presence of microstructural defects of constitution, configuration and conformation in the single macromolecules, which may be included in the crystals. On the other hand, it may be also a consequence of the inability of the polymer chains to completely disentangle and line up properly owing to the long-chain nature and subsequent entanglements. Since these requirements are not completely satisfied, crystals of polymers are very far from the ideality, and thus structural disorder inside polymer crystals is a rule rather than an exception. So, the main characteristic of polymeric materials is that, unlike other crystalline materials, they are never totally crystalline but are semicrystalline (de Rosa & Auriemma, 2013; Sperling, 2005). By the way, the term "configuration" refers to the geometrical organization of the atoms along the chain that is determined by chemical bonds; while the term "conformation" denotes the spatial arrangement of the atoms and substituents of a polymer chain that arises from the simple rotation about single bonds. Different conformations are obtained simply by rotation around the single primary bonds. Unlike the conformation, the configuration of a polymer chain cannot be altered without breaking chemical bonds.

Several others studies carried out at the sub-microscopic scale emphasized the discontinuous character of microfibrils (*i.e.* the biphasic nature of its structure). Experimental evidence was provided by wide angle (Fink *et al.*, 1987) and small angle X-ray diffraction (Grigoriew & Chmielewski, 1998), solid state ^{13}C NMR (nuclear magnetic resonance) experiments (Earl and VanderHart, 1981), and tensile tests performed on cellulose fibers (Ishikawa *et al.*, 1997). As mentioned in the previous section on cellulose biosynthesis, the crystallization follows very closely the polymerization of glucopyranose residues in a way that allows the present proteins of the TCs to govern the microfibril crystalline form. Analogously to Figure 8d, a simplified view of the organization of crystalline and amorphous domains in cellulose microfiber is shown in Figure 11. Thus, as a basic rule, microfibrils can be considered as a slender rod-like element composed of highly ordered regions (the cellulose crystals) linked along the fiber axis by less organized ones.

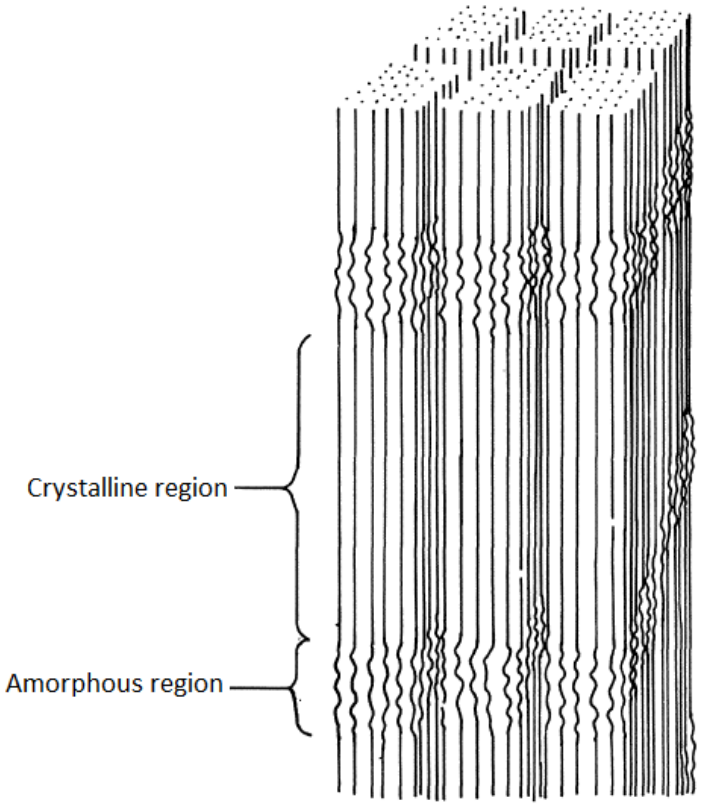

Figure 11 – Possible microstructure of cellulose microfibrils showing the highly ordered regions (the crystallites) that alternate with less organized ones according to the traditional two-phase model system.

The secondary interactions (*i.e.* non-covalent interactions) such as van der Waals and hydrogen bonds are intrinsically related to the cohesion between cellulose chains and

their strong tendency to crystallize. But, considering that these hydrogen bonds in cellulose have strength on the order of ~20-40 kJ/mol and are significantly stronger than van der Waals forces which have strength of ~2-25 kJ/mol, these hydrogen bonds are thought to be the main responsible to the interchain cohesion, and therefore, to the formation of the crystalline domains in cellulose (Belgacem & Pizzi, 2016; Krassig, 1993).

Thermodynamically, the crystal formation can be explained by the balance between entropy and enthalpy effects during the packing of cellulose chains. According to Qian *et al.* (2005) the hydrogen bonds are stronger in the cellulose crystal in comparison to the single chains or sheets. This indicates that during the packing of the chains, the –OH groups are closer. In that situation there is a loss in the conformational degree of freedom of the molecules, causing the formation of hydrogen bonds as compensation. The formation of bonds is an exothermic process ($\Delta H < 0$) that causes a decrease in enthalpy and this can compensate the rigidity and decrease of the entropy. It can keep the system stable with a negative overall energy ($\Delta G < 0$). As expected by the Gibbs equation (Equation 1) (Qian *et al.*, 2005; Mariano, 2016).

$$\Delta G = \Delta H - T\Delta S \qquad \text{Eq. (1)}$$

Conversely, also according to Qian *et al.* (2005) the crystal size is able to increase by the deposition of new monomers, but after some point the hydrogen bonds can no longer compensate these effects. At this time, the system will be dominated by the entropy effects, causing disorder. This can explain the periodic nature of the distribution of the amorphous zones in the cellulose supramolecular structure that can be observed in Figure 11. This periodic nature of the distribution of disordered regions along ramie microfibrils was demonstrated by Nishiyama *et al.*, (2003) using small angle neutron diffraction. A periodicity of about 150 nm was found, corresponding to the sizes estimated by diffraction of hydrolyzed microfibrils. Earlier, it has been believed that disordered chains are located primarily on the surface of microfibrils (Kovalenko, 2010).

In view of the fact that in the crystalline site the hydrogen bonds are stronger and more numerous in comparison to non-crystalline one, the physical and mechanical properties of the crystalline and non-crystalline phase can be different. For instance, properties such as elastic modulus and density and are higher for crystalline zones than for non-crystalline ones (Sinko *et al.*, 2013; Kulasinski *et al.* 2014). In particular, the mechanical properties have been found to be substantially distinct. While the chain

molecules in the disordered regions contribute to the flexibility and the plasticity of the bulk material, those in the ordered regions contribute to the stiffness and elasticity of the material (Dufresne, 2012).

Concerning these mechanical properties, there are several modeling studies that are concerned with the contribution of hydrogen bonding to the stiffness of the cellulose chain (Wohlert *et al.*, 2012). By removing the hydrogen bonds from the computational model Eichhorn & Davies (2006) noted a decrease in elastic modulus in the chain direction by 15%, while Tashiro & Kobayashi (1991) calculated the contribution to 40%. Kroon-Batenburg *et al.* (1986) and, more recently, Cintrón *et al.* (2011) obtained values as high as 55–60%. These studies were carried out considering the crystalline structure of cellulose Iβ and are able to highlight the importance of the hydrogen bonds on mechanical properties.

The degree of crystallinity of polymers can be defined as the fraction of a polymer that is occupied in the crystalline region, being often expressed in percentage. The degree of crystallinity of cellulose microfibrils depends on their origin and also on the processing method used to obtain the microfibril, *e.g.* the percentage of crystalline domains in cellulose isolated from softwood ranges from 40 to 60%, whereas the percentage of ordered chains in cellulose from bacteria and algae are typically higher, reaching values greater than 80%. Thus, the degree of crystallinity definitely has a great practical importance, since the physical and mechanical properties of the fiber-like cellulose structure are directly related to its value.

Except physical and mechanical properties, also the physico-chemical behavior of the crystalline and non-crystalline domains is distinct, hence the physico-chemical behavior of cellulose is strongly related to its degree of crystallinity influencing directly the accessibility for chemical derivatization, swelling, water-binding *etc*. Therefore, the degree of crystallinity is a very important property which needs to be taken into account when considering the manufacturing and applications of cellulose and cellulosic materials (Schenzel *et al.*, 2005).

The degree of crystallinity of cellulose can be measured by several different techniques including wide-angle X-ray scattering, solid-state ^{13}C NMR, Fourier transform infrared spectroscopy and Raman spectroscopy. Even though results from different techniques show a good correlation, the values obtained for the degree of crystallinity can vary significantly depending on the technique used and also the data analysis method applied (Park *et al.*, 2009; 2010).

Other important distinct feature between the crystalline and non-crystalline phase is the rotational conformation of the hydroxymethyl group (see Figure 4). The *tg* conformation is characteristic for the crystal structure of native cellulose, called cellulose I. *gt* is characteristic for regenerated or mercerized cellulose crystals, cellulose II. *gg* is found, together with *gt* and *tg*, in non-ordered regions (Habibi *et al.*, 2010; Nishiyama *et al.*, 2002; O'Sullivan, 1997).

The two-phase model is very sucessful to describe the property of semicrystalline polymers in general, however, this two-phase model considering only the crystalline and amorphous phase is a simplified view. Polymers consist, indeed, of various regions, each with a characteristic degree of internal order, ranging continuously from something close to the ideal crystalline state to the completely amorphous state. In the highly crystalline regions, the arrangement of atoms or molecules is not always perfectly regular, and even in amorphous regions, there are often areas in which the molecules are roughly parallel with an arrangement close to that of crystals (De Rosa & Auriemma, 2013; Sperling, 2005).

Whereas the crystalline cellulose is relatively well understood, there are numerous aspects pertaining to the structure and properties of amorphous cellulose that are less understood (Kulasinski *et al.*, 2014). It is probably associated to the current knowledge on the amorphous state of polymers in general, which remains very incomplete at this time (Sperling, 2005). For instance one interesting question from the point of view of fundamental understanding of the properties of cellulose, is whether the amorphous regions of cellulose microfibril are paracrystalline or fully amorphous. Indeed the amorphous portions within a cellulose microfibril may not be fully disordered but may rather behave like bundles of nearly parallel chain which are not well enough oriented to give a long-range highly ordered three-dimensional structure, but these amorphous regions of cellulose may contains some residual order chacaterized by short-range interactions. These amorphous regions with some residual order are known as paracrystalline domains. Kulasinski *et al.* (2014) in a recent study provided evidence in support of, and consistent with, the hypothesis of the existence of this paracystalline interphase which has intermediate mechanical properties between the crystalline and fully amorphous phases in wood microfibrils.

Apart from the dependency on the degree of crystallinity, the physical and mechanical properties of polymer materials also are strongly influenced by the crystalline structure and morphology. "Crystalline structure" refers to the way in which the chains,

in a particular conformation, are packed, giving rise to the regular three-dimensional structure, while "crystalline morphology" refers to the size and shape of the crystallites, their arrangement, and their interconnection with the amorphous phase.

3.1. Cellulose crystal structure and cellulose Polymorphs

Broadly speaking, in the context of chemistry, polymorphism is an inherent property of the solid state in which the solid phase of a given chemical compound can exhibit different crystal structures which, although possessing the same chemical composition, may manifest different properties. Each distinct form of the crystal structure for a given compound is called a polymorph or allomorph and they have a different arrangement and/or conformation of the molecules in the crystal lattice. The word polymorphism comes from a Greek word. The term "*poly*" means "many" and "*morph*" means "form or shape", so the word polymorphism can be translated to many forms. The investigation of crystal forms impacts on fundamental science as well as on utilitarian objectives because different polymorphs may display a range of different properties (*e.g.* density, solubility, melting point, free energy, rate of dissolution, tensile strength and tabeling *etc*), which may affect application and utilization of the solid materials (Bernstein, 2002).

Polymorphism is quite common for crystals of organic compounds whose molecules contain groups capable of hydrogen bonding (Bernstein, 2002). The repeating unit of cellulose, or cellobiose, includes six hydroxyl groups and three oxygen atoms. Therefore, the presence of six hydrogen bond donors and nine hydrogen bond acceptors provides several possibilities for forming various hydrogen bond systems. Due to different mutual arrangements of the glucopyranose rings and possibility of conformational changes of the hydroxymethyl groups, cellulose chains can exhibit different crystal packings (Kovalenko, 2010). As a result, cellulose has several polymorphs, namely cellulose I, II, III and IV and their varieties Iα, Iβ, III_I, IV_I, III_{II} and IV_{II}. Most of these polymorphs result from chemical treatments of polymorph I. These polymorphs differ by packing (*i.e.* unit cell parameters) and polarity of the constituting chains, as well as the hydrogen bond patterns established between them (Wada *et al.*, 2008). The first structural model was suggested in 1937 by Meyer and Misch (Meyer & Misch, 1937). Since then considerable progress has been made in elucidating the crystal structures of cellulose. However, on account of the structural variety of cellulose, the structural properties continue to be under intensive characterisation and there are still

many open questions. The possible transitions between the different cellulose polymorphs are presented schematically in Figure 12 (Dufresne, 2012). This review focuses on the Cellulose I and II structures.

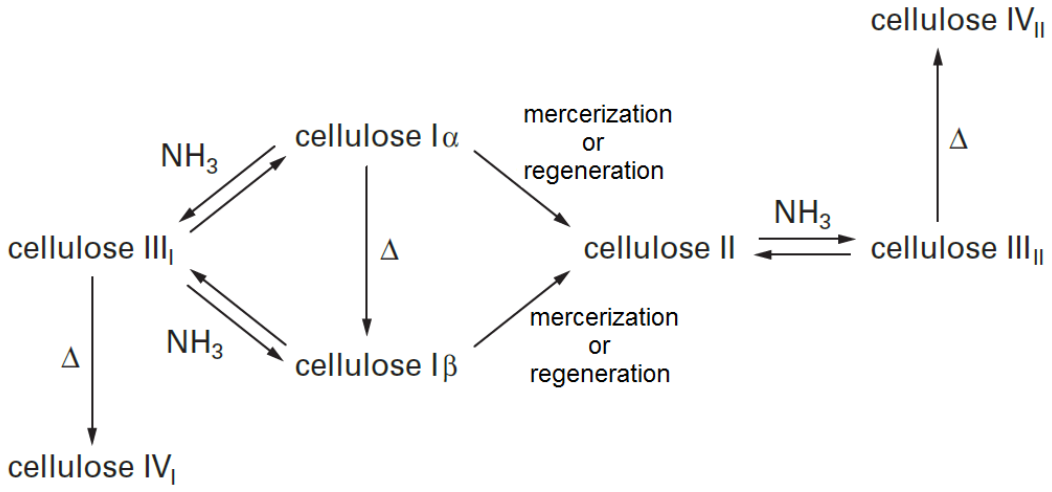

Figure 12 – Possible interconversions of cellulose polymorphs. Adapted from Dufresne (2012).

Cellulose I is the most abundant polymorph in nature. That is why it is known as native cellulose and it is the focus of major studies in the area. In 1984, Atalla and Vanderhart by high-resolution solid-state ^{13}C NMR spectroscopical studies demonstrated that native cellulose actually consists of two distinct polymorphic forms, namely cellulose Iα and Iβ (Atalla & VanderHart, 1984). These two different crystalline forms of cellulose I can be found alongside each other and the Iα/Iβ ratio depends on the source, *i.e.* origin of the cellulose. The Iα structure is dominant in most algae and bacteria (which are considered as primitive organisms), whereas Iβ is the dominant polymorph in higher plants and in tunicates (Dufresne, 2012; Wada *et al.*, 2008). Nishiyama and co-workers by means of synchrotron X-ray and neutron fiber diffraction have provided the most accurate characterization of the Iα and Iβ lattice structures to date. Cellulose Iα corresponds to a triclinic unit cell, space group *P1*, containing only one chain per unit cell and the unit-cell parameters are a = 0.672 nm, b = 0.596 nm, c = 1.040 nm, α = 118.08°, β = 114.80°, γ = 80.37°. The polymorph Iβ has a monoclinic unit cell, space group $P2_1$, with two chains per unit cell and the unit-cell parameters are a = 0.778 nm, b = 0.820 nm, c = 1.038 nm, α = β = 90°, γ = 96.51° (Nishiyama *et al.*, 2002; 2003b). The Iα and Iβ unit cells are shown in Figure 13b. The characteristic features of the complex hydrogen bond pattern established in each of these polymorphs (Iα and Iβ) and their differences are well discussed by Kovalenko (2010). The Iα phase is considered to be less thermodynamically

stable than the Iβ phase, because it can be irreversibly converted into Iβ by high-temperature annealing at 260 to 280°C in various media, such as organic solvents or helium. However, complete conversion to Iβ is typically not achieved (Dufresne, 2012; Wada *et al.*, 2008; Yamamoto & Horii, 1993).

Despite the differences between Iα and Iβ unit-cell parameters, the shifts in the cellulose chain arrangement are small when viewed along the chain axis (Figure 13a). Three lattice planes with approximate *d*-spacings of 0.39 nm, 0.53 nm, and 0.61 nm are shared and correspond to Iα lattice planes $(110)_{I\alpha}$, $(010)_{I\alpha}$, and $(100)_{I\alpha}$, and Iβ lattice planes $(200)_{I\beta}$, $(110)_{I\beta}$, and $(1\text{-}10)_{I\beta}$, respectively. As the projection perpendicular to the chain axis in the plane of the hydrogen-bonded sheets shows, the main difference between cellulose Iα and Iβ is the relative displacement of sheets (parallel stacking of cellulose chains in one plane) along the $(110)_{I\alpha}$ and $(200)_{I\beta}$ planes (called ‘‘hydrogen-bonded’’ planes) in the chain axis direction (Figure 13c and d). For Iα there is a relative displacement of *c*/4 between each subsequent hydrogen-bonded plane (*i.e.* neighboring sheets), while for Iβ the displacement alternates between *c*/4 and -*c*/4 (Moon *et al.*, 2011). An important common feature for both polymorph Iα and Iβ is that there are no intersheet O–H···O hydrogen bonds and, therefore, the cellulose sheets are held together by only hydrophobic interactions (van der Waals forces) and weak C–H···O hydrogen bonds. So, the most likely route for solid-state conversion of cellulose Iα → Iβ is the relative slippage of the cellulose chains past one another. Such a movement does not require the disruption of the hydrogen-bonded sheets but slippage by *c*/2 at the interface of the sheets (Nishiyama *et al.*, 2003b; Pérez & Mazeau, 2004).

In both phases (Iα and Iβ) the hydroxymethyl groups are oriented in the *tg* conformation and the cellulose chains are arranged in what is called the ‘‘parallel-*up*’’ configuration (Koyama *et al.*, 1997; Nishiyama *et al.*, 2002; 2003b). This parallel-*up* packing in cellulose Iα and Iβ unit cells was experimentally demonstrated by Koyama *et al.* (1997) through a combination of direct-staining the reducing ends of cellulose chains and microdiffraction-tilting electron crystallographic analysis. Since the cellobiose repeat unit has a different structure on either side of the 1–4 linkage, the directionality of the 1-to-4 linkage (1→4 linkage) along the length of the cellulose chain affects how neighboring chains interact with each other. The term ‘‘parallel’’ is used when all the cellulose chains are arranged such that the 1→4 link points in the same direction. In contrast “antiparallel” describes alternating stacking of the cellulose chains in the 1→4 link directionality between different hydrogen bonding planes. The direction of the

cellulose chain 1→4 link with respect to the c-axis of the unit cell is also defined because this alters the interaction between neighboring hydrogen bonding planes (Figure 13a). The ‘‘*up*’’ configuration corresponds to the 1→4 link direction pointing in the positive *c*-axis direction of the unit cell, while the ‘‘*down*’’ configuration the 1→4 link direction pointing in the negative *c*-axis direction (Moon *et al.*, 2011). Note that most of the literature uses a different convention, in which ‘‘*up*’’ versus ‘‘*down*’’ are defined in terms of the relative location of the O5 and C5 atoms along the positive *c*-axis of the unit cell. In the ‘‘*up*’’ configuration, the position of O5 is greater than that of C5, while in the ‘‘*down*’’ configuration the position of O5 is less than that of C5 (Koyama *et al.*, 1997). Both Iα and Iβ have the ‘‘parallel-*up*’’ configuration, thus all cellulose chain segments run parallel along the chain axis and are arranged such that the 1→4 link points in the same direction (Figure 13c, d) and that direction is in the positive *c*-axis direction of their respective crystalline unit cell (Moon *et al.*, 2011).

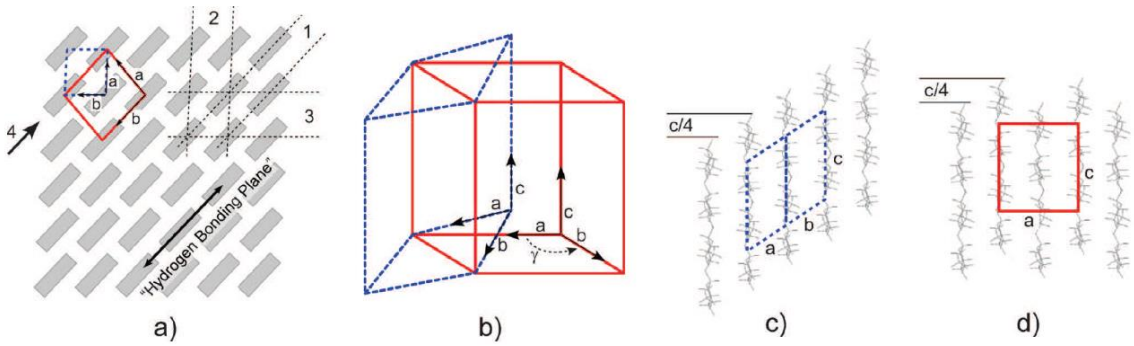

Figure 13 – Schematic of the unit cells for cellulose Iα (triclinic, dashed line) and Iβ (monoclinic, solid line): (a) projection along the chain direction with the Iα and Iβ unit cells superimposed on the cellulose I crystal lattice, showing the parallelogram shape of both unit cells when looking down the *c*-axis. In this orientation both unit cells have nearly identical molecular arrangements, sharing the three major lattice planes, labeled 1, 2, and 3, with the corresponding *d*-spacings of 0.39, 0.53, and 0.61 nm. The corresponding lattice planes for 1, 2, and 3, are $(110)_{I\alpha}$, $(010)_{I\alpha}$, and $(100)_{I\alpha}$, for Iα and $(200)_{I\beta}$, $(110)_{I\beta}$, and $(1\text{-}10)_{I\beta}$ for Iβ. (b–d) View along the direction labeled 4, (b) relative configuration of Iα with respect to Iβ unit cell and the displacement of the hydrogen bonding sheets for (c) Iα of +*c*/4, and for (d) Iβ alternating +*c*/4 and -*c*/4 (from Moon *et al.*, 2011).

Cellulose II is the second most extensively studied allomorph due to its technical relevance. Cellulose II, like cellulose Iβ, has the monoclinic unit cell, space group $P2_1$, containing two chains, but differ in the unit-cell parameters, which are a = 0.801 nm, b = 0.902 nm, c = 1.034 nm, α = β = 90°, γ = 117.11°. Unlike cellulose I which has a parallel-*up* orientation and the hydroxymethyl groups oriented in the *tg* conformation, the chains

in cellulose II are aligned in an antiparallel manner (*up* and *down* directions) with the hydroxymethyl groups near the *gt* conformation (Langan *et al.*, 1999, 2001, 2005). These diferences are regarded as the most significant differences between the cellulose polymorphs I and II. As previously mentioned, the term antiparallel refers to alternating stacking of the cellulose chains in the 1→4 link directionality between different hydrogen bonding planes (Pérez & Mazeau, 2004; Kovalenko, 2010). Recently, Kim *et al.* (2006) using a method of reductive amination, followed by gold labeling, visualized the reducing ends of cellulose I and cellulose II "crystals" by transmission electron microscopy (TEM) showing that the reducing groups are all located at the same end of the chain assembly (parallel arrangement) for cellulose I, while for the mercerized specimen (cellulose II) the reducing groups are alternatively on either side within the assembly (antiparallel arrangement). Owing to this antiparallel directionality of the chains, the polymorph II is often said to be less polar when compared to polymorph I. In effect, though there is a general consensus that the chains are packed in antiparallel mode in cellulose II, this is not unanimously accepted and such question is still raising many debates.

Other notable feature of cellulose II is that during the conversion from polymorph I to II, the exocyclic C_6H_2OH groups rotate from the *tg* to the *gt* conformation so that an inter-residue hydrogen bond is lost. However, new intersheet hydrogen bonds are established. This redistribution of hydrogen bonds is particularly interesting, because it provides a more uniform distribution of the H-bonds connecting all neighboring cellulose molecules and at the same time improves the interlayer attraction forces (*i.e.* the forces involved in the attraction of cellulose sheets to each other). In other words, in cellulose II the absence of the second hydrogen bond along the chain is compensated by the presence of four weak hydrogen bonds between the sheets, and although these new bonds are weaker, their number (four hydrogen bonds per glucopyranose residue) is sufficiently large to have an effect on the properties of this polymorph (Figure 14). Therefore, cellulose I and II possess different properties and advantages over the other, what make the polymorph II preferable for some applications (Langan *et al.*, 1999, 2001, 2005; Pérez & Mazeau, 2004; Kovalenko, 2010, Wada *et al.*, 2008; Yue *et al.*, 2012; Jin *et al.*, 2016).

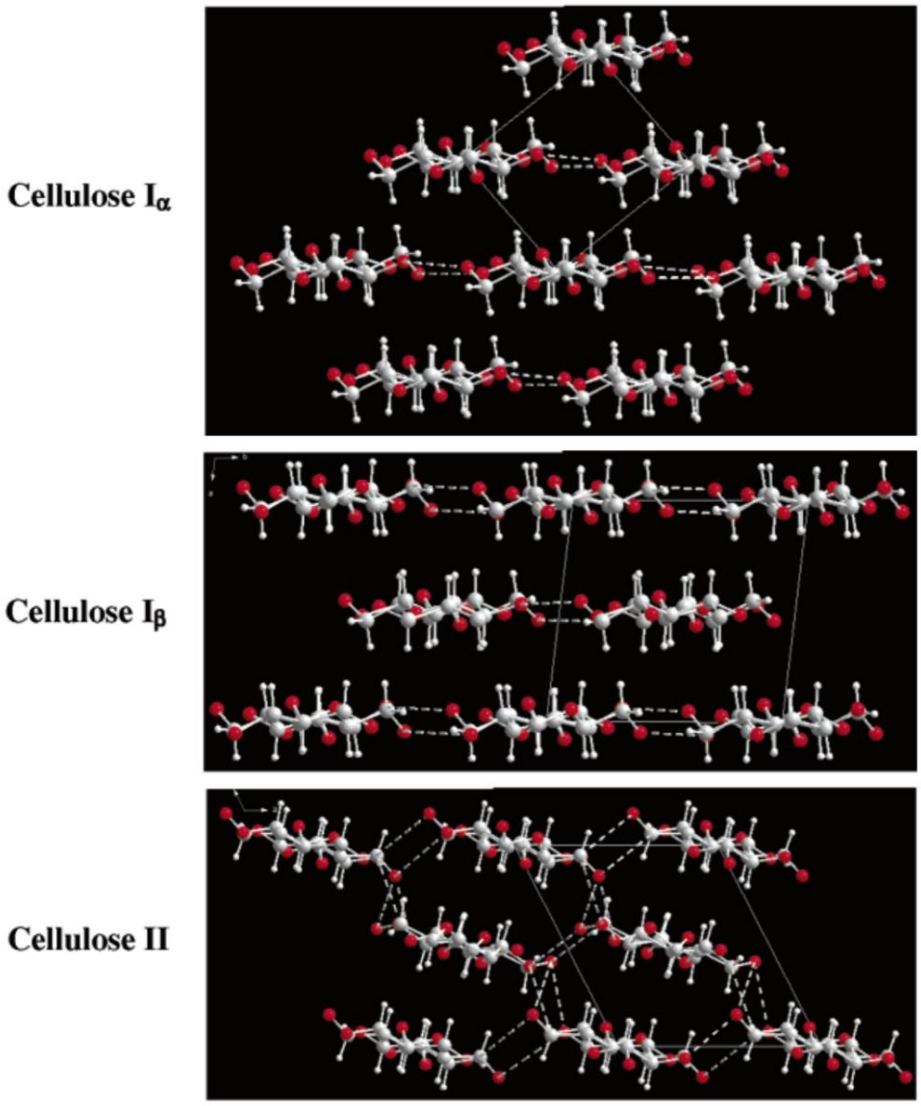

Figure 14 – Schematic projections of the crystal structures of cellulose Iα, Iβ and II down the chain axes directions. C, O, and H atoms are represented as gray, red, and white balls, respectively. Covalent and hydrogen bonds are represented as full and dashed sticks, respectively. Only the major components of hydrogen bonds are represented. Adapted from Wada *et al.* (2004).

The changes in hydrogen bonding network (mentioned above) imparts to cellulose II an additional stability compared to cellulose I, which could explain why it is possible to convert cellulose I to cellulose II, but not in the reverse direction. Thus, the transition from cellulose I to cellulose II is widely considered as irreversible, suggesting that polymorph II is thermodynamically more favorable than polymorph I. A detailed description of the complex hydrogen-bonding system in cellulose II, as well as the comparison with the hydrogen bond network present in cellulose I, is provided by Kovalenko (2010).

Cellulose II can be prepared from native cellulose (cellulose I) by two distinct processes: i) mercerization (alkaline treatment) or ii) regeneration (solubilization followed by recrystallization).

i) Mercerization, a universally recognized process the name of which is derived from its inventor John Mercer, is an essentially solid-state process during which cellulose fibers are swollen in concentrated alkali media and recrystallized into cellulose II upon washing and drying (removal of the swelling agent). The mercerization of cellulose leads only to its swelling, but not to solubilization.

ii) In the process known as regeneration, the native cellulose (polymorph I) is dissolved in a solvent and subsequent reprecipitated by adding a non-solvent, leading the chains to recrystallize into cellulose polymorph II.

Even though the unit cells of cellulose II obtained by these two distinct routes resemble each other closely, small differences have been reported. For example, the values of the *b* parameter in mercerized cellulose from ramie has been quoted as 0.810(3) nm and 0.801(5) nm in the case of regenerated specimen. In addition, the torsion angle χ of the center chain, representing the conformation of the hydroxymethyl group, is +148(6)° and -175(8)° for regenerated and mercerized samples, respectively (Langan *et al.*, 1999, 2001). So, it could be argued whether these different methods of preparation of cellulose II might account for some of the small differences. Facing these small differences reported between the mercerized and regenerated celluloses, which could be negligible on account of the different resolutions of X-ray data utilized, Langan *et al.* (2005) provided experimental data from which it is possible to conclude that these two singular ways for preparing cellulose II lead to essentially identical crystal and molecular structures.

It must be mentioned that cellulose II can, in rare cases, be formed naturally; two examples are that of the marine alga Halicystis (Sisson, 1938) and the gram-positive bacterium Sarcina (Canale-Parola, 1970). Other cases relate to conditions where the normal process of synthesis is perturbed, either by mutation (Kuga et al, 1993) or by addition of the dye Tinopal (Cousins & Brown, 1997), which alters crystal structure and leads to an antiparallel structure. Both are very useful to insights into the crystalline structure and morphology of cellulose II as will be discussed along the next sections.

3.2. Mercerization and regeneration processes

The main difference between these processes is that during regeneration the cellulose is solubilized, while mercerization leads only to its swelling. So, understanding the phenomena of swelling and dissolution can lead to deeper insights into regeneration and mercerization processes. Indeed, swelling and dissolution are two completely different phenomena. Polymer swelling is often defined as a process where the solvent molecules penetrate and labilize the polymer structure to a certain extent, leaving the volume and physical properties of the polymer significantly changed, although the solid or semi-solid state remains. On the other hand, dissolution is a transition from a two-phase system to a one-phase system (clear solution), in which the original supramolecular structure of the polymer is fully destroyed, resulting in a solution where the polymer is, at best, molecularly dispersed. Typically, polymer dissolution is preceded by polymer swelling. However there is no clear-cut borderline between a swelling process and a dissolution process, so that the same system can act either as a swelling agent or as a dissolution agent, depending on the properties of the polymer (cellulose) and operation conditions. In addition, both swelling and dissolution occur from the outside to the inside of the bulk of the polymer, being the kinetics considerably different regarding the amorphous and crystalline zones. Due to the higher free energy, the amorphous regions are preferentially and more easily accessed (Klemm *et al.*, 1998; Medronho & Lindman, 2014; Zhang *et al.*, 2006).

Despite the fact that Mercer introduced the “mercerization” transformation more than 150 years ago, the unraveling of its mechanism remains a question of intense debate and the elucidation of the detailed events that take place during the mercerization is of great interest, especially as the process does not appear to require solubilization of the cellulose chains (Lee *et al.*, 2013; Pérez & Mazeau, 2004). In general terms, the mercerization has been explained as an interdigitation mechanism in which, when sufficient swelling is applied, the cellulose chains from neighboring nanofibrils of opposite polarity would intermingle and recrystallize into the antiparallel mode upon removal of the swelling agent (Kim *et al.*, 2006; Nishiyama *et al.*, 2000; Okano & Sarko, 1985). Therefore, this mechanism apparently consists in a lateral reorganization of chains of opposite polarity from the swollen state.

In the mercerization, the interconversion from cellulose I to cellulose II passes through a kind of intermediary state called alkali-cellulose complex. By means of characterization by X-ray diffraction, evidence for the occurrence of different types of

this intermediary state that could be classified as a function of the cellulose chain conformation has been put forward (Okano & Sarko, 1984). Some studies have been focussed on these various types of alkali-cellulose complexes (Nishimura *et al.*, 1991a, 1991b; Okano & Sarko, 1985; Porro *et al.*, 2007; Schoeck *et al.*, 2007).

According to the literature about mercerization process, in concentrated alkaline solutions the cellulose lose most of their original hydrogen bonds either by polymer-solvent interactions and/or deprotonation of part of their hydroxyl groups, making both the amorphous and crystalline regions swell, increasing the distance between crystallographic planes and simultaneously leading to the formation of alkali-cellulose complexes. In this swollen state, the chains are able to undergo conformational changes without chain solubilization. Upon neutralization of the solution (*i.e.* ion removal), new interactions between hydroxyl groups of adjacent chains are possible and the chains crystallize into cellulose II, which is more thermodynamically favorable. Furthermore, on the morphological level, relevant changes in fibrilar architecture can take place (such as lumen collapse). Under these circumstances, mercerization is widely considered as a solid-phase transition or solid state process. Interestingly, despite the remarkable changes in the supramolecular structure, the gross structure of the cellulose sample as a moiety of particles or fibers or as a film can be largely maintained in the mercerization process (Kleem *et al.* 1998; Lee *et al.*, 2013; Pérez & Mazeau, 2004; Zhang *et al.*, 2006).

The absence of hydrogen bonds between the layers (sheets) explains the possibility of penetration of the sodium ions in the structure of native cellulose to transform it into a new crystalline structure containing these ions, which have the ideal size to fit between the sheets containing the network of hydrogen-bonded parallel cellulose chains (Belgacem & Pizzi, 2016).

It should be underlined that experimentally the conversion from cellulose I to II by the mercerization process depends primarily on the swelling agent system, alkali concentration, ratio of swelling agent to cellulose substract, temperature, time, pH *etc*. Treatment with alkali at a concentration below the transition value provides conditions that are not sufficient for hydroxide ions to penetrate into the cellulose I crystals and therefore no polymorphic transformation takes place.

Typically, mercerization is done in concentrated aqueous sodium hydroxide solutions, although many other swelling agents (such as aqueous solutions of other alkali metal hydroxides *e.g.* lithium, potassium hydroxides; alcohol/water/sodium hydroxide systems in which the alcohol can be metanol, etanol or butanol; or even similar systems

with other solvents instead alcohol) are also able to only swell cellulose and convert native fibers to cellulose II (Habibi *et al.*, 2010; Han *et al.*, 2013; Mansikkamaki *et al.*, 2005; Klemm *et al.*, 2005; Krassig, 1993; Wang *et al.*, 2014).

As already abovementioned, unlike mercerization, in the regeneration process the transiton from cellulose polymorph I to II occurs through cellulose dissolution, in which the original crystalline form of cellulose is expected to be fully destroyed, because to solubilize the polymer the solvent-solute attraction must be stronger than the numerous intermolecular cohesive forces which hold the cellulose chains together. Regarding the dissolution itself, the more consensual vision of experts in the field is that the key factor (and challenging) to dissolve cellulose in a given solvent resides in the solvent ability to break the strong hydrogen bond network. Other interactions among cellulose molecules have been mostly ignored. However, some works recently argued against this accepted picture, they have concluded that cellulose has clear amphiphilic properties and a careful examination of the interactions involved suggests that hydrophobic interactions play a significant role in governing cellulose solubility (Lindman *et al.*, 2010; Medronho *et al.*, 2012; Medronho & Lindman, 2014).

From a thermodynamic point of view the dissolution of a polymer, such as cellulose, in a solvent is, of course, governed by the free energy of mixing. The mixing process will occur spontaneously when the free energy change on mixing is negative. Otherwise, phase separation may result from the mixing process. The polymer molecular weight is a key parameter in dissolution; the higher the molecular weight, the weaker is the entropic driving force contribution for dissolution. Under these conditions, the enthalpy term is crucial in determining the sign of the Gibbs free energy change. One should mention that polymer dissolution is often controlled by kinetics rather than by thermodynamics and cellulose is a very clear example of this. Thermodynamically, a reasonable solvent for cellulose dissolution must be able to overcome the low entropy gain by favorable solvent/polymer interactions (Medronho & Lindman, 2014), *viz.* it is essential that the change in enthalpy be negligible or negative to assure a negative value for the change in free energy.

Reaching molecularly dispersed systems has been challenging for nearly all known solvent systems. Unlike non-polymeric materials, polymers do not dissolve fast, and the dissolution is controlled by either the disentanglement of the polymer chains or by the diffusion of the chains through a boundary layer adjacent to the polymer–solvent interface. The polymer changes then to a disentangled state which allows cellulose chains

to move out of the polymer matrix into the solvent. This process is usually very dependent on the solvent convection around the polymer. Convection acts first by removing pealing polymer chains out of the vicinity of the main polymer particle and bringing new solvent from the bulk. The second effect is to avoid the formation of a viscous polymer layer around the dissolving polymer, which usually hinders the fresh solvent to access the dissolving polymer particle (Medronho & Lindman, 2015; Miller-Chou & Koenig, 2003).

Once solubilized, adding a non-solvent to the system promotes the regeneration of cellulose polymer from solution, *viz.* the regeneration starts when the medium surrounding the cellulose molecules becomes energetically unfavorable for dispersion of individual chains. So, it is thought that the exchange of solvent with non-solvent (*i.e.* the coagulating process) leads to a desolvation of the cellulose molecules and to the supposed reformation of the intra and intermolecular interactions to yield the cellulose II polymorph having antiparallel chain packing. The kinetics of regeneration is mainly controlled by the relative velocities of the counter-diffusion process-diffusion of the solvent from the solution into the coagulation bath and the non-solvent from the bath into the solution (Medronho & Lindman, 2015).

Since regenerated cellulose is the cellulose precipitated from cellulose solutions, the mechanism underlying the structure formation of regenerated cellulose from the solution must be understood in more detail, because this knowledge could be useful to the better control of resulting structure and properties of regenerated cellulose. A three-step hypothetical mechanism for the structural formation of regenerated cellulose from its solution has been proposed as follows: (i) glucopyranose rings are stacked together by hydrophobic interaction with van der Waals forces, and monomolecular sheets are formed; (ii) association of these sheets by hydrogen bonds affords thin planar crystals incorporating amorphous chains; (iii) these structures, which are randomly dispersed in solution, contact and adhere with each other to form three-dimensional structures (Miyamoto *et al.*, 2009). Figure 15 shows schematically these different stages of the probable structural formation of regenerated cellulose in a water environment.

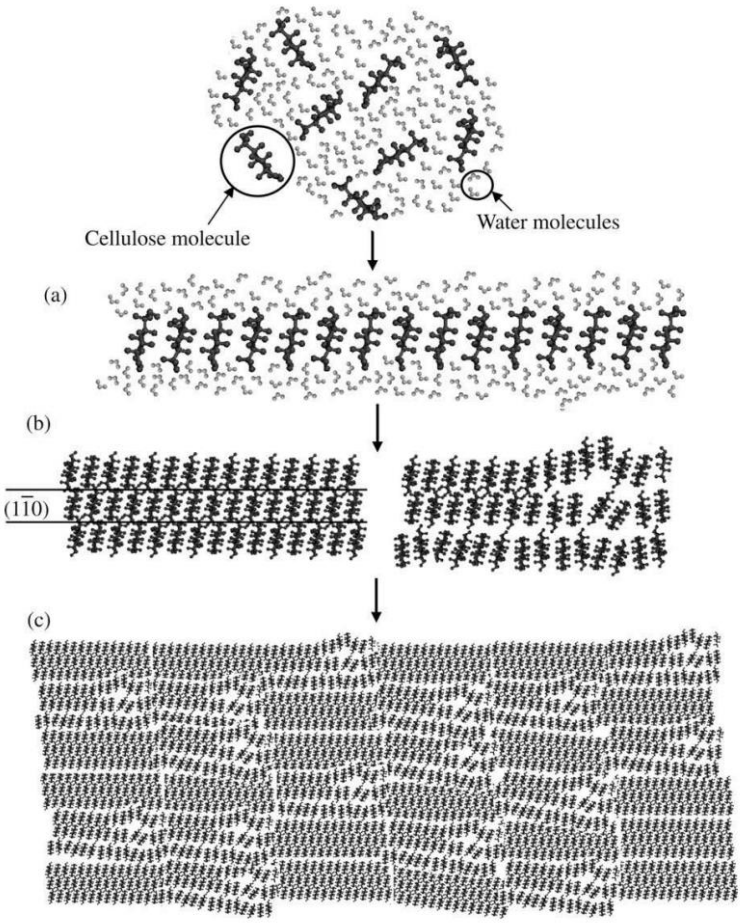

Figure 15 – Schematic model for the structural formation of regenerated cellulose in a water environment: (a) formation of the molecular sheets by van der Waals force; (b) piling up of the molecular sheets by hydrogen bonds to form seeds of crystal and amorphous; (c) contact and sticking together of the structural unites to form regenerated cellulose (Miyamoto *et al.*, 2009).

The existence of molecular sheets packed by hydrophobic interactions has been suggested by many studies. Hermans (1949) and Hayashi *et al.* (1974) separately reported that structural disorders lie mainly in the hydrogen-bonded intermolecular region, and both deduced the molecular sheet structures as a basic feature of regenerated cellulose. This sheet was named as "sheet-like structure" (Hermans) or "plane lattice structure" (Hayashi). In order to identify the initial structure of the cellulose crystal in the course of its regeneration process from solution Miyamoto *et al.* (2009) simulated regeneration of cellulose by molecular dynamics, reproducing hypothesized formation of the molecular sheet-like structure at the early stage. Based on their computer simulation, they stated that, in an aqueous environment, molecular sheets formed by hydrogen bonds changed to van der Waals-associated molecular sheets. Their proposed hypothetical mechanism for the formation of the cellulose crystal II is very similar to those previously theorized by

Cousins & Brown (1995) for polymorph Iβ, who also have indicated from computational calculations that van der Waals-associated molecular sheets formation is most likely to be the first stage in crystallization of cellulose due to the lower potential energy than that of hydrogen-bonded molecular sheets.

Recently, the first experimental evidence of the development of hydrophobically stacked monomolecular sheets at the initial stage of the structure formation of regenerated cellulose was provided in the work of Isobe *et al.* (2012) by means of time resolved synchrotron-radiation X-ray measurements. When the cellulose solution was coagulated using a heat-gap or coagulant, a diffraction peak first appeared at the position corresponding to the molecular period in the molecular sheets packed by hydrophobic interactions, therefore the changes in the X-ray profile indicates that the cellulose molecules first form hydrophobically stacked monomolecular sheets, followed by their mutual association via hydrogen bonding. Thus, this work is in good agreement with the regeneration mechanism previously assigned. Similarly, Yamane *et al.* (2015) also experimentally demonstrated by synchrotron X-ray radiation that the hydrophobically packed molecular sheets were the initial structure from solution. In addition, the dissolution of cellulose in aqueous sodium hydroxide solution was also investigated using the same X-ray diffraction measurement. It was found out that the molecular sheets remain in the dissolving system until the last stage of dissolving and finally disappear when the process is completed. These results indicate that structure formation and dissolution are ‘‘two sides of the same coin’’, *i.e.* they proceed on opposite courses of molecular processing of cellulose. Another important finding in this study was the detection of the trace of the molecular sheets from the non-crystalline region of regenerated cellulose films with low crystallinity, what could be related in some way with the existence of residual order in the amorphous regions as stated in the previous section.

According to Ostlund *et al.* (2013) the properties of regenerated cellulose material can be tuned by the proper choice of the experimental conditions such as temperature and coagulation medium. They reported that coagulation media with different polarity lead to regenerated materials with different morphologies and properties and this can be used to tune the properties of the end material. As the polarity of the coagulant is increased, more ordered (crystalline) materials were obtained, therefore the hydrophobic interactions between the polymer chains during regeneration are governed by the increased polarity of the coagulant. This way, less polar coagulants should yield low crystallinity

regenerated cellulose, because most likely it would prevent the formation of molecular sheets which is the inital stage of the recrystallization.

In practice, finding a non-derivatizing solvent that does not reduce the DP nor does react with the cellulose is one of the most challenging parts in cellulose dissolution. From the traditional viscose route, which is generally a slow process and environmentally hostile (*e.g.* discharge of toxic gases), up to state-of-art ionic liquid systems, several derivatizing and non-derivatizing (aqueous and non- aqueous) solvents, with strikingly unrelated properties, have been developed. The list is vast and includes quite unusual combinations and experimental conditions: simple or multicomponent mixtures, aqueous and organic media, inorganic and organic salts, high and low temperatures, high and low pHs, *etc*.

A few classical examples of non-derivatizing solvents can be mentioned, such as aqueous inorganic complexes (*e.g.*, cuprammonium hydroxide or cupriethylenediamine), concentrated salt solutions (*e.g.*, zinc chloride, ammonium, calcium and sodium thiocyanate solutions), salts dissolved in organic solvents (*e.g.*, lithium chloride/N,N-dimethylacetamide, ammonia/ ammonium salt, tetrabutylammonium fluoride/dimethyl sulfoxide), aqueous alkali (lithium hydroxide or sodium hydroxide solutions), ionic liquids like 1-butyl-3-methyl-imidazolium chloride (BMIMCl) *etc.* A more detailed and updated list can be found elsewhere (Heinze & Koschella, 2005; Liebert, 2009; Medronho & Lindman, 2014, 2015; Olsson & Westman, 2013). Independently of the solvent system used, typically, water is the most suitable coagulation agent.

3.3. Technical relevance of cellulose polymorph II

From an industrial perspective, cellulose II is used to prepare materials such as films (cellophane), textile fibers (rayon, lyocell), membranes for dialysis, filtration and chromatography (Cuprophan), papers (for packaging and printing purposes), pharmaceutical pellets (for drug release), food casing (cekicel) and cellulose derivatives (in particular cellulose ethers and esters) (Gupta *et al.*, 2013; Han *et al.*, 2013; Kleem et al;, 2005 ; Kumar *et al.*, 2002; Liu & Hu, 2008; Miyamoto *et al.*, 2011; 2016; Sasaki *et al.*, 2003). Therefore, cellulose II, produced either by mercerization or regeneration, has applications in several important commercial areas.

3.4. Crystall Orientation and folded-chain structure of cellulose II

The orientation of the chains in the crystal lattice can be defined with respect to the main axis of the fiber. As stated by imaging and diffraction studies in the crystal lattice of cellulose I polymorph the chain axis (*c* axis) is parallel to the long axis of the microfibril. As demonstrated for *Valonia* cellulose, after the conversion from polymorph I to II by mercerization, this orientation is maintained and the molecule axis of the cellulose chain (*c* axis) remains along the fiber axis (Chanzy & Roche, 1976). Needless to say that in the polymorphs I and II the cellulose chains align in a parallel-up and anti-parallel manner (*up* and *down* directions) in relation to the *c* axis, respectively. This orientation is consistent with the conclusions of Kim *et al.* (2006) from electron diffraction data collected on crystals from mercerized ramie cellulose. In contrast to this, some studies carried out with regenerated cellulose have put forward evidence that the chains are arranged perpendicular to the fiber long axis and parallel to their basal plane (Atkins *et al.*, 1979; Buléon &Chanzy, 1978). To illustrate, these findings are depicted in Figure 16.

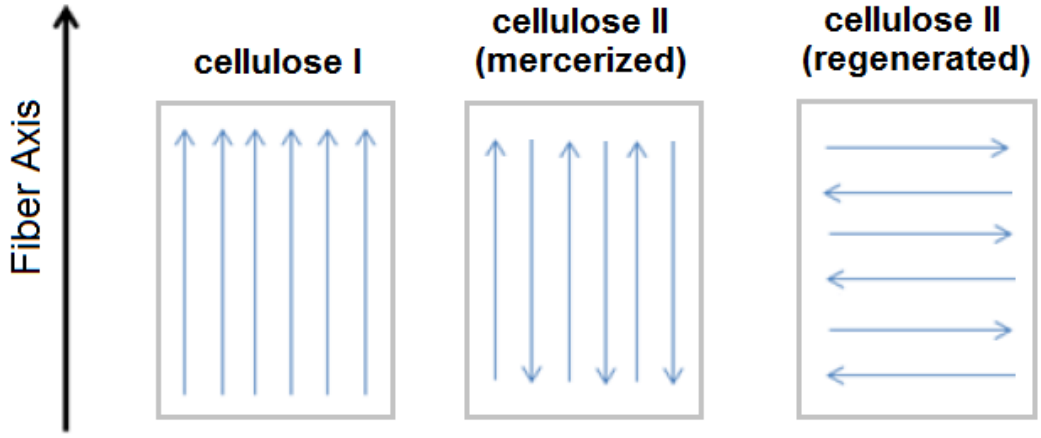

Figure 16 – Schematic representation of the chain orientation in the crystal lattice with respect to the main axis of the fiber for native, mercerized and regenerated cellulose. Each arrow represents one cellulose chain. Here is also represented the parallel-up and anti-parallel (*up* and *down* directions) alignment of cellulose polymorphs I and II, respectively.

These studies on regenerated cellulose pointed out that the ribbon-like lamellar crystalline morphology obtained looks like the lamellar chain-folded morphology, which is typical for linear stereoregular polymers crystallized from dilute solution (Atkins *et al.*, 1979; Buléon and Chanzy, 1978). From that, it was hypothesized that two models could be possible to these regenerated cellulose crystals: i) where the cellulosic chains fold

within the lamellae, similar to morphology encountered in other synthetic polymers, or ii) where straight chains traverse the lamellae, in which the thickness should correspond roughly to the length of the chain, which can be estimated by a measure of the DP. The latter model is the most reasonable for low-molecular-weight cellulose specimens.

Conversely, Kuga *et al.* (1993) provided evidence in support of, and consistent with, the folded-chain hypothesis. In their study Kuga *et al.* (1993) found out that a mutante strain of *Asetobacter xylinum* produced the cellulose II polymorph with anomalous strand-like morphology in contrast to straight crystalline microfibrils of cellulose I normally produced by the wild-type strain. Electron micrographs and electron diffraction diagrams revealed that these strand-like structures displayed lateral dimensions of 10 nm, in which the molecular chains were oriented perpendicularly to the strand axis. Because the average length of glucan chains in this material was determined to be about 10 times the width of the 10 nm wide strand, they concluded that it was highly likely that in this form of cellulose II chain folding was involved (as show in Figure 17), which gives rise to the antiparallel structure. This is the most plausible evidence for the occurrence of chain folding in cellulose II. In this context, Yamane *et al.* (2013) have investigated the possibility of a folded-chain crystal of the cellulose II polymorph by molecular dynamics (MD) simulation. According to them, the energy of the folded-chain crystal is higher than that of the extended-chain crystal at a short crystal length. However, the energy decreased with increasing crystal length and, finally, differences between the energy of folded- and extended-chain crystals became negligible at 20 nm, *viz.* at this point the higher energy of the turning point of the chain can be compensated by a large number of interactions in the crystalline lattice for a crystal size of 20 nm, which corresponded to the real crystal length of regenerated cellulose. Furthermore, the lattice parameters of the folded-chain crystal and original crystal were almost the same. Therefore, there is a possibility that the cellulose chain is folded in the case of regenerated cellulose (Yamane *et al.* 2013).

The orientation of the crystal and the chain folding are important issues directly related with the crystalline morphology, and thus it exerts influence on the polymer material properties (as already stated in the sections above). For instance, it has a strong influence on the axial and tranverse modulus of elasticity of the material (an anisotropic property), further the surface where cellulose folds would be especially vunerable to chemical attack.

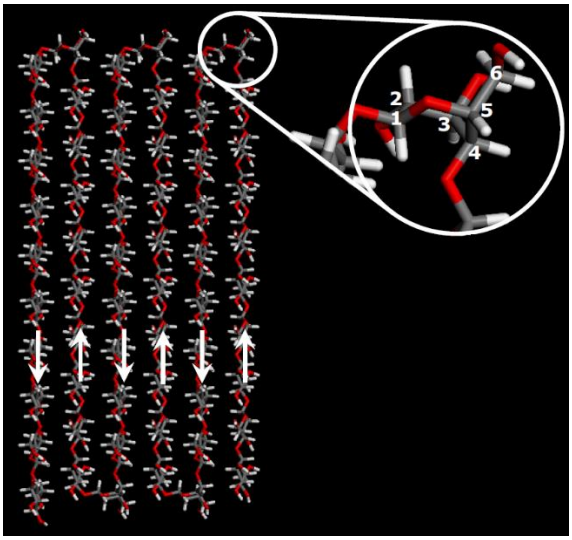

Figure 17 – Schematic projections of the folded-chain structure linked by the $B_{1,4}$ ring conformer. The molecular sheet was sliced off along the (1-10) crystal planes from the cellulose II crystal. White arrows show up and down cellulose molecules (adapted from Yamane *et al.*, 2013).

4. CELLULOSE NANOCRYSTALS: PROPERTIES, PRODUCTION AND APPLICATIONS

As mentioned in the previous sections, in nature, cellulose occurs as a slender rod-like or threadlike entity, formed during biosyntesis. This entity is called microfibril (collection of cellulose chains) and it forms the basic structural unit of the plant cell wall. Each microfibril can be considered as a string of cellulose crystals, linked along the chain axis by amorphous domains (see Figure 11). These highly ordered crystalline domains can be released/isolated from microfibrils by means of chemically induced destructuring strategy (such as acid hydrolysis) in the form of well-defined nano-sized particles, known as cellulose nanocrystals (CNCs). This is represented in Figure 18.

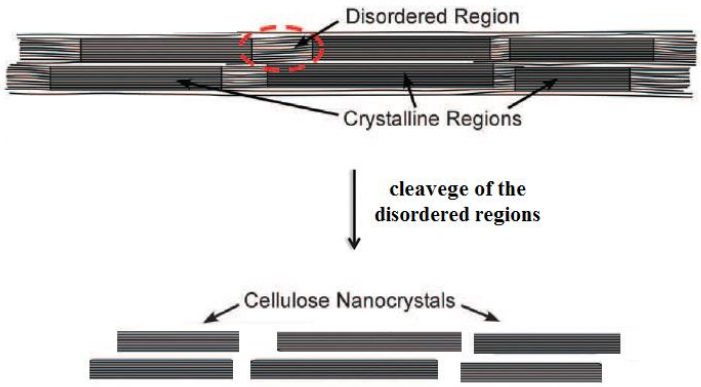

Figure 18 – Schematic drawing of a cellulose microfibril showing the suggested arrangement of crystalline and amorphous regions and the cellulose nanocrystals realeased/isolated after cleavage of the disordered regions (adapted from Moon *et al.*, 2011).

In the literature, many terminologies have been used to appoint this highly crystalline cellullosic nanomaterial, *e.g.* cellulose nanowhiskers, cellulose whiskers, cellulose crystallites, cellulose crystals, cellulose nanocrystals, nanocrystalline cellulose, cellulose monocrystals, cellulose micelles (in early literature) and cellulose microcrystals. Regarding this issue, in 2011 TAPPI's International Nanotechnology Division proposed that the most appropriate nomenclature to describe this nanosized material is "cellulose nanocrystals" (TAPPI, 2011).

Among the different types of nanomaterials CNCs are receiving growing attention in the last years owing to their unique combination of high physicochemical properties and environmental appeal. Such interest is supported by increasing annual number of scientific publications (papers, patents, books) concerning this topic as shown in Figure 19 (Dufresne, 2012; Durán *et al.*, 2012; Hamad, 2017). In addition, currently there are already commercial entities producing CNC at capacities beyond pilot-plant scale, namely CelluForce (www.celluforce.com) and American Process Inc. (www.americanprocess.com), which are located in Canada and USA, respectively (http://www.tappinano.org/media/1114/cellulose-nanomaterials-production-state-of-the-industry-dec-2015.pdf). Nevertheless, it seems that most of the production volume is still intended for research purposes.

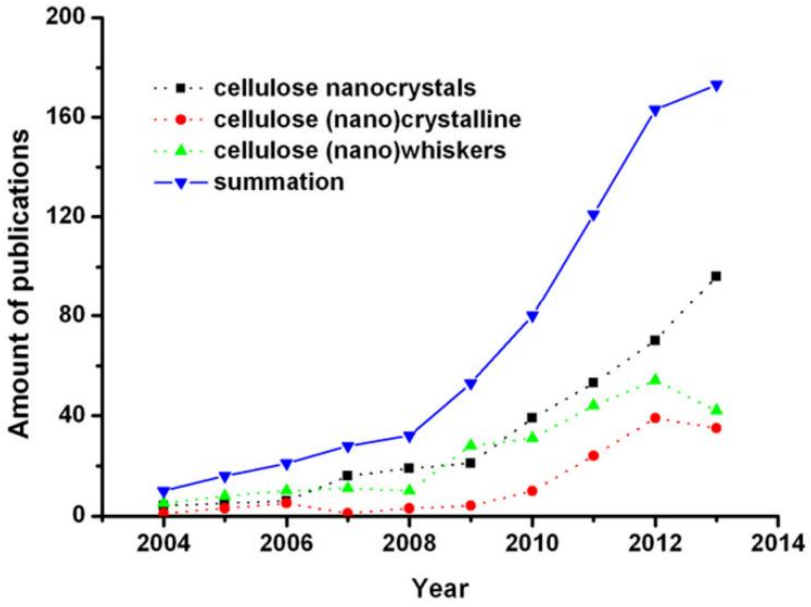

Figure 19 – Evolution of the number of research publications on cellulose nanocrystals from 2004 to 2013 according to ISI Web of Knowledge system (Lin, 2014).

CNCs are a very high-value material, since they can transform the performance of existing products as well as helping to create new, unique and improved products. CNCs can be applied as reinforcing additive, thickener and rheology modifier, emulsion stabilizer, fat replacer (low-calorie food additive), hydrogel, aerogel, liquid crystals, support matrix for catalysts or protein/enzyme immobilization, scaffolds, vehicles for delivery and targeting of therapeutics, pharmaceutical binder, biosensing and bioimaging agents and some others. Thus, CNCs offer a broad range of potential applications in fields ranging from packaging to biomedicine. At present, the most promising application of CNCs is as reinforcement material in polymer nanocomposite field. Others fields of potential applications are paints, coatings, adhesives, emulsions, special papers, cosmetics, pharmaceuticals, biomedical devices, textiles, the automotive industry, aerospace, building/construction materials, the electronic and electrical industry, and many others (dos Santos *et al.*, 2013; Filpponen & Argyropoulos, 2010; Lam *et al.*, 2012; Mandal & Chakrabarty, 2011; Moon *et al.*, 2011; Peng *et al.*, 2011; Yang & Pan, 2010). Actually, as more researchers from various scientific fields become interested in CNC, other possible uses have been proposed and explored (Brinchi *et al.*, 2013). So, in recent years, the number of possible applications for this nanomaterial has grown continuously.

Large specific surface area, high specific strength and modulus, high aspect ratio (L/D), low density, reactive hydroxyl groups that can facilitate grafting chemical species to tailor the surface properties, non-abrasive nature, non-toxic character, biocompatibility and biodegradability are some specific useful features of CNCs which make them promising nanoparticles. Moreover, they are derived from cellulose, which is the most abundant renewable natural polymer available on Earth, therefore low cost. Conversely, the strong tendency for agglomeration, high hydrophilicity and the non-thermoplastic behavior (decomposition prior to the onset of melting) are the main drawbacks related to CNC and eventually limiting its application (Brinchi *et al.*, 2013; Flauzino Neto *et al.*, 2016a; Dufresne, 2012; Ng *et al.*, 2015; Mariano *et al.*, 2014).

4.1. Isolation of CNC from cellulose source material

The isolation of CNC from cellulose source materials occurs in two stages. The first one is the pretreatment of the source material to remove the non-cellulosic constituents, so that the cellulose molecules becomes accessible to react more consistently in the subsequent stage. The second one is a well-controlled and chemically induced treatment (generally chemical hydrolysis) where a “complete” regioselective degradation

of the less organized and more accessible fraction of the cellulosic material takes place, so releasing the crystalline domains from the "purified" material obtained after the first stage.

The goal of the pretreatment stage is the complete or partial removal of the non-cellulosic components (such as lignin, hemicelluloses, protein, *etc*) to obtain high purity cellulosic fibers and get acess to them. The particular pretreatment is dependent on the cellulose source material. Classicaly, for lignocellulosic biomass source this pretreatment consist in similar techniques that are employed in pulp and paper industry. It is usually done as a two-step chemical processing, the alkali delignification followed by bleaching. The alkali step purpose is to degradate and solubilize the lignin, pectins, hemicelluloses and proteins, being commonly performed with aqueous solution of NaOH 2% at 80 or 100°C. The subsequent bleaching step aims in removing the residual phenolic molecules like lignin by oxidizing agents such as hydrogen peroxide (H_2O_2), ozone (O_3) or sodium hypochorite ($NaClO_2$). Both steps must be carefully done to eliminate the non-cellulosic constituents, while leaving cellulose moieties intact, *i.e.* avoiding the breakdown of cellulose chains (Brinchi *et al.*, 2013, Mariano, 2016; Moon et al 2011). Deeper descriptions of the deconstruction of non-cellulosic contents in lignocellulosic biomass are available, for instance in the paper by Ng *et al.* (2015).

The second stage can be performed by many different top-down chemically induced deconstructing strategies, among them the controlled strong acid hydrolysis is the most well-known and widely used (Peng *et al.*, 2011). During acid hydrolysis the amorphous domains surrounding and embedded within cellulose microfibrils are preferentially hydrolyzed, then releasing well-defined crystals from microfibrils (Figure 18). This procedure is based in the quicker hydrolysis kinetics presented by the amorphous domains, as compared to the crystalline ones (Habibi *et al.*, 2010). Owing to some drawbacks related to acid hydrolysis (which will be discussed later), several alternatives methods have also been studied, *e.g.* enzyme-assisted hydrolysis (George *et al.*, 2011; Hayashi *et al.*, 2005; Satyamurthy *et al.*, 2011), sono-chemical-assisted hydrolysis using weak organic acid (Filson & Dawson-Andoh, 2009; Li *et al.*, 2011), hydrolysis with oxidative reagents such as ammonium persulfate (Cheng *et al.*, 2014; Leung *et al.*, 2011) or sodium metaperiodate (Visanko *et al.*, 2014) or 2,2,6,6-Tetramethylpiperidine-1-oxyl (TEMPO)–NaBr–NaClO system (Qin *et al.*, 2011; Brinchi *et al.*, 2013), subcritical water hydrolysis (Novo *et al.*, 2015), hydrolysis mediated by ionic liquids (Han *et al.*, 2013; Lazko *et al.*, 2016; Mao *et al.*, 2015; Yang *et al.*, 2013).

Concerning the second stage, it should be noted that the vast majority of the technologies used are top-donw deconstructing strategies, and only few recent works have reported a bottom-up approach for the production of CNC, such as the works of Yang *et al.* 2013 and Han *et al.*, 2013. This "new" approach to CNC production involves the regeneration process of cellulose, and could be very interesting toward a better control of nanomaterial formed and its properties (*e.g.*, control of size, shape, aspect ratio, crystallinity, *etc*).

4.2. Influence of cellulose source and isolation process on CNC properties

The structure and properties (such as crystallinity, specific strength and modulus, aspect ratio, specific surface area, crystal structure), especially the morphological features (shape and size) of the CNCs, depend on: (i) the source of the original cellulose, which is linked to the biosynthesis of cellulose microfibrils, and (ii) the isolation process of the CNCs from the cellulose microfibrils, including any pretreatment or deconstruction processes (Flauzino Neto *et al.*, 2016a; Moon *et al.*, 2011; Yang *et al.*, 2013).

CNCs have been isolated from a broad range of cellulose sources, *e.g.* from higher plants (da Silva *et al.*, 2015) and algae (Revol, 1982), sea animals, such as tunicates (Sacui *et al.*, 2014), and bacteria (George *et al.*, 2011), and in pricinple could be extracted from almost any cellulosic material. In practice, for most studies, researchers have shown preferences to commercial microcrystalline cellulose (MCC), filter paper, bleached wood pulp or related products, owing to their purity and availability in laboratories. Tunicin has also been a favored source of CNC because of its larger dimensions, high crystallinity and aspect ratio. However, its widespread use is restricted by the high cost of harvesting and limited availability (Brinchi *et al.*, 2013; Klemm *et al.*, 2011). Some different CNC images are shown in Figure 20, from which it is possible to observe the influence of the cellulose source as well as polymorphism on the final shape and size of the nanoparticles. Therefore, specific pretreatments and extraction procedures have been developed depending on the source of cellulose. Although, if often composed of few laterally bound elementary crystallites that are not separated by conventional acid hydrolysis and sonication process (Elazzouzi-Hafraoui *et al.*, 2008), the length and width of cellulose nanocrystals is generally in the order of few hundred nanometers and few nanometers, respectively.

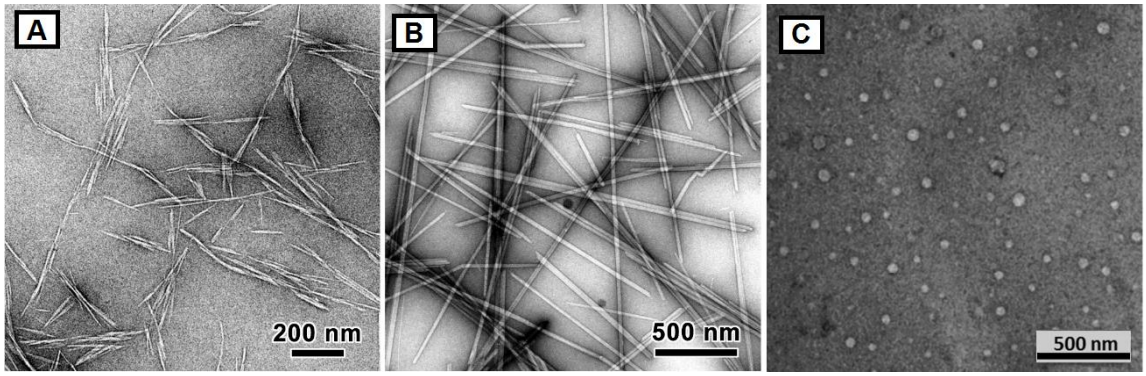

Figure 20 – Transmission electron micrographs of negatively stained preparations of cellulose nanocrystals of various origins: a) wood; b) Glaucocystis (adapted from Kaushik *et al.* 2015); c) Lyocell (adapted from Beaumont *et al.* 2016). a) and b) correspond to cellulose I polymorph, while c) correspond to cellulose II polymorph.

4.3. Acid hydrolysis

Rånby (1951) is considered as the pioneer in the production of coloidal suspensions of cellulose crystals by controlled sulfuric acid hydrolysis of cellulose fibers. The method of choice for the isolation of CNC is still based on controlled sulfuric acid hydrolysis, probably owing to the stability of the resulting suspensions and simplicity at laboratory scale. As aforementioned, the amorphous regions act as structural defects which are susceptible to acid attack and, under controlled conditions they can be removed leaving crystalline regions intact. This transformation consists in the disruption of amorphous regions surrounding and embedded within cellulose microfibrils. During the acid hydrolysis process, the hydronium ions (H_3O^+) can penetrate the cellulose chains in the amorphous domains promoting the hydrolytic cleavage of the glycosidic bonds and releasing individual crystallites. It is ascribed to the faster hydrolysis kinetics of amorphous domains compared to crystalline ones. Figure 21 shows a representation of the mechanism of acid hydrolysis reaction. From this process, CNC may be released and extracted from the cellulose substrate (Brinchi *et al.*, 2013; Dufresne, 2012).

Typical procedures currently employed consist of the following steps: (1) Strong acid hydrolysis of pure cellulosic material under strictly controlled conditions of temperature, time, agitation, and with control of other conditions such as nature and concentration of the acid and the acid-to-cellulose ratio; (2) Dilution with water to stop the hydrolysis reaction and repeated washing by successive centrifugation to remove the excess acid; (3) Extensive dialysis against distilled water to fully remove free acid molecules and eventually soluble sugars; (4) Mechanical treatment, usually sonication, to disperse the nanocrystals as a more or less uniform stable suspension. Additional steps of

post-treatment such as filtration, differential centrifugation, ultracentrifugation or high-pressure homogenization to obtain particles with reduced polydispersity of size and/or effectively disperse and homogenize the CNC suspension have been also reported (Brinchi *et al.*, 2013; Dufresne, 2012; Habibi *et al.*, 2010).

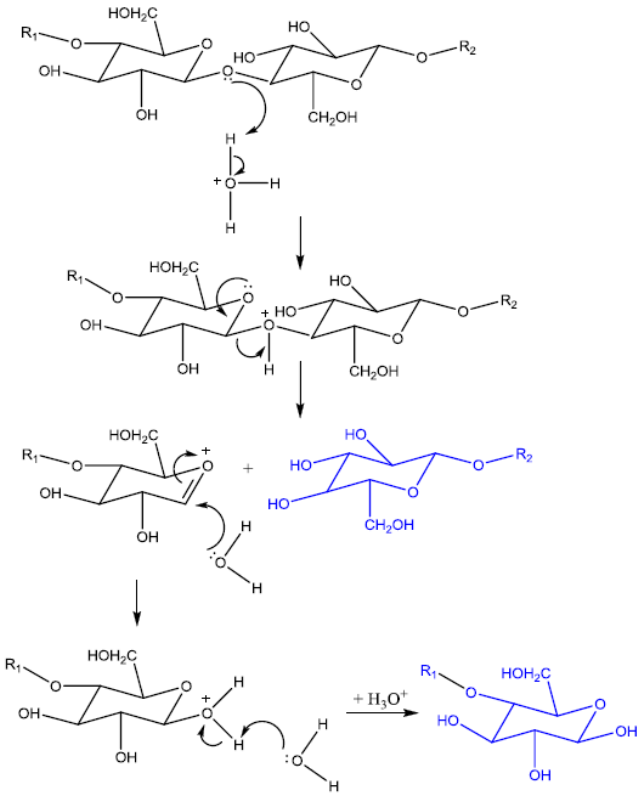

Figure 21 – Representation of the mechanism for the acid hydrolysis reaction.

Regarding acid hydrolysis, the temperature and the time of reaction, acid nature, acid concentration and the acid-to-cellulose ratio have been identified as the most important parameters that affect the morphology, polymorphism and final properties of the resulting CNC (Flauzino Neto et al, 2013; Sèbe *et al.*, 2012).

Sulfuric acid is the most often used process for CNC preparation. However, the use of other acids such as hydrochloric, nitric, phosphoric and hydrobromic acids has been also reported. If CNCs are prepared using hydrochloric acid, their ability to disperse in polar solvents is limited and the suspension is unstable tending to flocculate. On the other hand, when sulfuric acid is used as a hydrolyzing agent, it reacts with the surface hydroxyl groups of cellulose to yield surface sulfate esters groups ($-OSO_3^-$) leading to the formation of a negative electrostatic layer covering the nanocrystals and promoting their dispersion in water by repulsive forces between individual nanoparticles. However, the introduction of charged sulfate groups compromises the thermostability of the

nanocrystals. Nevertheless, the stability can be achieved by performing a proper neutralization of the nanoparticle suspension by sodium hydroxide (NaOH) (Habibi *et al.*, 2010; Lin & Dufresne, 2014a). Thus, one of the main reasons for using sulfuric acid is to obtain stable aqueous suspensions. The density of charges on the CNC surface depends on the hydrolysis conditions and can be determined by elementary analysis or conductimetric titration to exactly determine the sulfur content.

In the case of sulfuric acid-catalyzed hydrolysis, usually, the concentration of sulfuric acid does not vary much from a typical value of 65 wt%, the temperature ranges from room temperature up to 70°C, the hydrolysis time can be varied from 30 min to overnight, being that variations from 30 to 60 min are commoner, and the acid-raw material ratio values range from 8.3 to 35 $mL \cdot g^{-1}$ (Dufresne, 2012; Silva & D'Almeida, 2009b).

4.4. Degree of polymerization

As the hydrolysis proceeds, the degree of polymerization (DP) of the cellulose molecules is expected to decrease. In general, upon acid hydrolysis, cellulose depolymerizes rapidly down to a certain level after which the degradation is much slower, the so-called level-off DP (LODP). It was verified that regardless of the hydrolysis conditions, the same LODP was reached (Battista, 1950; Battista *et al.*, 1956; Hakansson & Ahlgren, 2005). Obviously a longer time was needed under milder conditions to reach the LODP. A good correlation between DP and length of the nanocrystals measured by microscopic observations was reported (Battista *et al.*, 1956). This LODP was also found to match the periodicity observed for ramie cellulose microfibrils in small angle neutron scattering studies (Nishiyama *et al.*, 2003a). It was considered that the microfibrils have 4–5 disordered residues every 300 residues.

4.5. Specific surface area

As could be expected, the large specific surface area of CNC is an intrinsic feature of its nanoscale dimensions. The reported specific surface area of CNC is estimated to be greater than 100 $m^2 \cdot g^{-1}$ and even up to several hundreds of $m^2 \cdot g^{-1}$. Specific surface area can be increased with increasing aspect ratio or decreasing diameter of CNC. Figure 22 shows the evolution of the specific surface area as a function of the diameter of rod-like nanoparticles. A sharp increase is observed when the diameter falls below a value of 20 nm, which corresponds to the diameter range of cellulose nanocrystals. The surface area

is an issue particularly important for CNC-based nanocomposites compared to conventional composites, because the effect of interfacial interaction and bondability between the filler and compatible polymer can be amplified by the larger specific surface area of CNC, and thus improving some of the composite properties. However, due to this high surface area and the presence of many OH groups the CNCs have a strong tendency for agglomeration driven by their high hydrophilic nature. So, once dried the CNC suspension will form aggregates which are difficult to be re-dispersed. This aggregated CNC is absolutely not desirable for effective processing and even reinforcement purpose.

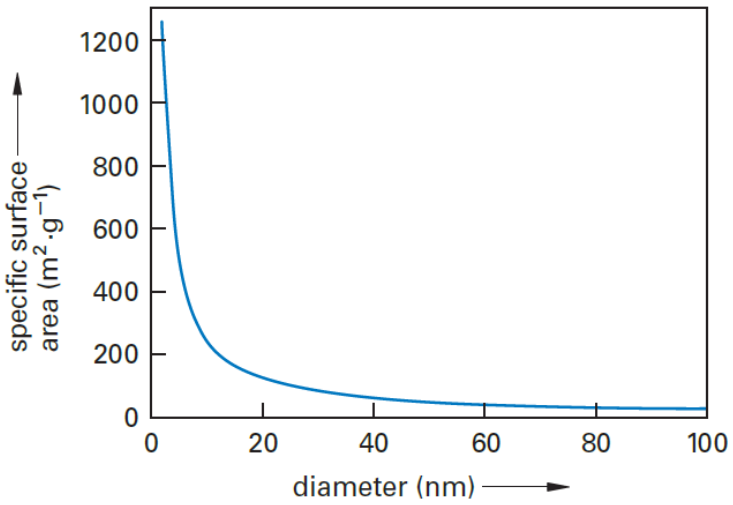

Figure 22 – Evolution of the specific surface area of rod-like nanoparticles as a function of their diameter, assuming a density of 1.5 $g \cdot cm^{-3}$ for crystalline cellulose (Dufresne, 2012).

The CNC aggregation upon drying makes the experimental determination of its specific surface area difficult. Determination of the specific surface area from gas adsorption isotherm is often incorrect because of the irreversible aggregation of the nanoparticles upon drying. Therefore, often the specific surface area of CNCs can be estimated from the average geometrical dimensions of the nanoparticles, assuming a rod-like geometry and a density 1.5 or 1.6 $g \cdot cm^{-3}$ for crystalline cellulose. For example, values of 170 (Dufresne, 2000) and 533 $m^2 \cdot g^{-1}$ (Siqueira *et al.*, 2010) have been reported for nanocrystals extracted from tunicin and sisal, respectively. The corresponding diameters were 15 and 5 nm, respectively, and the density of crystalline cellulose was assumed to be 1.5 $g \cdot cm^{-3}$ (Dufresne, 2012).

4.6. Excellent mechanical properties

There is limited understanding on the intrinsic mechanical properties of single CNC. The small particle size combined with the limited metrology techniques available to characterize the CNC along multiple axes has made quantitative mechanical properties measurement extremely challenging. In addition, several factors may influence the measured mechanical properties and will contribute to the wide scatter in the reported values. These factors include: crystal structure (polymorphism), crystallinity, anisotropy, and the property measurement methods and techniques (including sample preparation, assumptions made, *e.g.* regarding the stress transfer in the sample and cross sectional area, *etc*). Thus, it is crucial to consider these factors when comparing reported mechanical properties values for CNC (Moon *et al.*, 2011; Wohlert *et al.*, 2012).

In view of the anisotropy within crystalline cellulose (*i.e.* non symmetric structure of the cellulose chain and its arrangement within the crystal structure) there will be differences in the mechanical properties as a function of direction with respect to the cellulose crystalline structure. Most studies have focused on elastic properties along the more readily measureable axial direction of the cellulose crystal, while only few ones have been attempted measuring the properties in the transverse direction (Mariano *et al.*, 2014; Moon *et al.*, 2011; Wohlert *et al.*, 2012).

For native cellulose (mixture of cellulose Iα and Iβ) the average value of the longitudinal elastic modulus is around 137* GPa when considering intramolecular hydrogen bonding, and 92** GPa without intramolecular hydrogen bonding, evidencing the important role of intramolecular bonding on the determination of the crystallite modulus and chain deformation mechanism. For cellulose II, the average value of the longitudinal elastic modulus is around 113* GPa. The lower value observed for form II is ascribed to lower intramolecular hydrogen bonds, showing again the importance of this parameter, whereas the intermolecular hydrogen bonds were found to play a minor role. These striking mechanical properties make CNC an ideal candidate for the processing of reinforced polymer composites. Its Young's modulus, with a density for crystalline cellulose around 1.5–1.6 $g \cdot cm^{-3}$, is much higher than for glass fibers, around 70 GPa with a density around 2.6 $g \cdot cm^{-3}$, which are classically used in composite applications. It is similar to Kevlar (60–125 GPa, density around 1.45 $g \cdot cm^{-3}$) and potentially stronger than steel (200–220 GPa, density around 8 $g \cdot cm^{-3}$). Indeed, the specific Young's modulus, which is the ratio between the Young's modulus and the density of cellulose crystal is around 85 $J \cdot g^{-1}$ whereas it is around 25 $J \cdot g^{-1}$ for steel (Dufresne, 2013; Mariano *et al.*,

*considering experimental and theoretical data
**theoretical data

2014). Therefore, owing to the high stiffness and strength associated to its renewable nature and low density, CNC has emerged as a promissing reinforcing nanoelement for the preparation of nanocomposites with enhanced mechanical performance.

4.7. Crystallinity

Since CNC can be considered as a crystal with no apparent defect or containing only a small number of defects, its degree of crystallinity is expected to be very high. The reported values for this parameter ranges from 46 to 96% and significantly depends on the measurement method and data analysis method applied (Dufresne, 2012; Park *et al.*, 2010). As alredy indicated, the degree of crystallinity is highly dependent on the original cellulose source (*i.e.* it depends on the crystallization which takes place during biosynthesis process) and isolation process. Furthermore, the degree of crystallinity has a strong correlation with CNC mechanical properties, especially with the modulus of the crystalline domains, as previously shown. The higher the crystallinity, the higher the modulus of the CNC which becomes close to the theoretical modulus of the perfect crystal.

4.8. Aspect ratio (L/D)

The rod-like shape is the most often found for CNC. The average length is generally of the order of a few hundred nanometers, whereas the width is of the order of a few nanometers. Then, like for fiber materials, CNC is often described in terms of its aspect ratio. The values reported in the literature vary roughly between 10 and 75 for cotton and *Posidonia oceanica* leaves, respectively (Bettaieb *et al.*, 2015; Ebeling *et al.*, 1999). This morphological feature depends on the origin of the cellulose substrate and on the extraction method (including its conditions and any pretreatment). However, it is widely accepted that the raw starting material is the most important factor (Beck-Candanedo *et al.*, 2005; Dufresne, 2012; Elazzouzi-Hafraoui *et al.*, 2008).

The aspect ratio has a close relation with the CNC mechanical properties when incorporating it into a polymeric matrix. A higher aspect ratio can provide higher reinforcement effect compared to nanofiller with lower aspect ratio, and therefore it is a key parameter with strong influence on the mechanical properties of CNC-based nanocomposites. Thus, at this point, it is clear that the source of CNC can influence its applications.

4.9. Challenges on commercial CNC production

To date, the development of cost-efficient and environmentally friendly CNC extraction processes stands out as the major challenge to be overcome. In particular the reduction in the cost of CNC production is often addressed, because it could increase the number of markets appropriate for CNC applications. The commercial production of nanocrystals is based on the hydrolysis with sulfuric acid. The use of a concentrated strong acid, especially sulfuric, has a number of important drawbacks such as hazard, corrosivity (corrosion resistant reactors have to be used) and environmental incompatibility. Other relevant challenges to be met, are: i) valorization of the waste liquor stream which contains sugars, in monomeric and oligomeric forms, and residual sulfuric acid, thus its use could reduce the production costs; ii) the low yield which has a important impact on the final cost of CNC; iii) reliable recipe for production with uniform size, aspect ratio, surface chemistry needs to develop, because it would provide more control in CNC suspensions, and in the design and processing of CNC-based composites; iv) effective drying method of aqueous CNC suspensions which will maintain nanoscale dimensions for material applications (where a dry form is necessary) and mitigate the higher transportation costs of aqueous suspensions (Brinchi et al 2013; Ng *et al.*, 2015).

4.10. Toxicology assessment and biodegradability

Manufactured nanomaterials have recently caused societal concerns about their possible adverse effects on human health and environment. Properties of nanomaterials typically differ from those of their parent bulk materials because of their larger surface area to volume ratio, leading to a greater activity, their smaller size, resulting in their ability to cross cellular membranes (*i.e.* penetrate into cells), and intrinsic effects caused by nanometric size, including electronic and plasmonic effects. Since such particles may have a negative effect on biological systems and ecosystems, their toxicological risks must be evaluated and an accurate description of the product in terms of dimensions, chemistry, and toxicity is required by the authorities.

While the production and application of CNC are growing exponentially, research into the toxicological impact and possible hazard of these nanoparticles is still restricted at a very preliminary stage (mainly on the level of cytotoxicity) (Lin & Dufresne, 2014b; Roman, 2015). CNCs have been evaluated using several standard ecotoxicological and mammalian test protocols and, so far, the results seem to point towards the same direction suggesting that CNCs have no or low toxicity (*i.e.* are practically non-toxic). Moreover,

CNCs have recently obtained regulatory approval under Canada's New Substances Notification Regulations for unrestricted use in Canada and it is the first organic nanomaterial to be added to Canada's domestic substance list (Kaushik *et al.*, 2015; Kovacs *et al.*, 2010). Anyway, further testing is necessary especially regarding evaluation on the environmental fate, potential CNC uptake and exposure studies, so that a detailed risk assessment can be determined. In doing so, are taken steps protect workers, consumers and the environment from suspect CNC materials and guide the development of safer materials in the future (Brinchi *et al.*, 2013; Roman, 2015).

Knowledge on the biodegradability is also of utmost importance for risk assessment of this nanomaterial. The biodegradability of CNC in aqueous environment has been investigated according to OECD (Organisation of Economic Cooperation and Development) standards. CNCs were found to degrade faster than its macroscopic counterpart, whereas other important and widely used nanoparticles such as fullerenes and carbon nanotubes did not biodegrade at all (Kümmerer *et al.*, 2011). Here, it is important to note that these findings are crucial issues directly associated to practical applications of CNC, *e.g.* biomedical applications requiring biocompatibility such as drug delivery and cellular growth systems.

4.11. Durability of CNC based products

As stated by Hubbe *et al.* (2008), at an academic level it is likely that long-term durability issues can be addressed by considering the strengths of materials, the methods by which the components of a composite are mixed, and the chemical strategies by which the interfaces are compatibilized. However, at a practical level it may be difficult to make sure that a specific item purchased today will last nearly as long as an item made of standard materials, such as wood, metal, or plastic.

4.12. Cellulose nanocomposites based on cellulose nanocrystals

In general, a composite can be considered as any multiphase material which demonstrates a significant proportionality of the inherent properties of both phases that constitute it, such that a better combination of properties is obtained. According to this principle of jointness, best properties are achieved through a judicious combination of two or more different materials. In addition, the constituent phases must have physical and chemical properties different and must be separated by a distinct interface. Many composite materials are composed of only two phases; one is called matrix, which is

continuous and surrounds the other phase, which in turn is often called dispersed phase or filler. The properties of this multiphase system (including the mechanical ones) are a function of the properties of the constituent phases, their relative amounts and geometry of the dispersed phase (particle shape, size, its distribution and orientation) as well as the interfacial compatibility between the constituents of the mixture and morphology (spatial arrangement of the phases). A current trend in the composites field is the preparation of composites where at least one dimension of the dispersed phase (filler) is in the nanoscale range (1 nm -100 nm). The composites obtained in this way, called nanocomposites, may exhibit many unique and superior properties when compared to conventional composites. Because the high surface area of the particles with nanometric dimensions can promote greater interfacial interaction between filler and matrix, thus enabling more significant changes in physicochemical properties of nanocomposites compared to traditional composites.

As previously stated, to date, the most promising application of CNCs is in composite materials as reinforcing element of polymer systems. The incorporation of CNCs in polymer matrices generally leads to polymer-based nanocomposite materials with higher mechanical and barrier properties than the neat polymer or traditional composites. CNC is a potential alternative which could overcome the high cost, adverse environmental impact and health problems associated to the fillers traditionally used in the industry such as glass and carbon fibers. Aditionally, the use of natural and renewable materials, such as CNC, appear as a perfect option for the development of fully-biobased and biodegradagle nanocomposites systems with enhanced technical performance.

The first publications related to the use of CNC as reinforcing filler in polymer based nanocomposites was reported in 1995 by Favier *et al.* (1995a; 1995b) at CERMAV-France. In these pioneering studies, they produced nanocomposite films by casting and evaporating a mixture of poly(styrene-co-butyl acrylate) in latex form and cellulose nanocrystals isolated from tunicate. By DMA (dynamic mechanical analysis) experiments in the shear mode, the authors observed a huge improvement in the storage modulus after adding CNC into the host polymer even at low content. This increase was particularly striking above the glass-rubber transition temperature (T_g) of the thermoplastic matrix because of its poor mechanical properties in this temperature range. In the rubbery state of the polymeric matrix, it has been found that the modulus of the composite with a loading level as low as 6 wt% (around 4 vol.%) was more than two orders of magnitude higher than the one of the unfilled matrix (Figure 23a). Moreover, whereas the stiffness

of the unfilled matrix decreases with temperature, the relaxed modulus of nanocomposites with 6% of load remains remarkably constant up to the temperature at wich CNC starts to degrade (around 500 K) (Figure 23b).

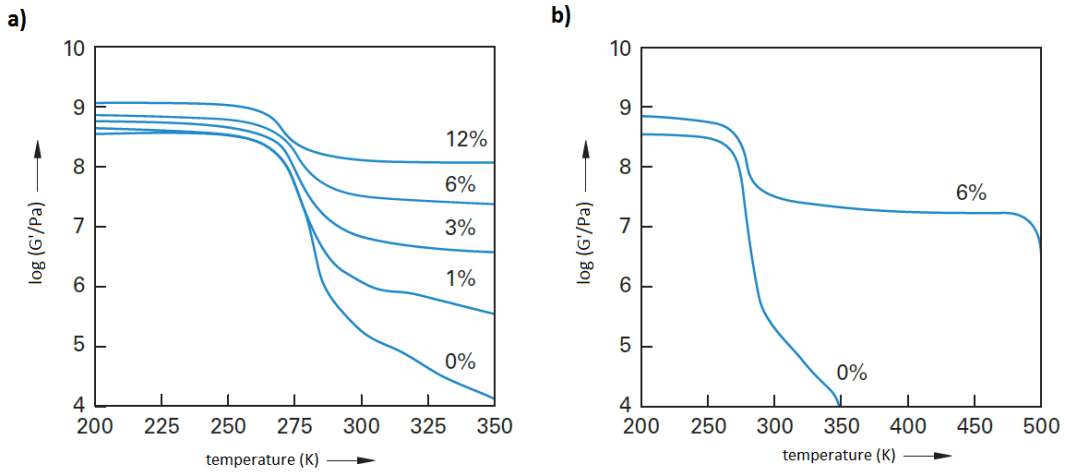

Figure 23 – Logarithm of the storage shear modulus as a function of temperature for poly(styrene-co-butyl acrylate) reinforced with tunicin nanocrystals. (a) Shows the reinforcing effect obtained for various filler contents and panel (b) shows the improvement of the thermal stability of the matrix (Favier *et al.*, 1995b).

Since then, there has been an increased interest in the preparation of CNC/polymer nanocomposites. Obviously this is largely due to the intrinsic CNC properties such as nanoscale dimensions, high surface area, unique morphology, low density, high stiffness and strength. So far, incorporation of CNC into a wide range of polymeric matrices was attempted, including synthetic and natural ones (such as starch, natural rubber, polylactic acid (PLA), low density polyethylene (LDPE), polystyrene (PS), polyoxyethylene (POE), *etc*). A list of papers relative to investigations in this field would be quite long, and there are available excellent reviews covering this research topic (Kalia *et al.*, 2011; Mariano *et al.*, 2014; Miao & Hamad, 2013; Moon *et al.*, 2011; Oksman *et al.*, 2016).

4.13. Mechanical properties of CNC/polymer nanocomposites and percolation theory

By far, the mechanical properties of CNC/polymer nanocomposites are their most important and most investigated asset. Like for any fiber-reinforced polymer composites, the mechanical properties of CNC/polymer nanocomposites depend on many factors, such as: filler loading (or filler volume fraction), filler dispersion, filler morphology (shape, size, and aspect ratio), filler surface area, filler orientation, filler-matrix interfacial adhesion, filler stiffness and strength, microstructural details of the composite, percolation phenomenon, processing technique, *etc*.

It has been observed that the huge and unusual mechanical reinforcement effect provided by the CNC can not be well described by the traditional mechanical models applied to composite materials, like the theoretical model of Halpin-Kardos (mean-field approach) which has been extensively used to explain and predict the elastic modulus of short-fiber composites and semicrystalline polymers. In such an approach, the modulus and the geometry of the particles are taken into account, but one assumes that there is no interaction between the fillers. On account of the failure of this model, it was suggested that interactions between the fillers and their topological arrangement must be considered. In view of this, the classic series-parallel model (Takayanagi *et al.* 1964) adapted to include a percolation approach (Ouali *et al.*, 1991) has been found to successfully describe, *i.e.* with sufficient accuracy, the mechanical behavior of polymer-based nanocomposites reinforced with CNC. According to this mechanical model based on percolation concepts the unusual mechanical properties of the CNC/polymer composite (especially those observed in the rubbery state) could be well understood by virtue of the formation of a stiff continuous network of CNC inside the host matrix, which occurs when the filler particles are present in quantities above the threshold where they start interacting. The formation of this rigid network is presumably caused by strong interactions between the CNC themselves, such as hydrogen bonds. The interconnected particle organization at the percolation point is represented in Figure 24 for rod-like particles. Percolation theory considers various parameters such as particle-particle interactions, orientation of particles and aspect ratio (Dufresne, 2012).

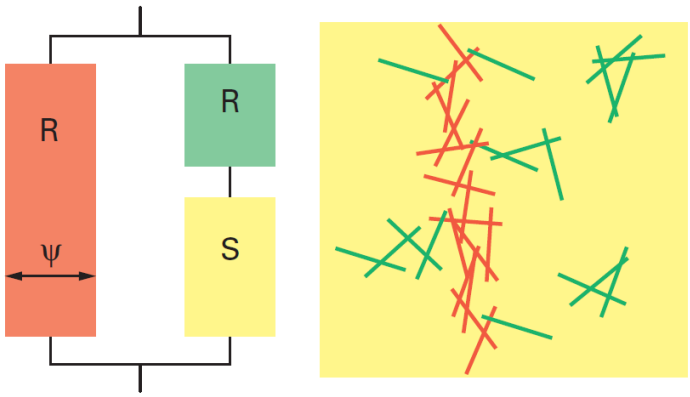

Figure 24 – Schematic representation of the series-parallel model adapted to include a percolation approach. R and S refer to the rigid (filler) and soft (polymeric matrix) phases, respectively, and ψ is the volume fraction of the percolating rigid phase. Red and green rods correspond to percolating and unpercolating nanoparticles, respectively. In this model the percolating filler network is set in parallel with a series part composed of the matrix and the non-percolating filler phase. (Dufresne, 2012).

Within the framework of the model, the elastic tensile modulus E_c of the composite is given by the following equation (Equation 2):

$$E_C = \frac{(1-2\psi+\psi V_R)\, E_S E_R + (1-V_R)\, \psi\, {E_R}^2}{(1-V_R)\, E_R + (V_R-\psi)\, E_S} \qquad \text{Eq. (2)}$$

Where E_S and E_R refer to the tensile modulus of the soft phase (polymeric matrix) and rigid phase (CNC), respectively; and V_R is the volume fraction of the reinforcing phase. The adjustable parameter, ψ, involved in the series-parallel model of Takayanagi *et al*. (1964) corresponds to the volume fraction of the percolating rigid phase. With b being the critical percolation exponent, it can be written as:

$$\psi = 0 \quad \text{for} \quad V_R < V_C \qquad \text{Eq. (3)}$$

$$\psi = V_R \left(\frac{V_R - V_{Rc}}{1-V_{Rc}}\right)^b \quad \text{for} \quad V_R > V_{Rc} \qquad \text{Eq. (4)}$$

Where b = 0.4 for a 3D network (de Gennes, 1979; Stauffer, 1985) and V_{Rc} is the percolation threshold, which means the lowest volume fraction of filler particles that can provide the necessary number of individual rods, arranged randomly, to form a uninterrupted 3D percolating network whitin the polymer matrix, *i.e.* the onset point of an infinite communication state. So, the geometrical percolating network is supposed to form only above the percalotion threshold. In this case, the percolation threshold V_{Rc} can be calculated according to the aspect ratio (L/D) of the CNC, as shown by Equation 5.

$$V_{Rc} = \frac{0.7}{L/D} \qquad \text{Eq. (5)}$$

At sufficiently high temperatures the stiffness of the polymeric matrix could be assumed to be much lower than the one of the reinforcing phase (ES ~0), then the stiffness of the composite is simply the product of the volume fraction and stiffness of the rigid percolating network, as given below:

$$E_C = \psi E_R \qquad \text{Eq. (6)}$$

Therefore, the predicted composite modulus depends on the volume fraction of the percolating rigid phase (Equations 3 and 4), which is directly related to the volume fraction and geometrical characteristics of the reinforcing phase (Equation 5). Here, it should be remembered that the CNC aspect ratio (geometrical characteristics) is directly

related to the origin of cellulose and to the isolation process of CNC, as already mentioned.

The other parameter involved in the prediction of the composite's modulus (Equation 4) is the modulus of the percolating nanoparticle network E_R, which is obviously different from the one of individual CNC and depends on the nature and strength of interparticle interactions. This modulus can be assumed to be similar, in principle, to the one of a paper sheet for which the hydrogen bonding forces provide the basis of its stiffness. However, because of the nanoscale effect stronger interactions are expected. This modulus can be experimentally determined from tensile tests performed on films prepared from the evaporation of a suspension of CNC (Bras *et al.*, 2011; Dufresne 2012, Mariano *et al.*, 2014). Values ranging from about 500 MPa to 15 GPa have been reported and this value was found to be roughly correlated to the aspect ratio of the CNC. As demonstrated by Bras *et al.* 2011 the modulus of the film was found to increase with the aspect ratio (Figure 25). Thus, from a mechanical point of view there is no doubt that the use of CNC with higher aspect ratio is more interesting, because it first induces a decrease of the critical percolation threshold and also stiffens the formed continuous network (Bras *et al.*, 2011; Dufresne et al 2012). In addition, the reduction of the percolation threshold allowing reduction of the filler loading necessary to reach an effective reinforcing effect, resulting in a lower number of rod ends under stress, and lower number of cracks. In general terms, the percolation mechanism states an optimal volume fraction of filler. Below this volume fraction, the reinforcement is only partial and over it the reinforcement cannot increase, or can even decrease.

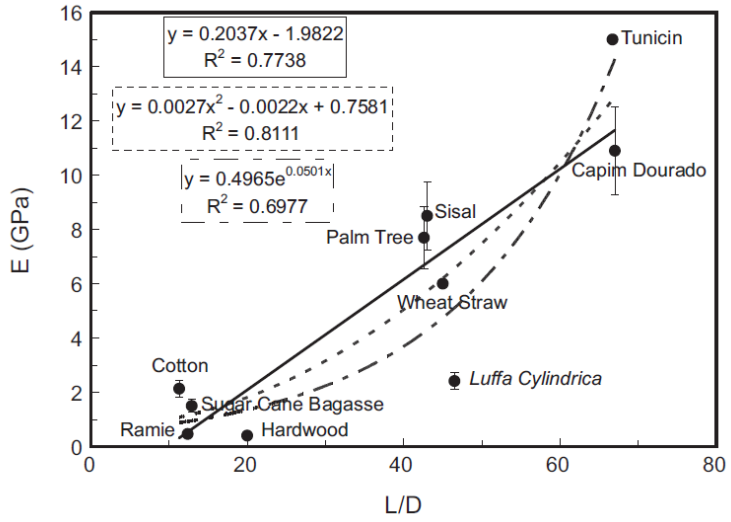

Figure 25 – Evolution of the Young's modulus of the cellulosic nanocrystals film determined from tensile tests as a function of the aspect ratio of the constituting CNC (Bras *et al.*, 2011).

The percolation model is consistent with the high reinforcement above the T_g and explain the thermal stabilization of the nanocomposite modulus. As the polymer chains gain mobility causing the matrix to soften, the CNC network remains strong leading to the significant improvement of the mechanical performance at high temperatures, such as the one obtained by Favier *et al.* (1995a; 1995b) (Figure 26). It should be pointed out that the following assumptions are made when fitting data with the mechanical percolation model: i) the cellulose particles are uniformly dispersed in the matrix; ii) the particles have uniform shape and size; iii) good interfacial interactions exist between the matrix and cellulose particles; iv) the matrix is free of voids; vi) initially there are no residual stresses in the matrix; vii) both the matrix and the CNC reinforcement behave as linearly elastic materials (Saxena, 2013).

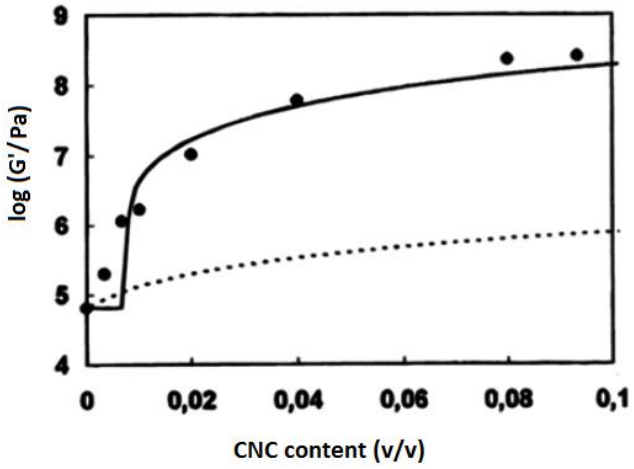

Figure 26 – Plot of the logarithm of the storage shear modulus (G') at 325 K (*Tg* + 50 K) as a function of the volume fraction of CNC. Comparison between the experimental (black dots) and calculated data with two different mechanical models: a meanfield model (dashed line) and a percolation model (continuous line). (Favier et al 1995b).

Any parameter that affects the formation of the percolating nanocrystal network or interferes with it is a critical issue that changes dramatically the mechanical performances of the composite. The main parameters that were identified to affect the mechanical properties of such materials are the morphology and dimensions of the nanoparticles, the processing method, and the microstructure of the matrix and matrix/filler interactions (Mariano *et al.*, 2014). As shown in Figure 25, higher aspect ratio nanocrystals provide higher reinforcement. Regarding the processing method, slow wet processes (casting/evaporation) involving pristine CNC were reported to give the highest mechanical performance materials compared to other processing techniques. Indeed, during liquid evaporation strong interactions between nanoparticles can settle and

promote the formation of a strong percolating network. During slow water (or polar liquid) evaporation, because of Brownian motions in the suspension or solution (whose viscosity remains low, up to the end of the process when the latex particle or polymer concentration becomes very high), the rearrangement of the nanoparticles is possible. They have time enough to interact and connect to form a percolating network which is the basis of their reinforcing effect. The resulting structure (after the coalescence of latex particles and/or interdiffusion of polymeric chains) is completely relaxed and direct contacts between pristine nanocrystals are then created.

To expand the range of polymers that can be used in association with CNC, homogeneous dispersion of the nanoparticles in any liquid medium, regardless its polarity, is desirable. To promote this dispersion it is necessary to lower the surface energy of the nanoparticles to fit with that of the liquid or polymer melt. This is usually achieved by coating their surface with a surfactant or by surface chemical modificadion (replacing part of the surface hydroxyl groups by less polar groups). But, even if the dispersion of the nanoparticles in the liquid medium (in which the polymeric matrix is generally solubilized) is improved, hindered interactions between physically or chemically modified nanocrystals limit the formation of a strong percolating nanoparticle network and then the reinforcing effect (Mariano *et al.*, 2014).

Another important issue concerning the mechanical properties is the hardening effect in the semi-crystalline polymer matrix induced by CNC, which act as nucleating agent in the system. Indeed, highly crystalline CNCs have excellent nucleation ability in reinforced polymer by offering numerous primary nucleation sites for growth of crystallites, intending to facilitate the recrystallization of the polymer chains at the interface. Consequently, the degree of crystallinity of the polymer matrix can be significantly enhanced, altering the resulting mechanical properties (Mariano, 2016; Ng *et al.*, 2015).

Today the enhancement in mechanical and barrier properties of nanocomposites by addition of CNC represents an opportunity for industrial sector. However, certain drawbacks need to be addressed, such as, incompatibility with the hydrophobic polymer matrix, the tendency to form aggregates during processing, the onset of thermal degradation at 200-300°C (which eventually limits the processing temperature).

5. REFERENCES

Atalla, R. H., & Vanderhart, D. L. (1984). Native Cellulose: A Composite of Two Distinct Crystalline Forms. *Science, 223*, 283-285.

Atkins, E. D. T., Blackwell, J., & Litt, M. H. (1979). Texture of cellulose crystallized from hydrazine. *Polymer, 20*, 145-147.

Battista, O.A. (1950). Hydrolysis and crystallization of cellulose. *Industrial & Engineering Chemistry, 42*, 502-507.

Battista, O. A., Coppick, S., Howsmon, J. A., Morehead, F. F. & Sisson, W.A. (1956). Level-off degree of polymerization -relation to polyphase structure of cellulose fibres. *Industrial & Engineering Chemistry, 48*, 333-335.

Beaumont, M., Nypelö, T., Kö nig, J., Zirbs, R., Opietnik, M., Potthast, A., & Rosenau, T. (2016). Synthesis of redispersible spherical cellulose II nanoparticles decorated with carboxylate groups. *Green Chemistry, 18*, 1465-1468.

Beck-Candanedo, S., Roman, M., & Gray, D. G. (2005). Effect of reaction conditions on the properties and behavior of wood cellulose nanocrystal suspensions *Biomacromolecules, 6*, 1048-1054.

Belgacem, M. N., Pizi, A. (2016). Lignocellulosic Fibers and Wood Handbook: Renewable Materials for Today's Environment. John Wiley & Sons/Scrivener Publishin, Hoboken/ Salem, Massachusetts.

Bernstein, J. (2002). Polymorphism in molecular crystals. Clarendon Press Oxford, New York.

Bettaieb, F., Khiari, R., Dufresne, A., Mhenni, M.F., & Belgacem, M. N. (2015). Mechanical and thermal properties of *Posidonia oceanica* cellulose nanocrystal reinforced polymer. *Carbohydrate Polymers, 123*, 99-104.

Boerjan, W., Ralph, J. & Baucher, M. (2003). Lignin biosynthesis. *Annual Review of Plant Biology, 54*, 519 -546.

Braconnot, H. (1819). Sur la conversion du corps ligneux en gomme, en sucre, et en un acide d'une nature particulière, par le moyen de l'acide sulfurique; conversion de la même substance ligneuse en ulmine par la potasse. *Annuaire de Chimie, 12*, 172-195.

Bras, J., Viet, D., Bruzzese, C., & Dufresne, A. (2011). Correlation between stiffness of sheets prepared from cellulose whiskers and nanoparticles dimensions. *Carbohydrate Polymers, 84*, 211-215.

Brejnholt, S. M. (2010). Pectin. In: Imerso, A. (eds). Food stabilizers, thickeners and gelling agents. John Wiley and Sons, pp. 237-264.

Brinchi, L., Cotana, F., Fourtunati, E., & Kenny, J. M. (2013). Production of nanocrystalline cellulose from lignocellulosic biomass: Technology and applications. *Carbohydrate Polymers, 94*, 154-169.

Buléon, A., & Chanzy, H. (1978). Single crystals of cellulose II. *Journal of Polymer Science, 16*, 833-839.

Campbell, F. C. (2010). Structural Composite Materials. ASM International.

Canale-Parola, E. (1970). Biology of the sugar-fermenting Sarcinae. *Bacteriological Reviews, 34*, 82-97.

Célino, A., Fréour, S., Jacquemin, F., & Casari, P. (2013). The hygroscopic behavior of plant fibers: a review. *Frontiers in Chemistry, 1*, 43.

Chanzy, H. D., & Roche, E. J. (1976). Fibrous transformation of *Valonia* cellulose I into cellulose II. *Applied Polymer Symposium, 28*, 701-711.

Chen, H. (2014). Biotechnology of lignocellulose: theory and practice. Chemical Industry Press, Beijing.

Cheng, M., Qin, Z., Liu, Y., Qin, Y., Li, T., Chen, L., & Zhu, M. (2014). Efficient extraction of carboxylated spherical cellulose nanocrystals with narrow distribution through hydrolysis of lyocell fibers by using ammonium persulfate as an oxidant. *Journal of Materials Chemistry A, 2*, 251-258.

Cherubini, F. (2010). The biorefinery concept: using biomass instead of oil for producing energy and chemicals. *Energy Conversion and Management, 51*, 1412-1421.

Cintrón, M.S., Johnson, G.P., French, A. (2011). Young's modulus calculations for cellulose I b by mm3 and quantum mechanics. *Cellulose, 18*, 505-516.

Cousins, S. K. & Brown, R. M. Jr. (1995). Cellulose I microfibril assembly: computational molecular mechanics energy analysis favours bonding by van der Waals forces as the initial step in crystallization. *Polymer, 36*, 3885-3888.

Cousins, S. K., & Brown, R. M. (1997). X-ray diffraction and ultrastructural analyses of dye-altered celluloses support van der Waals forces as the initial step in cellulose crystallization. *Polymer, 38*, 897-902.

da Silva, I. S.V., Flauzino Neto, W. P., Silvério, H. A., Pasquini, D., Andrade, M. Z., & Otaguro, H. (2015). Mechanical, thermal and barrier properties of pectin/cellulose nanocrystal nanocomposite films and their effect on the storability of strawberries (*Fragaria ananassa*). *Polymer Advanced Technologies.* doi: 10.1002/pat.3734.

de Gennes, P.G. (1976). On a relation between percolation theory and the elasticity of gels. *Journal of Physical Chemistry Letters, 37*, l-2.

de Rosa, C., & Auriemma, F. (2013). Crystals and Crystallinity in Polymers: Diffraction Analysis of Ordered and Disordered Crystals. John Wiley & Sons, Hoboken.

Delmer, D.P. & Amor, Y. (1995). Cellulose biosynthesis. *Plant Cell, 7*, 987-1000.

Ding, S., Zhao, S., & Zeng, Y. (2014). Size, shape, and arrangement of native cellulose fibrils in maize cell walls. *Cellulose, 21*, 863-871.

Dinwoodie, J. M. (1975). Timber- a review of the structure-mechanical property relationship. *Journal of Microscopy, 104*, 3-32.

Djahedi, C., Bergenstrahle-Wohlert, M., Berglund, L. A., & Wohlert, J., (2016). Role of hydrogen bonding in cellulose deformation: the leverage effect analyzed by molecular modeling. *Cellulose, 23*, 2315-2323.

dos Santos, R. M., Flauzino Neto, W. P., Silvério, H. A., Martins, D. F., Dantas, N. O., & Pasquini, D. (2013). Cellulose nanocrystals from pineapple leaf, a new approach for the reuse of this agro-waste. *Industrial Crops and Products, 50*, 707-714.

Dufresne, A. (2000). Dynamic mechanical analysis of the interphase in bacterial polyester/ cellulose whiskers natural composites. *Composite Interfaces, 7*, 53-67.

Dufresne, A. (2012). *Nanocellulose: From nature to high-performance tailored materials*. de Gruyter, Berlin/Boston.

Dufresne, A. (2013). Nanocellulose: a new ageless bionanomaterial. *Materials Today, 16*, 220-227.

Durán, N., Lemes, A. P., & Seabra, A. B. (2012). Review of cellulose nanocrystals patents: Preparation, composites and general applications. *Recent Patents on Nanotechnology, 6*, 16-28.

Earl, W. L., & VanderHart, D. L. (1981). Observations by high-resolution C-13 NMR of cellulose-I related to morphology and crystal-structure. *Macromolecules, 14*, 570-574.

Ebeling, T., Paillet, M., Borsali, R., Diat, O., Dufresne, A., Cavaille, J. Y. Chanzy, H. (1999). Shear-Induced Orientation Phenomena in Suspensions of Cellulose Microcrystals, Revealed by Small Angle X-ray Scattering. *Langmuir, 15*, 6123-6126.

Ebringerova, A., Hromadkova, Z. & Heinze, T. (2005). Hemicellulose. *Advances in Polymer Science, 186*, 1-67.

Eichhorn, S. J., Davies, G. R. (2006). Modelling the crystalline deformation of native and regenerated cellulose. *Cellulose, 13*, 291-307.

Elazzouzi-Hafraoui, S., Nishiyama, Y., Putaux, J-L., Heux, L., Dubreuil, F., & Rochas, C. (2008). The shape and size distribution of crystalline nanoparticles prepared by acid hydrolysis of native cellulose. *Biomacromolecules, 9*, 57-65.

Favier, V., Canova, G.R., Cavaillé, J.Y., Chanzy, H., Dufresne, A. & Gauthier, C. (1995a). Nanocomposites materials from latex and cellulose whiskers. *Polymers for Advanced Technologies, 6*, 351-355.

Favier, V., Chanzy, H. & Cavaillé, J.Y. (1995b). Polymer nanocomposites reinforced by cellulose whiskers. *Macromolecules, 28*, 6365-6367.

Fengel, D., Wegener, G. (1989). Wood: Chemistry, Ultrastructure, Reactions. de Gruyter, Berlin/New York.

Festucci-Buselli, R. A., Otoni, W. C., & Joshi, C. P. (2007). Structure, organization, and functions of cellulose synthase complexes in higher plants. *Brazilian Journal of Plant Physiology, 19*, 1-13.

Filpponen, I. & Argyropoulos, D. S. (2010). Regular Linking of Cellulose Nanocrystals via Click Chemistry: Synthesis and Formation of Cellulose Nanoplatelet Gels. *Biomacromolecules, 11*, 1060-1066.

Filson, P. B., & Dawson-Andoh, B. E. (2009). Sono-chemical preparation of cellulose nanocrystals from lignocellulose derived materials. *Bioresource Technology*, *100*, 2259-2264.

Fink, H. P., Philipp, B., Paul, D., Serimaa, R. & Paakkari, T. (1987). The structure of amorphous cellulose as revealed by wide-angle X-ray scattering. *Polymer, 28*, 1265-1270.

Flauzino Neto, W. P., Silvério, H. A., Dantas, N. O., & Pasquini, D. (2013). Extraction and characterization of cellulose nanocrystals from agro-industrial residue-soy hulls. *Industrial Crops and Products, 42*, 480-488.

Flauzino Neto, W.P., Mariano, M., da Silva, I.S.V., Putaux, J-L., Otaguro, H., Pasquini, D., & Dufresne, A., (2016a). Mechanical properties of natural rubber nanocomposites reinforced with high aspect ratio cellulose nanocrystals isolated from soy hulls. *Carbohydrate Polymers, 153*, 143-152.

Flauzino Neto, W.P., Putaux, J-L., Mariano, M., Ogawa, Y., Otaguro, H., Pasquini, D., & Dufresne, A., (2016b). Comprehensive morphological and structural investigation of cellulose I and II nanocrystals prepared by sulfuric acid hydrolysis. *Royal Society of Chemistry Advances, 6*, 76017-76027.

Gardner, K. H., & Blackwell, J. (1974). The structure of native cellulose. *Biopolymers, 13*, 1975-2001.

George, J., Ramana, K.V., Bawa, A.S., & Siddaramaiah. (2011). Bacterial cellulose nanocrystals exhibiting high thermal stability and their polymer nanocomposites. *International Journal of Biological Macromolecules, 48*, 50-57.

Grigoriew, H. & Chmielewski, A., G. (1998). Capabilities of X-ray methods in studies of processes of permeation through dense membranes. *Journal of Membrane Science, 142*, 87-95.

Gupta, P. K., Uniyal, V., & Naithani, S. (2013). Polymorphic transformation of cellulose I to cellulose II by alkali pretreatment and urea as an additive. *Carbohydrate Polymers*, *94*, 843-849.

Habibi, Y., Lucia, L. A., & Rojas, O. J. (2010). Cellulose nanocrystals: chemistry, self-assembly, and applications. *Chemical Reviews*, *110*, 3479-3500.

Håkansson, H. & Ahlgren, P. (2005). Acid hydrolysis of some industrial pulps: Effect of hydrolysis conditions and raw material. *Cellulose, 12*, 177-183.

Hamad, W. Y. (2017). Cellulose Nanocrystals: Properties, Production and applications. John Wiley & Sons, Hoboken.

Han, J. Q., Zhou, C. J., French, A. D., Han, G.P., & Wu, Q. L. (2013). Characterization of cellulose II nanoparticles regenerated from 1-butyl-3-methylimidazolium chloride. *Carbohydrate Polymers*, *94*, 773-781.

Hayashi, J., Masuda, S., & Watanabe, S. (1974). Plane Lattice Structure in Amorphous Region of Cellulose Fibers. *Nippon Kagaku Kaishi*, *1974*, 948-954.

Heinze, T., & Koschella, A. (2005). Solvents applied in the field of cellulose chemistry-a mini review. *Polímeros: Ciência e Tecnologia, 15*, 84-90.

Hermans, P. H. (1949). Degree of Lateral Order in Various Rayons as Deduced from X-Ray Measurements. *Journal of Polymer Science, 4*, 145-151.

Hon, D. N. S. (1994). Cellulose: a random walk along its historical path. *Cellulose, 1*, 1-25.

Hubbe, M. A., Rojas, O. J., Lucia, L. A., & Sain, M. (2008). Cellulosic nanocomposites: A review. *Bioresources, 3*, 929-980.

Ishikawa, A., Okano, T., & Sugiyama, J. (1997). Fine structure and tensile properties of ramie crystalline form of cellulose I, II, IIII and IVI, *Polymer, 38*, 463-468.

Isobe, N., Kimura, S., Wada, M., & Kuga, S. (2012). Mechanism of cellulose gelation from aqueous alkali-urea solution, *Carbohydrate Polymers, 89*, 1298-1300.

Jarvis, M. (2003). *Chemistry: cellulose stacks up*. *Nature, 426*, 611-612.

Jin, E., Guo, J., Yang, F., Zhu, Y., Song, J., Jin, Y., & Rojas, O. J. (2016). On the polymorphic and morphological changes of cellulose nanocrystals (CNC-I) upon mercerization and conversion to CNC-II. *Carbohydrate Polymers, 143*, 327-335.

John, M. J., & Thomas, S., (2008). Biofibres and biocomposites. *Carbohydrate Polymers, 71*, 343-364.

Kalia, S., Dufresne, A., Cherian, B. M., Kaith, B. S., Avérous, L., Njuguna, J., & Nassiopoulos, E. (2011). Cellulose Based Bio and Nanocomposites: A Review. *International Journal of Polymer Science, 2011*, 1-35.

Kamide, K. (2005). Cellulose and Cellulose Derivatives. Elsiever B. V., Amsterdam.

Kaushik, M., Fraschini, C., Grégory, C., Jean-Luc, P., & Moores, A. (2015). Transmission Electron Microscopy for the Characterization of Cellulose Nanocrystals. In: Khan Maaz (ed.) The Transmission Electron Microscope - Theory and Applications, InTech. doi: 10.5772/60985.

Kim, N., Imai, T., Wada, M., & Sugiyama, J. (2006). Molecular directionality in cellulose polymorphs. *Biomacromolecules, 7*, 274-280.

Klemm, D., Philipp, B., Heinze, T., Heinze, U., & Wagenknecht, W. (1998). Fundamentals and analytical methods. Comprehensive Cellulose Chemistry. Weinheim: Wiley - VCH, Darmstadt.

Klemm, D., Heublein, B., Fink, H. P., & Bohn, A. (2005). Cellulose: Fascinating biopolymer and sustainable raw material. *Angewandte Chemie Inernational Edition, 44*, 2-37.

Klemm, D., Kramer, F., Moritz, S., Lindström, T., Ankerfors, M., & Gray, D. (2011). Nanocelluloses: A new family of nature-based materials. *Angewandte Chemie International Edition, 50*, 5438-5466.

Kobayashi, J., Sakamoto, S., & Kimura, S. (2001). In vitro synthesis of cellulose and related polysaccharides. *Progress in Polymer Science, 26*, 1525-1560.

Kovacs, T., Naish, V., O'Connor, B., Blaise, C., Gagné, F., Hall, L., Trudeau, V., Martel, P. (2010). An ecotoxicological characterization of nanocrystalline cellulose (NCC). *Nanotoxicology, 2010*; 4, 255-70.

Kovalenko, V. I. (2010). Crystalline cellulose: structure and hydrogen bonds. *Russian Chemical Reviews, 79*, 231-241.

Koyama M., Helbert, W., Imai T., Sugiyama J., & Henrissat, B. (1997). Parallel-up structure evidences the molecular directionality during biosynthesis of bacterial

cellulose. *Proceedings of the National Academy of Sciences of the United States of America, 94*, 9091-9095.

Krässig, H. A. (1993). Cellulose: Structure, accessibility and reactivity. Gordon and Breach Science Publishers, Yverdon.

Kroon-Batenburg, L. M. J., Kroon, J., Northolt, M.G. (1986). Chain modulus and intramolecular hydrogen bonding in native and regenerated cellulose fibers. *Polymer, 27*, 290-292.

Kuga, S., Takagi, S., & Brown, R. M. Jr. (1993). Native folded-chain cellulose II. *Polymer, 34*, 3293-3297.

Kulasinski, K., Keten, S., Churakov, S. V., Derome, D. & Carmeliet, J. (2014). *Cellulose, 21*, 1103-1116.

Kumar, V., Reus-Medina, M. D. L. L., & Yang, D. (2002). Preparation, characterization, and tabletting properties of a new cellulose-based pharmaceutical aid. *International Journal of Pharmaceutics, 235*, 129–140.

Kümmerer, K., Menz, J., Schubert, J., & Thielmens, W. (2011). Biodegradability of organic nanoparticles in the aqueous environment. *Chemosphere, 82*, 1387-1392.

Lam, E., Male, K. B., Chong, J. H., Leung, A. C. W., Luong, J. H. T. (2012). Applications of functionalized and nanoparticle-modified nanocrystalline cellulose. *Trends in Biotechnology, 30*, 283-290.

Langan, P., Nishiyama, Y., & Chanzy, H. (1999). A revised structure and hydrogen-bonding system in cellulose II from a neutron fiber diffraction analysis. *Journal of the American Chemical Society, 121*, 9940-9946.

Langan, P., Nishiyama, Y., & Chanzy, H. (2001). X-ray structure of mercerized cellulose II at 1 angstrom resolution. *Biomacromolecules, 2*, 410-416.

Langan, P., Sukumar, N., Nishiyama, Y., & Chanzy, H. (2005). Synchrotron X-ray structures of cellulose I_β and regenerated cellulose II at ambient temperature and 100 K. *Cellulose, 12*, 551-562.

Lazko, J., Sénéchal, T., Landercy, N., Dangreau, L., Raquez, J.- M., & Dubois, P. (2014). Well defined thermostable cellulose nanocrystals via two-step ionic liquid swelling-hydrolysis extraction. *Cellulose, 21*, 4195-4207.

Lee, C. M., Mittal, A., Barnette, A. L., Kafle, K., Park, Y. B., Shin, H., Johnson. D. J.,Park. S., & Him, S. H. (2013). Cellulose polymorphism study with sum frequency-generation (SFG) vibration spectroscopy: identification of exocyclic CH2OH conformation and chain orientation. *Cellulose, 20*, 991-1000.

Leung, A. C. W., Hrapovic, S., Lam, E., Liu, Y., Male, K. B., Mahmoud, K. A., & Luong, J. H. T. (2011). Characteristics and properties of carboxylated cellulose nanocrystals prepared from a novel one-step procedure. *Small, 7*, 302-305.

Li, Q., & Renneckar, S. (2011). Supramolecular Structure Characterization of Molecularly Thin Cellulose I Nanoparticles. *Biomacromolecules, 12*, 650-659.

Li, S., Bashline, L., Lei, L., & Gu, Y. (2014). Cellulose Synthesis and Its Regulation. *The Arabidopsis Book/American Society of Plant Biologists, 12*, 1-21.

Libert, T. (2009). Cellulose solvents-remarkable history, bright future. In: Liebert, T., Heinz, T. J. & Edgar, K. J. (eds). Cellulose solvent: for analysis, shaping and chemical modifications. ACS symposium series Washington DC, pp. 3-54.

Lin, N., & Dufresne, A. (2014a). Surface Chemistry, Morphological Analysis and Properties of Cellulose Nanocrystals with Gradiented Sulfation Degrees. *Nanoscale, 6*, 5384-5393.

Lin, N., & Dufresne, A. (2014b). Nanocellulose in biomedicine: Current status and future prospect. *European Polymer Journal 59*, 302-325.

Lin, N. Cellulose Nanocrystals: Surface Modification and Advanced Materials. 2014. Doctoral Thesis- Materials, Mechanics, Civil Engineering, Electrochemistry, Université Grenoble Alpes, Grenoble, 2014.

Lindman, B., Karlstrom, G., & Stigsson, L. (2010). On the mechanism of dissolution of cellulose. *Journal of Molecular Liquids, 156*, 76-81.

Liu, Y. P., & Hu, H. (2008). X-ray diffraction study of bamboo fibers treated with NaOH. *Fibers and Polymers, 9*, 735-739.

Mandal, A., & Chakrabarty, D. (2011). Isolation of nanocellulose from waste sugarcane bagasse (SCB) and its characterization. *Carbohydrate Polymers, 86*, 1291-1299.

Mansikkamaki, P., Lahtinen, M., & Rissanen, K. (2005). Structural changes of cellulose crystallites induced by mercerisation in different solvent systems; determined by powder X-ray diffraction method. *Cellulose, 12*, 233-242.

Mao, J., Heck, B., Reiter, G., & Laborie, M.-P. (2015). Cellulose nanocrystals' production in near theoretical yields by 1-butyl-3- methylimidazolium hydrogen sulfate ([Bmim]HSO_4) – mediated hydrolysis. *Carbohydrate Polymers, 117*, 443-451.

Mariano, M., El Kissi, N., & Dufresne, A. (2014). Cellulose nanocrystals and related nanocomposites: Review of some properties and challenges. *Journal of Polymer Science B, 52*, 791-806.

Mariano, M. Applications of Cellulose Nanocrystals: Thermal, rheological and mechanical properties of new materials. 2016. Doctoral Thesis- Materials, Mechanics, Civil Engineering, Electrochemistry, Université Grenoble Alpes, Grenoble, 2016.

Medronho, B., Romano, A., Miguel, M. G., Stigsson, L., & Lindman, B. (2012). Rationalizing cellulose (in) solubility: reviewing basic physicochemical aspects and role of hydrophobic interactions. *Cellulose, 19*, 581-587.

Medronho, B., & Lindman, B. (2014). Competing forces during cellulose dissolution: From solvents to mechanisms. *Current Opinion in Colloid & Interface Science, 19*, 32-40.

Medronho, B., & Lindman, B. (2015). Brief overview on cellulose dissolution/regeneration interactions and mechanisms. *Advances in Colloid and Interface Science, 222*, 502-508.

Meyer, K., & Misch, L. (1937). Position des atomes dans le nouveau modele spatial de la cellulose. Sur la constitution de la partie cristallisse´e de la cellulose VI. *Helvetica Chimica Acta, 20*, 232-244.

Miao, C., & Hamad, W. Y. (2013). Cellulose reinforced polymer composites and nanocomposites: a critical review. *Cellulose, 20*, 2221-2262.

Miller-Chou, B. A., & Koenig, J. L. (2003). A review of polymer dissolution. *Progress in Polymer Science, 28*, 1223-1270.

Miyamoto, H., Ago, M., Yamane, C., Seguchi, M., Ueda, K., & Okajima, K. (2011) Supermolecular structure of cellulose/amylose blends prepared from aqueous NaOH solutions and effects of amylose on structural formation of cellulose from its solution. *Carbohydrate Research, 346*, 807-814.

Miyamoto, H., Umemura, M., Aoyagi, T., Yamane, C., Ueda, K., & Takahashi, K. (2009). Structural reorganization of molecular sheets derived from cellulose II by molecular dynamics simulations, *Carbohydrate Research, 344*, 1085-1094.

Miyamoto, H., Yuguchi, Y., Rein, D. M., Cohen Y., Ueda, K., & Yamane, C. (2016). Structure of cellulose/direct dye complex regenerated from supercritical water *Cellulose, 23*, 2099-2115.

Monica, E. K., Gellerstedt, G., & Henriksson, G. (2009). *Wood Chemistry and Wood Biotechnology Volume 1*. de Gruyter, Berlin, Boston.

Moon, R. J., Martini, A., Nairn, J., Simonsen, J., & Yougblood, J., (2011). Cellulose nanomaterials review structure, properties and nanocomposites. *Chemical Society Reviews, 40,* 3941-3994.

Mülhaupt, R., (2004). Hermann Staudinger and the Origin of Macromolecular Chemistry. *Angewandte Chemie International Edition, 43,* 1054-1063.

Nechyporchuk, O. Cellulose nanofibers for the production of bionanocomposites. 2015. Doctoral Thesis- Chemical and Process Engineering, Université Grenoble Alpes, Grenoble, 2015.

Ng, H.-M., Sin, L.T., Tee, T. T., Bee, S-T., Hui, D., Low, Chong-Yu., & Rahmat, A. R. (2015). Extraction of cellulose nanocrystals from plant sources for application as reinforcing agent in polymers, *Composites Part B: Engineering, 75*, 176-200.

Nishimura, H., Okano, T., & Sarko, A. (1991a). Mercerization of cellulose: 5. Crystal and molecular structure of Nacellulose I. *Macromolecules, 24*, 759-770.

Nishimura, H., Okano, T., & Sarko, A. (1991b). Mercerization of cellulose: 6. Crystal and molecular structure of Nacellulose I. *Macromolecules, 24*, 771-778.

Nishiyama, Y., Kuga, S., & Okano, T. (2000). Mechanism of mercerization revealed by X-ray diffraction. *Journal of Wood Science, 46,* 452-457.

Nishiyama, Y., Langan, P., & Chanzy, H. (2002). Crystal structure and hydrogen-bonding system in cellulose 1β from synchrotron X-ray and neutron fiber diffraction. *Journal of the American Chemical Society, 124*, 9074-9082.

Nishiyama, Y., Sugiyama, J., Chanzy, H. & Langan, P. (2003b). Crystal structure and hydrogen bonding system in cellulose 1(alpha), from synchrotron X-ray and neutron fiber diffraction. *Journal of the American Chemical Society, 125,* 14300-14306.

Nishiyama, Y., Kim, U. J., Kim, D.Y., Katsumata, K. S., May, R. P. & Langan, P. (2003a). Disorder along ramie cellulose microfibrils. *Biomacromolecules, 4*, 1013-1017.

Nishiyama, Y. (2009). Structure and properties of the cellulose microfibril. *Journal of Wood Science, 55*, 241-249.

Novo, L. P., Bras, J., García, A., Belgacem, N., & Curvelo, A. A. S. (2015). Subcritical water: A method for green production of cellulose nanocrystals. *ACS Sustainable Chemistry & Engineering, 3,* 2839-2846.

Okano, T., & Sarko, A. (1984). Mercerization of cellulose I. X-ray Diffraction evidence for intermediate structures. *Journal of Applied Polymer Science, 29*, 4175-4182.

Okano, T., & Sarko, A. (1985). Mercerization of cellulose: II. Alkali cellulose intermediates and a possible mercerization mechanism. *Journal of Applied Polymer Science, 30*, 325-332.

Oksman, K., Aitomäki, Y., Mathewa, A. P., Siqueira, G., Zhoud, Q., Butylina, S., Tanpichai, S., Zhou, X., & Hooshmand, S. (2016). Review of the recent developments in cellulose nanocomposite processing. *Composites Part A: Applied Science and Manufacturing, 83*, 2-18.

Olsson, C., & Westman, G. (2013). Direct Dissolution of Cellulose: Background, Means and Applications. In: van de Ven, T., & Goldbout, L. (eds). Cellulose - Fundamental Aspects. InTech, pp143-178. DOI: 10.5772/52144.

Ostlund, A., Idstrom, A., Olsson, C., Larsson, P. T., & Nordstierna, L. (2013). Modification of crystallinity and pore size distribution in coagulated cellulose films. *Cellulose, 20*, 1657-1667.

O'Sullivan, A. C. (1997). Cellulose: the structure slowly unravels. *Cellulose, 4*, 173-207.

Ouali, N., Cavaillé, J. Y., & Perez, J. (1991). Elastic, viscoelastic and plastic behavior of multiphase polymer blends. *Plastics and Rubber Processing and Applications, 16*, 55-60.

Park, S., Johnson, D. K., Ishizawa, C. I., Parilla, P. A., & Davis, M. F. (2009). Measuring the crystallinity index of cellulose by solid state ^{13}C nuclear magnetic resonance. *Cellulose, 16*, 641-647.

Park, S., Baker, J. O., Himmel, M. E., Parilla, P. A., & Johnson, D. K. (2010). Cellulose crystallinity index: Measurement techniques and their impact on interpreting cellulase performance. *Biotechnology for Biofuels, 3*, 1-10.

Payen, A. (1838). Memoire sur la composition du tissu propre des plantes et du ligneux. *Comptes Rendus Chimie, 7*, 1052-1056.

Peng, B. L., Dhar, N., Liu, H. L., & Tam, K. C. (2011). Chemistry and applications of nanocrystalline cellulose and its derivatives: a nanotechnology perspective. *The Canadian Journal of Chemical Engineering, 9999*, 1-16.

Pérez, S., & Mazeau, K. (2004). Conformations, Structures and Morphologies of Celluloses. In: Dimitriu, S. (eds). Polysaccharides: Structural Diversity and Functional Versatility. Marcel Dekker, pp 41-68.

Porro, F., Bedue, O., Chanzy, H., & Heux, L. 2007. Solid-state C-13 NMR study of Na-cellulose complexes. Biomacromolecules 8, 2586-2593.

Qian, X., Ding, S.-Y., Nimlos, M., R., Johnson, D., K., & Himmel, M., E. (2005). Atomic and Electronic Structures of Molecular Crystalline Cellulose Iβ: A First-Principles Investigation. *Macromolecules, 38,* 10580-10589.

Qin, Z. Y., Tong, G. L., Frank Chin, Y. C., & Zhou, J. C. (2011). Preparation of ultrasonicassisted high carboxylate content cellulose nanocrystals by TEMPO oxidation. *BioResources, 6,* 1136-1146.

Ramos, L. P. (2003). The chemistry involved in the steam treatment of lignocellulosic materials. *Química Nova, 26,* 863-871.

Rånby, B. G. (1951). III. Fibrous macromolecular systems. Cellulose and muscle. The coloidal properties of cellulose micelles. *Faraday Society, 11,* 158-164.

Revol, J.-F. (1982). On the cross-sectional shape of cellulose crystallites in *Valonia ventricosa*. *Carbohydrate Polymers, 2,* 123-134.

Ritter, S. K. (2008). Sustainability. *Chemical & Engineering News, 86,* 59-68.

Roman, M. (2015). Toxicity of Cellulose Nanocrystals: A Review. *Industrial Biotechnology, 11,* 25-33.

Sacui, I. A., Nieuwendaal, R. C., Burnett, D. J., Stranick, S. J., Jorfi, M., Weder, C., Foster, E. J., Olsson, R. T., & Gilman, J. W. (2014). Comparison of the properties of cellulose nanocrystals and cellulose nanofibrils isolated from bacteria, tunicate, and wood processed using acid, enzymatic, mechanical, and oxidative methods. *Applied Materials & Interfaces, 6,* 6127-6138.

Sasaki, M., Adschiri, T., & Arai, K. (2003). Production of cellulose II from native cellulose by near- and supercritical water solubilization. *Journal of Agricultural and Food Chemistry, 51,* 5376-5381.

Satyamurthy, P., Jain, P., Balasubramanya, R. H., Vigneshwaran, N. (2011). Preparation and characterization of cellulose nanowhiskers from cotton fibres by controlled microbial hydrolysis. *Carbohydrate Polymers, 83,* 122-129.

Saxena, I. M., & Brown, R. M. (2005). Cellulose Biosynthesis: Current Views and Evolving Concepts. *Annals of Botany, 96,* 9-21.

Saxena, A. Nanocomposites based on nanocellulose whiskers. 2013. Doctoral Thesis-Chemistry and Biochemistry, Georgia Institute of Technology, 2013. Atlanta, 2013.

Schenzel, K., Fischer, S. & Brendler, E. (2005). New Method for Determining the Degree of Cellulose I Crystallinity by Means of FT Raman Spectroscopy. *Cellulose 12,* 223-231.

Schoeck, J., Davies, R. J., Martel, A., & Riekel, C. (2007). Na-cellulose formation in a single cotton fiber studied by synchrotron radiation microdiffraction. *Biomacromolecules, 8*, 602-610.

Sèbe G., Ham-Pichavant, F., Ibarboure, E., Koffi, A. L. C., & Tingaut, P. (2012). Supramolecular structure characterization of cellulose II nanowhiskers produced by acid hydrolysis of cellulose I substrates. *Biomacromolecules, 13*, 570-578.

Silva, R., Haraguchi, S. K., Muniz, E. C., & Rubira, A. F. (2009a). Aplicações de fibras lignocelulósicas na química de polímeros e em compósitos. *Química Nova, 32*, 661-671.

Silva, D. J., & D'Almeida, M. L. O. (2009b). Cellulose Whiskers. *O Papel, 70*, 34-52.

Sinko, R., Mishra, S., Ruiz, L., Brandis, N., & Keten, S. (2013). Dimensions of biological cellulose nanocrystals maximize fracture strength. *ACS Macro Letters, 3*, 64-69.

Siqueira, G., Bras, J. & Dufresne, A. (2010). New process of chemical grafting of celulose nanoparticles with a long chain isocyanate. *Langmuir, 26*, 402-411.

Siró, I., & Plackett, D. (2010). Microfibrillated cellulose and new nanocomposite materials: a review. *Cellulose, 17*, 459-494.

Sisson, W. (1938). The existence of mercerized cellulose and its orientation in *Halicystis* as indicated by x-ray diffraction analysis. *Science, 87*, 350-351.

Sperling, L. H. (2006). Introduction to Physical Polymer Science. Wiley John Wiley & Sons, Hoboken.

Staudinger, H. (1920). Über Polymerisation. *European Journal of Inorganic Chemsitry, 53*, 1073-1085.

Staudinger, H. (1926). Die Chemie der hochmolekularen organischen Stoffe im Sinne der Kekule`schen Strukturlehre. *Berichte der deutschen chemischen Gesellschaft, 56*, 3019-3043.

Stauffer, D. (1985). Introduction to Percolation Theory. Taylor and Francis, London /Philadelphia.

Šturcova, A., Davies, G. R., & Eichhorn, S. J. (2005). Elastic modulus and stress-transfer properties of tunicate cellulose whiskers. *Biomacromolecules, 6*, 1055-1061.

Takayanagi, M., Uemura, S., & Minami, S. (1964). Application of equivalent model method to dynamic rheo-optical properties of crystalline polymers. Journal of *Polymer Science Part C: Polymer Symposia 5*, 113-122.

Tashiro, K., & Kobayashi, M. (1991). Calculation of crystallite modulus of native cellulose. *Polymer Bulletin, 14*, 213-218.

TAPPI 2011. “Roadmap for the development of international standards for nanocellulose”. Published at October 24th 2011. http://www.tappinano.org/media/1070/2011-roadmapfornanocellulosestandards.pdf

Varshney, V. K., & Naithani, S. (2011). Chemical Functionalization of Cellulose Derived from Nonconventional Sources. In: Kalia, S., Kaith, B. S., & Kaur, I. (eds). Cellulose Fibers: Bio- and Nano-Polymer Composites. Springer Berlin Heidelberg, pp 43-60.

Visanko, M., Liimatainen, H., Sirviö, J. A., Heiskanen, J. P., Niinimäki, J., & Hormi, O. (2014). Amphiphilic cellulose nanocrystals from acid free oxidative treatment: Physicochemical characteristics and use as an oil-water stabilizer. *Biomacromolecules, 15*, 2769-2775.

Wada, M., Chanzy, H., Nishiyama, Y., & Langan, P. (2004). Cellulose IIII Crystal Structure and Hydrogen Bonding by Synchrotron X-ray and Neutron Fiber Diffraction. *Macromolecules, 37*, 8548-8555.

Wada, M., Nishiyama, Y., Chanzy, H., Forsyth, T., & Langan, P. (2008). The structure of celluloses. *Powder Diffraction, 23*, 92-95.

Wang, H., Li, D., Yano, H., & Abe, K. (2014). Preparation of tough cellulose II nanofibers with high thermal stability from wood. *Cellulose, 21*, 1505-1515.

Wohlert, J., Bergenstrahle-Wohlert, M., & Berglund, L. A. (2012). Deformation of cellulose nanocrystals: entropy, internal energy and temperature dependence. *Cellulose, 19*, 1821-1836.

Yamamoto, H. & Horii, F. (1993). CP/MAS 13C NMR analysis of the crystal transformation induced for valonia cellulose by annealing at high temperatures. *Macromolecules, 26*, 1313-1317.

Yamane, C., Aoyagi, A., Ago, M., Sato, K., Okajima, K., & Takahashi. T. (2006). Two different surface properties of regenerated cellulose resulting from structural anisotropy. *Polymer Journal, 38*, 819-826.

Yamane, C., Miyamoto, H., Hayakawa, D., & Ueda, K. (2013). Folded-chain structure of cellulose II suggested by molecular dynamics simulation. *Carbohydrate Research, 379*, 30-37.

Yamane, C., Hirase, R., Miyamoto, H., Kuwamoto, S., & Yuguchi, Y. (2015). Mechanism of structure formation and dissolution of regenerated cellulose from cellulose/aqueous sodium hydroxide solution and formation of molecular sheets deduced from the mechanism. *Cellulose, 22*, 2971-2982.

Yang, Q., & Pan, X. (2010). A Facile Approach for Fabricating Fluorescent Cellulose. *Journal of Applied Polymer Science, 117*, 3639-3644.

Yang, D., Peng, X-W., Zhong, L-X., Cao, X-F., Chen, W., & Sun, R-C. (2013). Effects of pretreatments on crystalline properties and morphology of cellulose nanocrystals. *Cellulose, 20*, 2427-2437.

Yue, Y., Zhou, C., French, A. D., Xia, G., Han, G., Wang, Q., & Wu, Q. (2012). Comparative properties of cellulose nanocrystals from native and mercerized cotton fibers. *Cellulose, 19*, 1173-1187.

Zhang, Y. H., Cui, J., Lynd, L. R., Kuang, L. R. (2006). A transition from cellulose swelling to cellulose dissolution by o-phosphoric acid: evidence from enzymatic hydrolysis and supramolecular structure. *Biomacromolecules, 7*, 644-648.

http://www.celluforce.com (accessed 16 September 2016)

http://www.americanprocess.com (accessed 16 September 2016)

http://www.tappinano.org/media/1114/cellulose-nanomaterials-production-state-of-the-industry-dec-2015.pdf (accessed 16 September 2016)

CHAPTER II

Comprehensive morphological and structural investigation of cellulose I and II nanocrystals prepared by sulfuric acid hydrolysis

This chapter is based on paper "*Comprehensive morphological and structural investigation of cellulose I and II nanocrystals prepared by sulfuric acid hydrolysis*", published in 2016 in RSC Advances, 6, 76017-76027.

CONTENT CHAPTER II

ABSTRACT 78
1. INTRODUCTION 79
2. EXPERIMENTAL 80
2.1. Materials 80
2.2. Preparation of cellulose nanocrystals 81
2.2.1. Nanocrystals from native cellulose 81
2.2.2. Nanocrystals from mercerized cellulose 81
2.2.3. Nanocrystals from regenerated cellulose 81
2.3. CNC powders 82
2.4. Shear-oriented CNC fibers 82
2.5. Characterization 82
2.5.1. Elemental analysis 82
2.5.2. Zeta potential 82
2.5.3. Viscometry 82
2.5.4. Scanning electron microscopy 83
2.5.5. Transmission electron microscopy 83
2.5.6. X-ray diffraction 84
2.5.7. Fourier-transform infrared spectroscopy 84
2.5.8. Solid-state nuclear magnetic resonance 85
3. RESULTS 85
3.1. Characterization of native and mercerized cellulose fibers 85
3.2. Characterization of cellulose nanocrystals 87
3.2.1. Yield, chain length, sulfur content, surface charge and zeta potential 87
3.2.2. Morphology and crystal structure 88
4. DISCUSSION 97
4.1. Sulfur content and surface charge 97
4.2. Three-dimensional shape and crystal orientation of the CNCs 97
5. CONCLUSIONS 101
6. REFERENCES 101
7. APPENDIX A 108

ABSTRACT

Cellulose nanocrystals (CNCs) were produced from eucalyptus wood pulp using three different methods: i) classical sulfuric acid hydrolysis (CN-I), ii) acid hydrolysis of cellulose previously mercerized by alkaline treatment (MCN-II), and iii) solubilization of cellulose in sulfuric acid and subsequent recrystallization in water (RCN-II). The three types of CNCs exhibited different morphologies and crystal structures that were characterized using complementary imaging, diffraction and spectroscopic techniques. CN-I corresponded to the type I allomorph of cellulose while MCN-II and RCN-II corresponded to cellulose II. CN-I and MCN-II CNCs were acicular particles composed of a few laterally-bound elementary crystallites. In both cases, the cellulose chains were oriented parallel to the long axis of the particle, although they were parallel in CN-I and antiparallel in MCN-II. RCN-II particles exhibited a slightly tortuous ribbon-like shape and it was shown that the chains lay perpendicular to the particle long axis and parallel to their basal plane. The unique molecular and crystal structure of the RCN-II particles implies that a higher number of reducing chain ends are located at the surface of the particles, which may be important for subsequent chemical modification. While other authors have described nanoparticles prepared by regeneration of short-chain cellulose solutions, no detailed description was proposed in terms of particle morphology, crystal structure and chain orientation. It was provided such a description in the present study.

Keywords: cellulose nanocrystals, sulfuric acid hydrolysis, crystal morphology, regenerated cellulose, mercerized cellulose, cellulose allomorphs.

1. INTRODUCTION

Cellulose is a linear biopolymer consisting of *β*-(1,4)-linked *D*-glucopyranose units, occurring in nature in the form of slender semicrystalline nanofibrils where highly ordered regions (the crystallites) alternate with less organized ones (Gardner & Blackwell, 1974). In this so-called cellulose I (Cel-I), the chains are parallel and can be packed into two allomorphs, namely Iα (triclinic) and Iβ (monoclinic). Most native celluloses contain a mixture of both allomorphs in various ratios (Atalla & VanderHart, 1984). Several other allomorphs have been described, most of which result from chemical treatments of Cel-I. These allomorphs differ by the packing and polarity of the constituting chains, as well as the hydrogen bond patterns established between them (Wada *et al.*, 2008).

Among these allomorphs, cellulose II (Cel-II), in which the chains are antiparallel (Kolpak & Blackwell, 1976; Langan *et al.*, 2001, 2005), can be prepared from Cel-I by two distinct processes. Mercerization is an essentially solid-state process during which cellulose fibers are swollen in alkali and recrystallized into cellulose II upon washing (Warwicker, 1967). An interdigitation mechanism was proposed to account for the fibrous transition from Cel-I to Cel-II: upon swelling, the cellulose chains from neighboring nanofibrils of opposite polarity would intermingle and recrystallize into the antiparallel form upon washing and drying (Nishiyama *et al.*, 2000; Okano & Sarko, 1985). In the second process, cellulose is first dissolved and then regenerated by recrystallizing the chains into Cel-II upon washing (Medronho & Lindman, 2015). The Cel-I to Cel-II transition is irreversible, which suggests that Cel-II is thermodynamically more stable.

From an industrial point of view, Cel-II is used to prepare materials such as films (cellophane), textile fibers (rayon, lyocell), membranes for dialysis, filtration and chromatography (Cuprophan), papers (for packaging and printing purpose), pharmaceutical pellets (for drug release) and cellulose derivatives (such as methylcellulose and carboxymethylcellulose) (Gupta *et al.*, 2013; Han *et al.*, 2013; Kumar *et al.*, 2002; Liu & Hu, 2008; Sasaki et al, 2003).

Due to the combination of unique physicochemical properties and environmental appeal, cellulose nanocrystals (CNCs) have enjoyed a large interest in the recent years (Dufresne, 2012; Habibi *et al.*, 2010). CNCs are usually prepared by strong sulfuric acid hydrolysis that preferentially degrades the disordered regions of the native cellulose nanofibrils. An additional mechanical or sonication treatment releases rod-like

nanocrystals that form stable colloidal suspensions (Marchessault *et al.*, 1959; Mukherjee & Woods, 1953). In addition, the shape and size of the CNCs depend on the source of cellulose (Brito *et al.*, 2012; Chauve *et al.*, 2013; Elazzouzi-Hafraoui *et al.*, 2008). CNCs offer a wide range of potential applications in fields ranging from packaging to biomedicine. Several unique properties, such as high specific strength and modulus, high aspect ratio, low density, large specific surface area and reactive surfaces that can facilitate the grafting of chemical species to confer and tailor new properties, stimulate their use in new functional and advanced materials (dos Santos *et al.*, 2013; Dufresne, 2012; Eichhorn, 2011; Mariano *et al.*, 2014; Moon *et al.*, 2011).

So far, investigations of Cel-II have mostly focused on fibers and only a few recent studies have been carried out on CNCs. Cel-II nanocrystals have been prepared either by acid hydrolysis of mercerized fibers (Hirota *et al.*, 2012; Kim *et al.*, 2006; Yue *et al.*, 2012), mercerization of Cel-I CNCs (Jin *et al.*, 2016), or after recrystallization of fractions of short cellulose chains in solution (Dhar *et al.*, 2015; Hirota *et al.*, 2012; Hu *et al.*, 2014; Sèbe *et al.*, 2012). However, while these studies have generally combined the data from several imaging, diffraction and spectroscopic techniques, a complete structural picture of the nanocrystals has not been reported so far. The purpose of our work was thus to produce and characterize cellulose nanocrystals prepared from native eucalyptus Cel-I fibers by i) sulfuric acid hydrolysis, ii) acid hydrolysis of fibrous Cel-II obtained by mercerization of Cel-I, and iii) recrystallization (regeneration) of cellulose chains produced by stronger acid hydrolysis of native cellulose. We compared the morphology, crystal structure, crystallinity index, surface charge and degree of polymerization of the three types of nanocrystals that were characterized by complementary techniques, namely elemental analysis, zetametry, viscometry, transmission electron microscopy (TEM), atomic force microscopy (AFM), X-ray diffraction (XRD), Fourier-transform infrared and solid-state nuclear magnetic resonance spectroscopies (FTIR and NMR, respectively).

2. EXPERIMENTAL

2.1. Materials

Sulfuric acid (95.0-98.0 wt%, Vetec, P.A.), bis(ethylenediamine) copper(II) hydroxide solution 1.0 M in H_2O (Panreac) and cellulose membrane (Spectra/Por 1 Dialysis Membrane) were used as received. Bleached Kraft wood pulp sheets of eucalyptus urograndis hybrid (*Eucalyptus urophylla* and *grandis*) were provided by

Conpacel Company (Limeira, São Paulo, Brazil). This pulp was chosen as raw material because it has high cellulose content. Its chemical composition was determined as described by dos Santos *et al.* (2013): 92% cellulose, 6% hemicelluloses, 0% lignin and 0.3% minerals.

2.2. Preparation of cellulose nanocrystals

2.2.1. Nanocrystals from native cellulose

The bleached Kraft eucalyptus wood pulp (WP) was ground in a Fourplex mill equipped with a 16-*mesh* sieve and then hydrolysed with sulfuric acid. The hydrolysis was performed at 45°C for 50 min under vigorous stirring. For each gram of WP, it was used 20 mL of 60 wt% H_2SO_4. Immediately following the hydrolysis, the material (an ivory-white dispersion) was diluted 10-fold with cold deionized water to stop the hydrolysis reaction, and centrifuged twice for 10 min at 10,000 rpm to remove the excess acid. The precipitate was then dialyzed against deionized water to remove non-reactive sulfate groups, salts and soluble sugars, until a neutral pH was reached. The resulting dialyzed suspension was ultrasonicated for 15 min in an ice bath (Branson sonifier 250 - maximum power of 200 W - operating at a duty cycle of 50% and output of 40%) and stored in a refrigerator. Drops of sodium hypochlorite were added to avoid bacterial growth. The resulting nanocrystals will be referred to as "CN-I" in the following.

2.2.2. Nanocrystals from mercerized cellulose

The milled WP was treated with a 20 wt% sodium hydroxide aqueous solution under mechanical stirring for 5 h at 25°C, using 30 mL of solution per gram of material. The material was washed several times with distilled water until the alkali was completely removed, and dried at 40°C for 12 h in an air-circulating oven. The mercerized pulp (MWP) was milled again and submitted to sulfuric acid hydrolysis, using the same conditions as those applied for the preparation of CN-I. This sample will be referred to as "MCN-II".

2.2.3. Nanocrystals from regenerated cellulose

The hydrolysis of ground eucalyptus WP was carried out with 64 wt% H_2SO_4 at 40°C for 20 min. The subsequent steps of dilution with water, centrifugation, and dialysis were carried out using the same conditions as those used for the preparation of CN-I. Following hydrolysis, the solution was transparent and upon addition of water, it became

an ivory-white dispersion. Under these hydrolysis conditions, the cellulose fibers were thus solubilized and the soluble chains precipitated by addition of water, which corresponds to the so-called regeneration process. The resulting nanocrystals will be referred to as "RCN-II".

2.3. CNC powders

CNC powders of the three samples were prepared by freeze-drying 0.5 wt% suspensions.

2.4. Shear-oriented CNC fibers

Oriented fibers were prepared from the CNC suspensions using the method described by Nishiyama *et al.* (2008). Briefly, the suspensions were centrifuged and the pellets were mixed with polyvinyl alcohol (PVA). A saturated solution of sodium borate (borax) was added to cross-link PVA and yield a viscoelastic gel that was uniaxially stretched with tweezers to form a fiber and left to dry under load.

2.5. Characterization

2.5.1. Elemental analysis

The total sulfur content S% of the samples was determined by elemental analysis using an Element Analyser (Perkin-Elmer Series II, CHNS/O Analyzer 2400) from the freeze-dried CNC powders. The values were converted to the number *n* of $–OSO_3H$ groups of the CNC samples per 100 anhydroglucose units, using the method described in details by Hu *et al.* (2014).

2.5.2. Zeta potential

The zeta-potential ζ of 0.01 wt% CNC suspensions was measured on a Malvern DTS0230 instrument. All suspensions were diluted in an aqueous standard solution at pH 7, 5 mmol ionic strength and 200 $\mu S.cm^{-1}$ conductivity, prepared by the addition of diluted NaOH solution and solid NaCl into deionized water.

2.5.3. Viscometry

The viscosimetric average degree of polymerization ($\overline{\mathbf{DP}_v}$) of CNC samples was calculated according to TAPPI T 230 OM-99 (1999) standard, from the value of intrinsic viscosity [η] of the samples. The [η] value was obtained by measuring the flow of solvent

and solutions with Ostwald's viscometer (type n° 50, 100 or 150 depending on the sample molecular weight). The solvent used was a mixture of a solution of bis(ethylenediamine) copper (II) hydroxide and deionized water. The intrinsic viscosity [η] was determined from Equation (7).

$$[\eta] = \frac{\sqrt{[2(\eta_{sp} - \ln \eta_{rel})]}}{C} \qquad \text{Eq. (7)}$$

where η_{rel} is the relative viscosity given by the ratio of the flow time of the CNC suspension and the flow time of the solvent, η_{sp} is the specific viscosity given by (η_{rel} - 1), and C is the concentration of the CNC suspension in g·mL^{-1}. The $\overline{DP_v}$ was calculated using the equation recommended by the standard method SCAN-C15:62 (1980):

$$\overline{DP_v}^{0.905} = 0.75[\eta] \qquad \text{Eq. (8)}$$

where the values of 0.905 and 0.75 are constants characteristic of the polymer-solvent system and [η] is expressed in mL·g^{-1}.

2.5.4. Scanning electron microscopy (SEM)

Fragments of wood pulp were fixed on metal stubs using double-sided carbon tape. Some fibers were cut with a razor blade in order to visualize their cross-section. All specimens were coated with Au/Pd and observed in secondary electron mode in a Quanta 250 FEI microscope operating at 10 kV.

2.5.5. Transmission electron microscopy (TEM)

Drops of 0.001 wt% CNC suspensions were deposited onto glow-discharged copper grids coated with a carbon support film. The specimens were negatively stained with 2 wt% uranyl acetate. Other specimens were kept unstained for electron diffraction purpose and mounted in a Gatan 626 specimen holder. After introduction in the microscope, the holder was cooled with liquid nitrogen and the specimen was observed at low temperature (-180°C) under low illumination. All specimens were observed with a Philips CM200 'Cryo' transmission electron microscope (FEI) operating at 200 kV. Images and diffraction patterns were recorded on a TVIPS TemCam F216 camera. The average dimensions of CNC populations were determined from the TEM images by measuring the length and width of about 100 particles using the ImageJ software.

2.5.6. X-ray diffraction (XRD)

Strips of CNC films prepared by casting were fixed on a 0.2 mm collimator in such a way that the films were oriented either perpendicular or parallel to the X-ray beam. Fragments of PVA/CNC fibers were directly taped on the collimator. All specimens were placed in a vacuum chamber and X-rayed in transmission mode using a Philips PW3830 generator producing a Ni-filtered CuKα radiation (λ = 0.1542 nm), and operating at 30 kV and 20 mA. Two-dimensional (2D) diffraction patterns were recorded on Fujifilm imaging plates read with a Fujifilm BAS-1800II bioimaging analyser. Diffraction profiles were obtained by radially averaging the intensity over fan-shaped portions of the 2D spectra. A crystallinity index (CI) was calculated after peak deconvolution of the diffraction profiles (Park *et al.*, 2010). The peak fitting was carried out using pseudo-Voigt functions. CI was calculated using Equation 9:

$$\mathbf{CI} = \mathbf{100} \times \left(\frac{\boldsymbol{A_c}}{\boldsymbol{A_c + A_a}}\right) \qquad \text{Eq. (9)}$$

where A_c and A_a are the areas under the crystalline peaks and the amorphous halo, respectively, determined by deconvolution between 2θ = 10 and 30°.

The dimension D_{hkl} of the crystallites perpendicular to the hkl diffracting planes was estimated from the peak broadening in the XRD profiles after deconvolution, using Scherrer's equation:

$$\mathbf{D_{hkl}} = \frac{\boldsymbol{K\lambda}}{\boldsymbol{\beta_{1/2}\cos\theta}} \qquad \text{Eq. (10)}$$

where K is a correction factor usually taken as 0.9 for cellulose, λ is the X-ray wavelength, θ is the diffraction angle and $\beta_{1/2}$ is the peak width at half maximum intensity (Klug & Alexander, 1974).

2.5.7. Fourier-transform infrared spectroscopy (FTIR)

CNC powders were mixed with KBr in a ratio sample/KBr of 1:100 by mass to prepare compressed pellets and absorption spectra were recorded with a Perkin-Elmer Spectrum One instrument, in the range of 600-4000 cm^{-1}, a resolution of 4 cm^{-1} and a total of 16 scans for each sample.

2.5.8. Solid-state nuclear magnetic resonance (NMR)

Solid-state ^{13}C-NMR experiments were performed on a Bruker AVANCE 400 spectrometer using a combination of cross-polarization, high power proton decoupling and magic angle spinning (CP/MAS). ^{13}C-NMR spectra were acquired at 298 K, with a 4 mm probe operating at 100.13 MHz. MAS rotation was 12 kHz, CP contact times 2 ms and repetition time 1 s. The CI of the samples was also estimated from ^{13}C-NMR data by comparing the areas for the peaks of crystalline and amorphous C4. By analogy with equation (10), the calculation was done by dividing the area of crystalline peak (86 to 94 ppm) by the total area assigned to the C4 peak (80 to 94 ppm).

3. RESULTS

3.1. Characterization of native and mercerized cellulose fibers

The SEM images in Figure 27 show the morphological differences between the native wood pulp (WP) fibers and the mercerized ones (MWP).

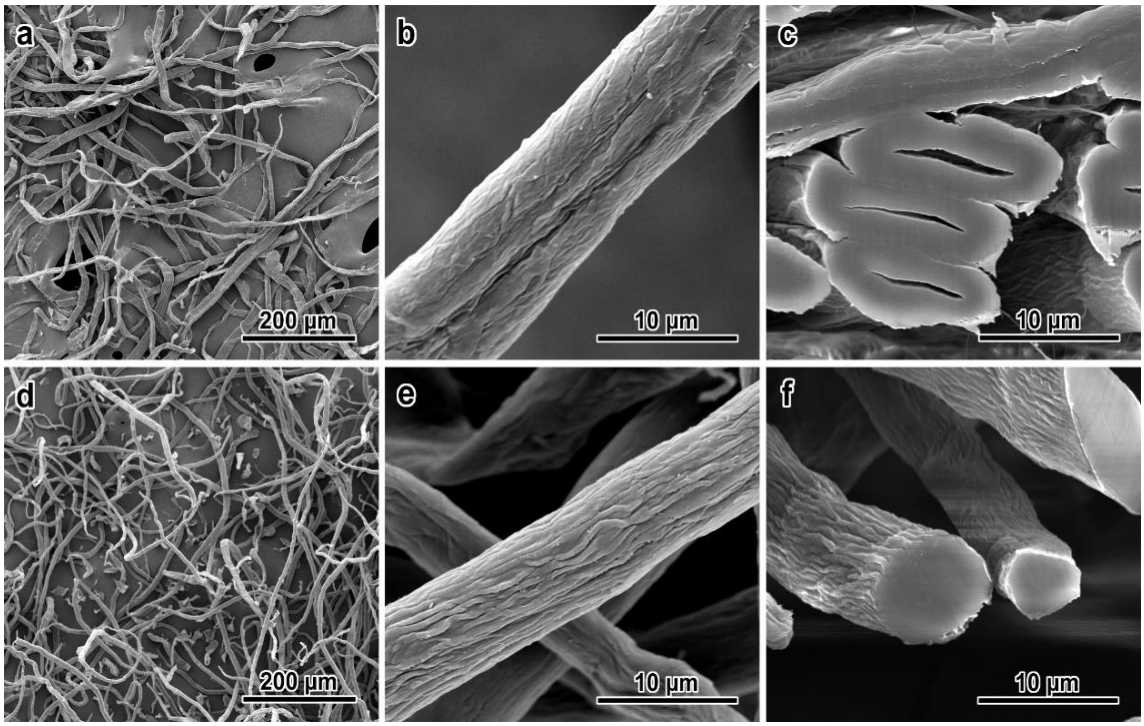

Figure 27 – SEM images of initial (a–c) and mercerized (d–f) wood pulp fibers (WP and MWP, respectively). In (c) and (f), the fibers were cut with a razor blade revealing their cross-section.

The raw WP fibers are long tortuous and sometimes twisted flat tubes with a relatively smooth surface (Figure 27a-c), whereas the MWP fibers are solid cylinders, the lumen having collapsed during the alkaline treatment (Figure 27d-f). The surface of the

MWP fibers exhibits a sub-fibrillar structure that most likely corresponds to bundles of nanofibrils, which is consistent with what was observed for mercerized pinewood pulp (Sharma *et al.*, 2015) and cotton fibers (Yue *et al.*, 2013). The mercerization process also affects the tortuosity and swelling of the fibers (*i.e.*, the fiber untwists and swells). However, the fibrous structure is largely kept intact after mercerization. The mercerized material is whiter, indicating that, after the alkali treatment, a part of the initial non-cellulosic components (hemicellulose, pectins, *etc*) was removed by this process. The yield of mercerization, calculated on the initial amount of dried cellulose fibers was 83% (Table 1). In addition, there was no significant change in the $\overline{\mathbf{DP}_v}$ values estimated by viscosity measurements: 898 and 920 for WP and MWP, respectively.

The XRD patterns recorded from WP and MWP fibrillar bundles are shown in Figure 28. The fiber pattern of WP is typical of native wood Cel-I. It contains 3 equatorial arcs assigned to $(\mathbf{1\bar{1}0})_{\mathbf{I}}$, $(110)_{\mathrm{I}}$, and $(200)_{\mathrm{I}}$ planes (indices of allomorph Iβ), as well as the characteristic thin meridional arc corresponding to the $(004)_{\mathrm{I}}$ planes (Figure S3a in Appendix A) (French, 2014). The CI calculated for this sample after peak deconvolution is 33% (Table 2).

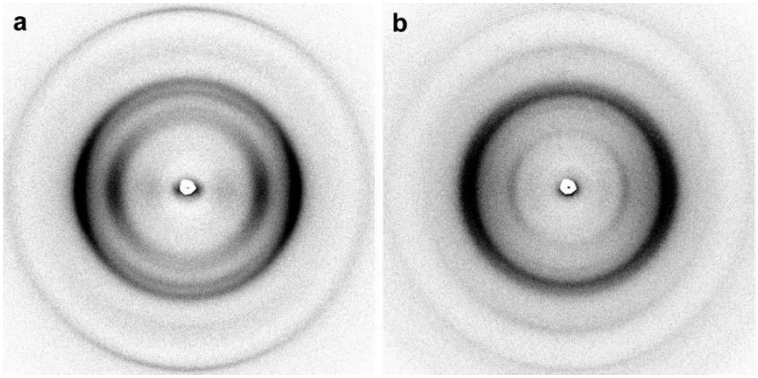

Figure 28 – X-ray diffraction patterns of initial (a) and mercerized (b) wood pulp fibers (WP and MWP, respectively). The fibrillar bundles are vertical with respect to the patterns.

The XRD pattern of MWP is clearly different and typical of Cel-II, displaying three main arcs on the equator, corresponding to the $(\mathbf{1\bar{1}0})_{\mathbf{II}}$, $(110)_{\mathrm{II}}$, and $(020)_{\mathrm{II}}$ planes (Figure S3b) (French, 2014). The mercerization process thus resulted in a total allomorphic conversion from Cel-I to Cel-II. The calculated CI was 53% (Table 2) but its comparison with that of WP is not straightforward since the crystal structure for both specimens is different.

3.2. Characterization of cellulose nanocrystals

3.2.1. Yield, chain length, sulfur content, surface charge and zeta potential

The yield of the three preparation protocols as well as $\overline{\mathbf{DP}_v}$, sulfur content, surface charge and zeta potential ζ of the resulting CNC samples are given in Table 1. Seeing that lower yields around 30% are often reported in the literature, our values can be considered as high and are consistent with other reports (Bendahou *et al.*, 2009; Han *et al.*, 2013; Hu *et al.*, 2014; Tonoli *et al.*, 2012). The $\overline{\mathbf{DP}_v}$ of CNC samples were 115, 54 and 17 for CN-I, MCN-II and RCN-II, respectively. The formula used in this study to calculate the $\overline{\mathbf{DP}_v}$ is recommended for characterization of unsulfated celluloses with a DP between 90 and 3,000. Thus, the DP values assessed by means of viscosity-average molecular weight are only an estimate of the chain length of the samples.

Table 1. Yield, sulfur content, surface charge, number of $–OSO_3H$ groups per 100 anhydroglucose units, zeta potential (ζ) and viscometric average degree of polymerization ($\overline{\mathbf{DP}_v}$) of the fibers and CNCs. "na": not applicable.

Sample	Yield (%)	Sulfur content (%)	Surface charge (mmol.g^{-1})	Number of $–OSO_3H$ groups per 100 anhydroglucose units	ζ (mV.cm^{-1})	$\overline{DP_v}$
WP	n. a.	0.94	Na	Na	Na	898 ± 18
MWP	83[a]	0.98	Na	Na	Na	920 ± 14
CN-I	64[a] / 70[b]	1.36	0.424	7.12	-33.5 ± 2.0	115 ± 3
MCN-II	55[a] / 60[b] / 66[c]	1.43	0.464	7.49	-35.7 ± 1.5	54 ± 3
RCN-II	44[a] / 48[b]	1.75	0.546	9.25	-30.0 ± 0.9	17 ± 1

[a] calculated with respect to the initial amount of dried wood pulp.

[b] based on the initial cellulose content.

[c] calculated with respect to the initial amount of mercerized fibers.

The sulfur content (Table 1) is related to the presence of anionic sulfate ester groups on the CNC surface created by esterification of hydroxyl groups during the sulfuric acid treatment, thus leading to colloidal CNC dispersions in water electrostatically stabilized by repulsive forces, as indicated by the negative ζ values (Table 1). The differences between the sulfur content values can be ascribed to the acid treatment conditions, since stronger sulfuric hydrolysis conditions are expected to result in higher levels of esterification sulfation (Lin & Dufresne, 2014; Roman & Winter, 2004). The ζ values of the three samples are rather close (-33.5 ± 2.0 mV·cm^{-1} for CN-I,

-35.7 ± 1.5 mV·cm^{-1} for MCN-II and -30.0 ± 0.9 mV·cm^{-1} for RCN-II), and considering that the zeta potential may also depend on the shape, size and structure of the particles, the small difference may not be significant and directly related to the sulfur content.

Table 2. Crystallinity index (CI) of the samples estimated from XRD data (CI^{XRD}) and ^{13}C-NMR data (CI^{NMR}) after peak deconvolution.

Sample	CI^{XRD} (%)	CI^{NMR} (%)
WP	33	-
MWP	53	-
CN-I	56	50
MCN-II	68	63
RCN-II	66	60

3.2.2. Morphology and crystal structure

Figure S1 shows the formation of birefringent domains induced by shear alignment of CNCs in aqueous suspensions under agitation. This effect results from the intrinsic shape and optical anisotropy of rod-like CNCs (Cranston & Gray, 2008). Thus, this behavior hints that well-dispersed of anisometric nanosized cellulose particles were obtained in all three isolation procedures. In general, the critical concentration at which the particles self-organize depends on their aspect ratio and on the electrostatic repulsion (Heux *et al.*, 2000). Consequently, for the same concentration, the weaker shear-induced birefringence exhibited by the RCN-II suspension may be explained by a smaller particle aspect ratio.

TEM micrographs of the different CNC samples are shown in Figure 29 and the CNC dimensions measured from TEM (average length $\bar{L}$ and width $\bar{D}$) and AFM (average thickness $\bar{H}$) images (Figure S2) are summarized in Table 3.

Table 3. Average dimensions of the CNCs. The length $\bar{L}$ and width $\bar{D}$ have been calculated from TEM images of negatively stained preparations of CN-I, MCN-II and RCN-II while the thickness $\bar{H}$ has been determined from height profiles in AFM images. The aspect ratio was calculated as $\bar{L}$ / $\bar{D}$.

Sample	$\bar{L}$ (nm)	$\bar{D}$ (nm)	$\bar{H}$ (nm)	Aspect ratio
CN-I	240 ± 52	15.1 ± 1.4	3.8 ± 0.9	16
MCN-II	132 ± 19	18.9 ± 2.2	5.2 ± 1.0	7
RCN-II	102 ± 10	12.0 ± 1.2	2.7 ± 0.6	8.5

The shape and size of the three types of particles are clearly different. CN-I (Figure 29a-b) contains rod-like particles typical of nanocrystals prepared by conventional acid hydrolysis of native higher plant cellulose (Brito at al., 2012; Chauve *et al.*, 2013). They are generally composite objects made of a few laterally-bound crystallites, in agreement with what was shown for cotton CNCs by Elazzouzi-Hafraoui *et al.* (2008). As illustrated for CN-I particles shown in Figure 30a-c, the shape and number of constituting crystallite significantly vary so that it is rather difficult to clearly define a 'typical' particle. Their average length and width determined from TEM images of negatively stained preparations are $\bar{L}$ = 240 ± 52 nm and $\bar{D}$ = 15.1 ± 1.4 nm, respectively (Figure 29a-b), while a thickness $\bar{H}$ = 3.8 ± 0.9 nm was measured from height profiles on AFM images (Figure S2a).

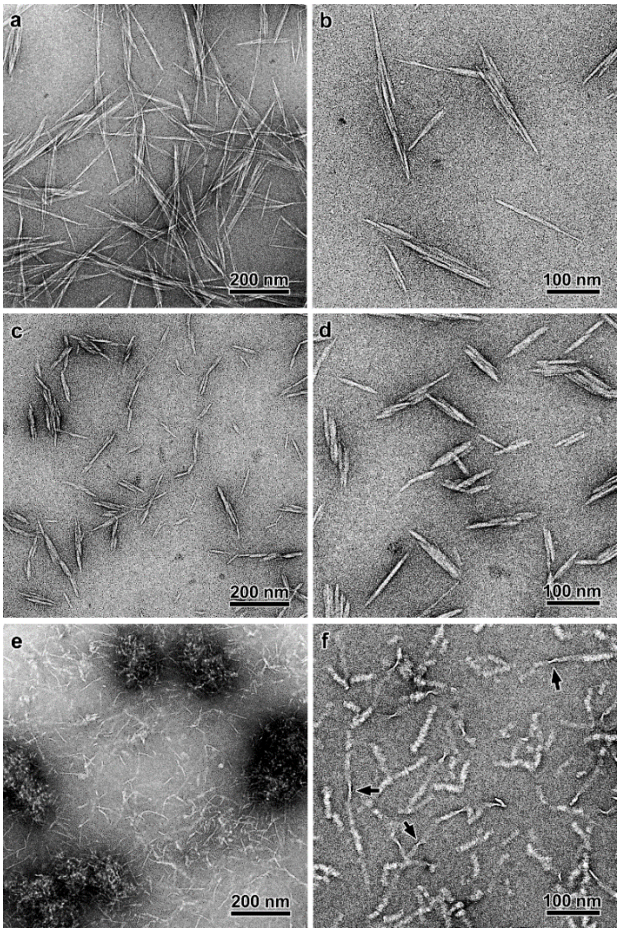

Figure 29 – TEM images of negatively stained CN-I (a and b), MCN-II (c and d) and RCN-II (e and f) nanocrystals. The arrows in (f) indicate twist regions.

MCN-II particles are also rod-shaped but shorter and wider: $\bar{L}$ = 132 ± 19 nm, $\bar{D}$ = 18.9 ± 2.2 nm, $\bar{H}$ = 5.2 ± 1.0 (Figures 29c-d and Figure S2b). Like for CN-I, these particles are composite objects (Figure 30d-f).

As seen in Figure 29e, the RCN-II suspension contains dense aggregates coexisting with vermicular objects. As these aggregates resisted mild sonication, we could not study them in details and focused our analysis on the individual particles. These acicular particles are more tortuous, longer ($\bar{L}$ = 102 ± 10 nm) and thinner ($\bar{D}$ = 12.0 ± 1.2) than MCN-II nanocrystals (Figure 29f). The thickness measured from AFM images ($\bar{H}$ = 2.7 ± 0.6 nm) (Figure S2c) and the distribution of negative stain in TEM images (Figures 29f, 30h and 30i) suggests that the particles are ribbon-shaped. As indicated by arrows in Figures 29f, 30h and 30i, white regions are locally observed that likely correspond to local twists of the ribbons. The ribbons would thus be seen edge-on and the width of these regions is about 3 nm, in good agreement with the thickness measured by AFM (Table 3). Although the resolution of these TEM images is mainly limited by the granularity of the dry stain, the particles seem to be composed of imperfectly stacked lamellar subunits (Figure 30g).

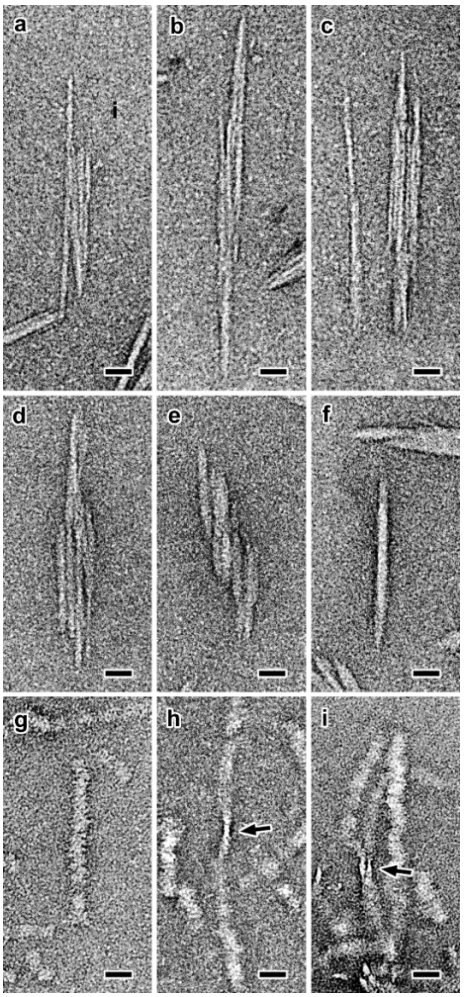

Figure 30 – Higher magnification TEM images of CN-I (a-c), MCN-II (d-f) and RCN-II (g-i) particles (negative staining). The arrows in (h) and (i) indicate twist regions. Scale bars: 20 nm.

The two-dimensional XRD patterns recorded from CNC films and shear-oriented PVA/CNC fibers are shown in Figure 31. When the films were oriented perpendicular to the X-ray beam (Figure 31a-c), the patterns were mostly of powder type, exhibiting a number of concentric diffraction rings. When the films were oriented parallel to the X-ray beam (Figure 31d-f), all samples yielded fiber patterns with a distribution of diffraction arcs. This is consistent with the fact that rod-shaped particles tend to take an in-plane orientation during drying. Their long axis lies parallel to the plane of the film but the azimuth of this axis is randomly oriented. The rings in the pattern of the CN-I film (Figure 31a) are not strictly uniform in intensity due to some orientation of the rod-like particles during drying, an effect previously reported by Elazzouzi-Hafraoui *et al.* (2008) for nanocrystals prepared from other cellulose sources. Like for the parent fibers, the XRD pattern of CN-I is typical of Cel-I, although the five main diffraction rings are more clearly defined. The CI value is 56% (Table 2). This increase with respect to the CI of the initial WP fibers (33%) is consistent with the fact that acid hydrolysis has preferentially degraded disorganized regions that contributed to the amorphous background in the XRD pattern for WP.

The XRD patterns for MCN-II and RCN-II films (Figures 31b and 31c, respectively) correspond to Cel-II, exhibiting the $1\bar{1}0_{II}$ and well-separated 110_{II} and 020_{II} rings (Figures S3b and S3c). For MCN-II, the intensities of the latter two are similar whereas for RCN-II, the intensity of 110_{II} is higher, suggesting some uniplanarity of the particles in the film. The *d*-spacings, summarized in Table 4, are consistent with previously reported measurements (Atkins *et al.*, 1979; Hu *et al.*, 2014; Sèbe *et al.*, 2012). The CI value for MCN-II is 68% (Table 2), higher than that of the mercerized fibers (53%), and the CI of RCN-II is 66%, which is lower than the value that Hu *et al.* (2014) estimated for their regenerated Cel-II nanocrystals using a similar deconvolution method (93%).

The CN-I fiber pattern recorded from a film parallel to the X-ray beam is similar to that of the parent WP fibers but it is better resolved and contains equatorial arcs assigned to $(1\bar{1}0)_I$, $(110)_I$, and $(200)_I$ planes, and a thin meridional arc corresponding to the $(004)_I$ planes (Figures 31d and S3a). The pattern of the MCN-II film contains the $1\bar{1}0_{II}$, 110_{II} and 020_{II} arcs in equatorial position whereas a thin 002_{II} meridional reflection can be seen (Figures 31e and S3b). The $1\bar{1}0_{II}$ reflection remains equatorial in the pattern of the RCN-II film but the strong 110_{II} arc is now oriented along the meridian. The 020_{II} reflection is expected to lie at a 65° angle with respect to the equator (Atkins *et al.*, 1979)

but due to some degree of misorientation, this reflection and its mirror counterpart with respect to the meridian are merged into a unique larger arc (Figures 31f and S3c).

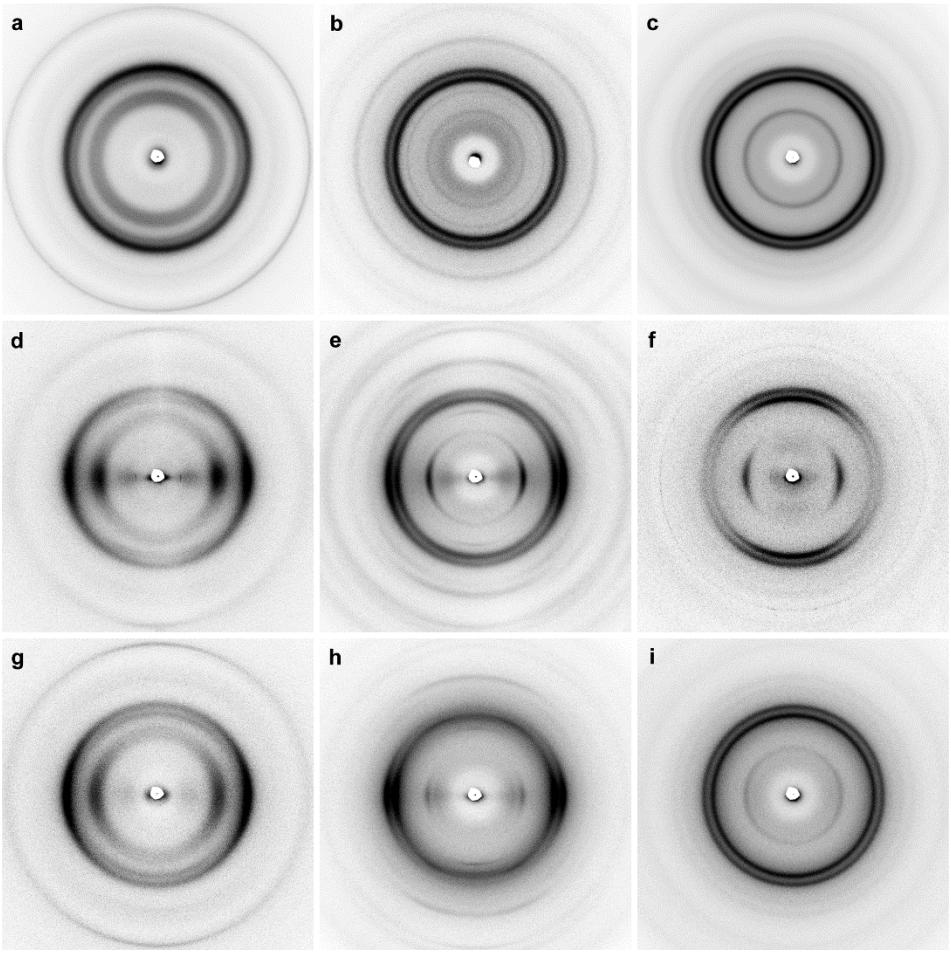

Figure 31 – Two-dimensional wide-angle X-ray diffraction patterns of CN-I (a,d and g), MCN-II (b,e and h) and RCN-II (c,f and i) specimens: a-c) the films were oriented perpendicular to the X-ray beam; d-f) the films were parallel to the X-ray beam and vertical with respect to the patterns; g-i) PVA/CNC fibers oriented vertical with respect to the patterns. In f, the thin ring at large diffraction angle was attributed to some contaminant.

Figures 31g-i show the XRD patterns for shear-oriented PVA/CNC fibers. In the case of CN-I and MCN-II, the resulting fiber patterns are a proof that the acicular nanocrystals were oriented along the stretching direction. This did not seem to be the case for RCN-II whose pattern only exhibits a very weak orientation (Figure 31i). The reason for this lack of orientation is unclear since the aspect ratio of RCN-II particles is close to that of MCN-II nanocrystals that aligned well along the shear direction (Table 3). Particle aggregation during the preparation of the PVA/CNC mixture may have occurred, or a large amount of the aggregates seen in Figure 29e was present, thus limiting the orientation during shear. In addition, the ribbon shape and associated twisting effect may

induce some flexibility in the particles which would also add to the lack of orientation. However, one can note that the relative intensity of the $\mathbf{1\bar{1}0_{II}}$ reflection is significantly lower compared to that in Figure 31f, and that the intensity of the 110_{II} ring is still stronger than that of 020_{II}.

Table 4. *d*-Spacings and associated crystal widths corresponding to the three main reflections in the XRD profiles of the fibers and CNCs. The indexes are those defined by French (2014).

	hkl	$\mathbf{1\bar{1}0_{I}}$	110_{I}	200_{I}
	d-spacing (nm)	0.60	0.53	0.39
CN-I	crystallite size (nm)	2.98	3.01	4.35
	hkl	$\mathbf{1\bar{1}0_{II}}$	110_{II}	020_{II}
	d-spacing (nm)	0.73	0.44	0.40
MCN-II	crystallite size (nm)	5.85	5.03	4.71
RCN-II	crystallite size (nm)	5.03	5.82	5.58

Selected area electron diffraction patterns were recorded from unstained specimens at low temperature, as shown in Figure S4. For CN-I and MCN-II, it was possible to find bundles of locally aligned nanocrystals so that fiber patterns were recorded. The patterns from the three samples are thus similar to the XRD diagrams of the corresponding shear-oriented PVA/CNC fibers (Figs. 31g-i). For CN-I, the thin 004_{I} meridional reflection is clearly marked, as well as the strong equatorial 200_{I} and the merged $\mathbf{1\bar{1}0_{I}}$ and 110_{I} reflections (Figure S4a). For MCN-II, the thin meridional 004_{II} reflection appears and the strong equatorial 110_{II} and 020_{II} arcs have similar intensities (Figure S4b). The pattern of the RCN-II sample does not reveal any clear orientation, probably because the nanocrystals are shorter which does not promote the formation of locally oriented bundles upon drying. However, the fact that the 110_{II} reflection is more intense than 020_{II} indicates a strong uniplanarity of the nanocrystals on the supporting carbon film (Figure S4c). These data recorded by electron diffraction on a small number of particles are thus in good agreement with those collected by XRD from larger populations of CNCs.

The size of the elementary crystallites constituting the three types of CNC was evaluated from the broadening of the three stronger peaks in the XRD profiles corresponding to the powder patterns in Figure 31a-c, using Scherrer's equation (Eq. 10).

The results are summarized in Table 4 and were used to propose shapes of the cross-sections of the crystallites (Figure S5). The cross-section of CN-I crystallites is squarish (approximately 3 × 3 nm^2), with surfaces corresponding to $(\mathbf{1\bar{1}0})_{\mathbf{I}}$ and $(110)_I$ planes (Figure S5a), which is consistent with the thickness determined from AFM images (Table 3) and the estimation of the width of the laterally associated crystallites that constitute CN-I CNCs (Figure 30a-c). This shape and dimensions were also reported for CNC prepared from Avicel (Elazzouzi-Hafraoui *et al.*, 2008) and wood pulp from various sources (Brito *et al.*, 2012). By dividing the average width of CN-I particles by that of the elementary crystallites, one finds that the CNC contains an average of 5 laterally bound units, in good agreement with the TEM images in Figures 29a,b and 30a-c. The elementary crystallites in MCN-II particles are wider than those in CN-I, which is consistent with the TEM observations (Figure 30d-f), and would have the shape of a truncated parallelogram (Figure S5b). MCN-II particles would thus be made of 3-4 crystallites.

From the XRD data, the cross-section of the RCN-II elementary crystallites would have a more or less hexagonal shape with an average diameter of 5.5 nm (Figure S5c). The direct comparison with the TEM images is more difficult since, as suggested by diffraction analyses, the chains would be oriented perpendicular to the long axis of the particle. Consequently, the cross-section of the ribbons cannot be visualized, except, possibly, in the twist regions (Figure 30h-i). However, the width of these regions, in agreement with the thickness measured by AFM, is close to 3 nm, which is about twice smaller than the size deduced form the XRD data. Figure S5d describes the cross-section that was deduced from the analysis of TEM and AFM micrographs. The reason of the discrepancy between the images and the XRD data is unclear. One possibility is that the aggregates that coexist with the ribbon-like nanocrystals contain Cel-II particles with a different morphology and that the XRD data correspond to an average of both types of particles. In that stage, the TEM images cannot be used to quantitatively evaluate the relative amounts of aggregates and individual ribbons and further work is needed to clarify this point.

Figure 32 shows the FTIR spectra for the three types of CNCs. All spectra exhibit the typical absorption peaks and bands assigned to cellulose, although small differences can be seen between them due to the different crystal structures. Considering the broad band for the –OH stretching vibration in the range of 3700-3000 cm^{-1}, the spectra for MCN-II and RCN-II display two distinctive peaks at 3491 and 3447 cm^{-1} related to

intramolecular hydrogen bonding in Cel-II. The intensity of the peak at 1430 cm^{-1} associated to the $–CH_2–(C_6)–$ bending vibration decreases significantly in the spectra for MCN-II and RCN-II compared to CN-I, owing to the change in conformation of hydroxymethyl group from *tg* to *gt* form. The CO at C-6 stretching vibration peak at 1035 cm^{-1} for CN-I was shifted to 1029 and 1027 cm^{-1} for MCN-II and RCN-II, respectively. This could be explained by changes in the torsional angles of *β*-(1,4)-D-glycosidic linkages. Similarly, the COC vibration at *β*-glycosidic linkage was switched from 898 in CN-I to 895 cm^{-1} for MCN-II and RCN-II. The absorption band at 711 cm^{-1} assigned to Iβ cellulose was detected for CN-I, while the absorption band at 750 cm^{-1} ascribed to Iα was not clearly seen. It means that this sample (CN-I) is rich in the Iβ allomorph. These FTIR results indicate that both mercerization and regeneration procedures transformed the cellulose crystal structure from Iβ to II. Moreover, these results are consistent with other reports in the literature (Dhar *et al.*, 2015; Han *et al.*, 2013; Oh *et al.*, 2005; Zuluaga *et al.*, 2009).

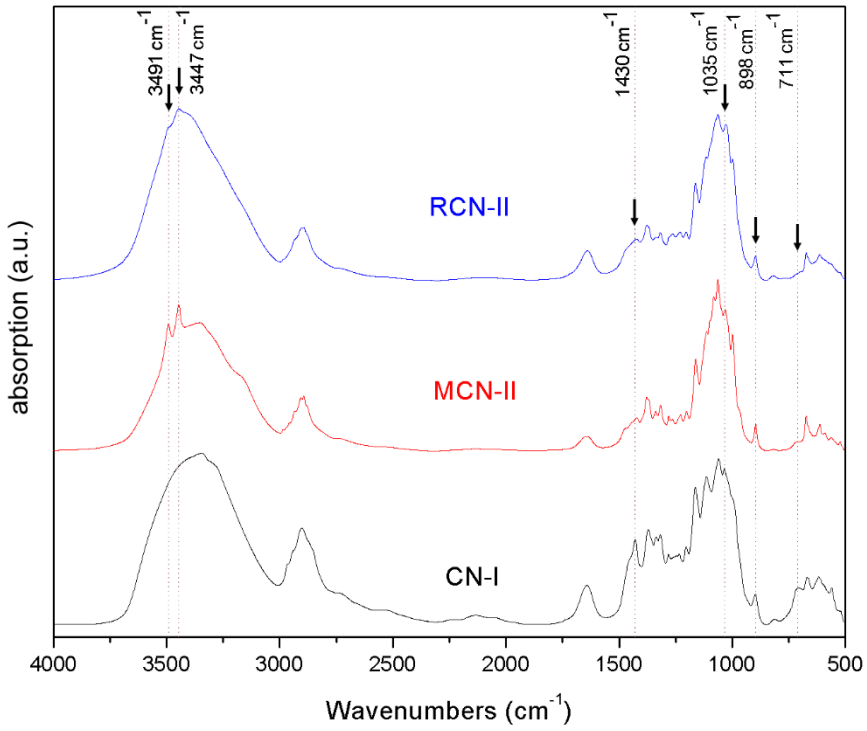

Figure 32 – Fourier-transform infrared absorption spectra of CN-I, MCN-II and RCN-II powders in KBr pellets.

The ^{13}C-NMR spectra recorded from the three CNC samples are shown in Figure 32. The peaks common to all spectra are those from the carbons of the carbohydrate moiety, which appear between 58 and 110 ppm. The signal from 58 to 67 ppm is attributed

to the C6 of the primary alcohol group. The cluster between 69 and 80 ppm is associated to the C2, C3, and C5 carbons. The region between 80 and 94 ppm corresponds to C4 and that between 95 and 110 ppm with the anomeric carbon C1 (Martins *et al.*, 2006; Sèbe *et al.*, 2012). The CN-I spectrum displays the typical chemical shifts assigned to the crystal lattice of (Iβ rich type). The signals at 104 and 106 ppm can be identified (zoom-in view in Figure 32). The spectra for MCN-II and RCN-II are typical of Cel-II, as revealed by the presence of peaks at 76 and 107 ppm and the absence of a peak at 65 ppm (Zuluaga *et al.*, 2009). The main difference was observed near 97 ppm, where a small peak only present for RCN-II has been attributed to C1 anomeric carbons of the end monomer units (C1 reducing end of cellulose), which can be detected when the DP of cellulose is sufficiently low (Sèbe *et al.*, 2012; Sharma *et al.*, 2014). Hence, this suggests that the cellulose chains are shorter in RCN-II than in CN-I and MCN-II. This is in agreement with the DP values determined from viscometry measurements (Table 1), and with the results of Hu *et al.* (2014) that showed that the acid-soluble cellulose chains that recrystallize have a low DP.

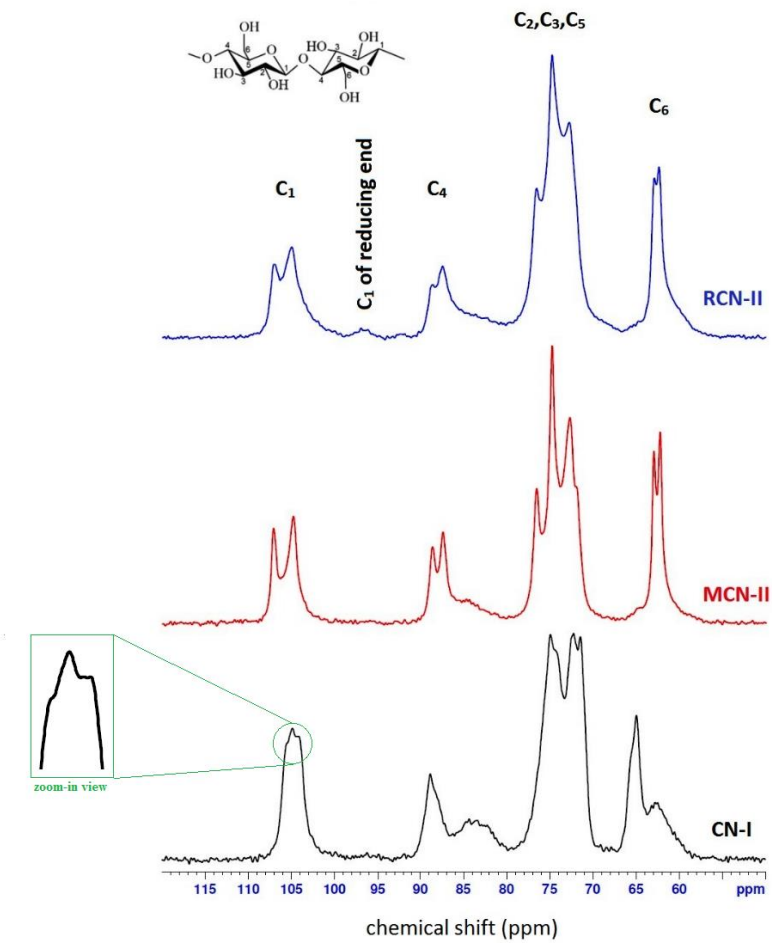

Figure 33 – ^{13}C CP/MAS NMR spectra of CN-I, MCN-II and RCN-II powders.

Distinct peaks corresponding to carbon atoms in the crystalline and disordered regions could be detected. The signal at around 89 ppm is assigned to the C4 of the highly ordered cellulose chains in the crystallite core, whereas the signal at 84 ppm corresponds to the C4 of disordered cellulose (Martins *et al.*, 2006; Novo *et al.*, 2015). The peaks around 65 ppm were assigned to the less ordered cellulose C6 carbons. The CI was also calculated from the ^{13}C-NMR spectra and the results are listed in Table 2. Similar results for CI^{NMR} can be found in the literature, usually around 60 ± 5% for cellulose nanocrystals (Park *et al.*, 2009, 2010; Sacui *et al.*, 2014). Although the CI values calculated from XRD and NMR data are different, their relative variation are similar and the conclusions based upon these variations are consistent.

4. DISCUSSION

4.1. Sulfur content and surface charge

Taking into account the number of $–OSO_3H$ groups per 100 anhydroglucose units (Table 1), the number of cellulose chains exposed on CNC surface according to the cross-section of the elementary crystallites for each type of CNC deduced from XRD data (Figure S5), and assuming that only 3 –OH groups are accessible for each cellobiose repeating unit, the percentage of esterified hydroxyl groups relative to the amount of available hydroxyl groups at the CNC surface was estimated to be 9.1, 15.8 and 19.3% for CN-I, MCN-II and RCN-II, respectively. The surface area that is not accessible due to the association of crystallites in the particles was neglected for these estimates. These values are consistent with those reported by Lin and Dufresne (2014) for nanocrystals extracted from native cotton by hydrolysis at 45°C using 65 wt% H_2SO_4.

4.2. Three-dimensional shape and crystal orientation of the CNCs

As shown from images and diffraction data, the elementary crystallites in CN-I particles have a square cross-section and the chain axis is parallel to the long axis of the nanocrystal (Figure 34a). The CN-I particles are made of a few parallel crystallites whose lateral association by hydrogen bonds has not be broken by acid hydrolysis (Elazzouzi-Hafraoui *et al.*, 2008). As the particles are rather flat, some uniplanarity might have been promoted during drying as a film. However, no such preferential orientation was detected in XRD powder patterns (Figure 31a), which means that in each particle, the associated elementary crystallites are randomly oriented with respect to one another around the common chain axis.

Mercerization is considered to be a solid-state transition in which the cellulose chains from neighbouring nanofibrils with opposite polarity can mix upon swelling in alkali. As demonstrated for *Valonia* cellulose, after recrystallization into Cel-II, the fibrous texture is preserved and the chain axis is still parallel to the fiber axis (Chanzy & Roche, 1976). This orientation is the one that was determined for MCN-II particles (Figure 34b) and is consistent with the conclusions of Kim *et al.* (2006) from electron diffraction data collected on CNCs from mercerized ramie cellulose. Yue *et al.* (2012) reported a similar morphology for CNCs prepared by acid hydrolysis of mercerized cotton cellulose. Such rod-like nano-elements were also described by Hirota *et al.* (2012) after TEMPO-mediated oxidation of mercerized cotton cellulose. MCN-II CNCs are shorter than CN-I particles. Indeed, one can expect that the intermingling of the chains upon swelling and subsequent recrystallization generate a significant number of disorganized regions that were thus preferentially degraded during acid hydrolysis. This assumption is confirmed by the 66% yield which means that a significant amount of material was dissolved during acid hydrolysis. Like for CN-I, MCN-II particles are made of a few associated elementary crystallites with no specific orientation relative to each other since no in-plane uniplanarity was detected in the XRD pattern. However, the crystallization upon washing generates larger crystalline domains as shown by broader constituting crystallites (Figure S5b), in agreement with the observations of mercerized ramie CNCs by Kim *et al.* (2006).

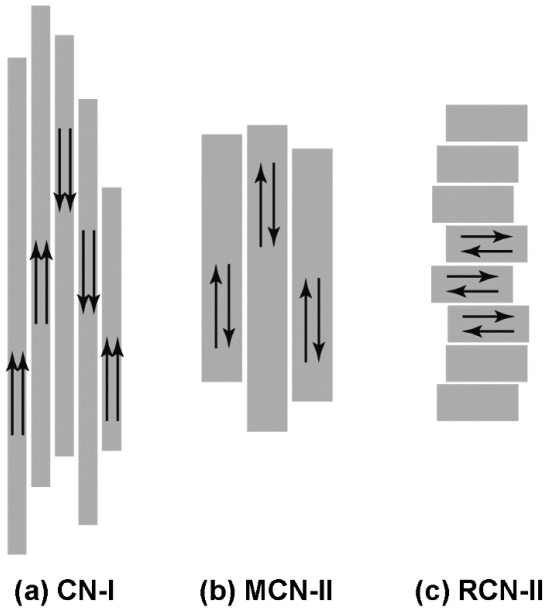

Figure 34 – Scheme describing the orientation of the Cel-I and Cel-II crystallites with respect to the CN-I (a), MCN-II (b) and RCN-II (c) composite particles.

The coarse morphology of RCN-II crystals resembles that of the particles prepared in similar conditions by Sèbe *et al.* (2012), Hirota *et al.* (2012), Martins *et al.* (2015) and Henrique *et al.* (2015). However, the images shown by these authors were recorded either by AFM and lack the lateral resolution of TEM images, or by TEM but often from crowded assemblies, which make the comparison of finer details difficult. The crystal orientation that we propose and that is illustrated in Figure 34c, was deduced from several results: i) since the 110_{II} is in meridional position in the pattern of Figure 31f, the chain axis is perpendicular to the long axis of the particle, in agreement with the conclusion of Atkins *et al.* (1979) who characterized fibers extruded from solutions of cellulose in hydrazine; ii) the 110_{II} reflection is meridional and very strong (Figures 31f and S4c), hence the $(110)_{II}$ planes are parallel to the observation direction and perpendicular to the base plane of the ribbons; iii) the $\mathbf{1\bar{1}0_{II}}$ reflection is weak in the XRD pattern of Figure 31c and absent in the electron diffraction pattern in Figure S4c, hence, the $\mathbf{(1\bar{1}0)_{II}}$ planes are parallel to the base plane of the ribbons and perpendicular to the observation axis. As a consequence, the *c*-axis, that is normal to the $(110)_{II}$ and $\mathbf{(1\bar{1}0)_{II}}$ planes should lie parallel to the ribbon plane. In that case, the width of the ribbons should more or less correspond to the length of the cellulose chains. An extended cellulose chain with $\overline{\mathbf{DP}}$ 17 would have a length of about 9 nm that is in rather good agreement with the average width measured from TEM images (12 nm), considering the irregular and rough aspect of the ribbons. Surprisingly, no $00l_{II}$ reflection was observed in the diffraction patterns of Figures 31f and S4c, as opposed to the patterns of MCN-II particles (Figures 31e, 31h and S4b) in which the 002 and/or 004_{II} reflections are visible. Since the number of $(00l)_{II}$ planes, which is directly related to the width of the RCN-II ribbon, is small, and if the degree of order is lower in the *c*-direction, it is possible that the 00*l* signals are very weak and thus not clearly visible. To verify this assumption, it would be necessary to record low-temperature electron diffraction patterns from individual ribbons, like those recorded by Kim *et al.* (2006) from individual nanocrystals of mercerized ramie cellulose (thus equivalent to our MCN-II particles). This is a real challenge considering the small volume of material probed by the electrons, the irregular morphology of the ribbons and the very high beam sensitivity of cellulose.

Ribbon-like cellulose II crystals have also been prepared by Buléon and Chanzy (1978) by deacetylating a fraction of short-chain cellulose triacetate in a water/methylamine solution at 90°C. Helbert and Sugiyama (1998) prepared fractions of short chains by hydrolysis of Avicel cellulose with phosphoric acid according to the

method of Isogai and Usuda (1991). When crystallized at 90°C, long lamellar crystals were obtained, exhibiting the same shape as those previously described by Buléon and Chanzy (1978). The crystal orientation was confirmed by electron diffraction and high-resolution lattice imaging (Helbert & Sugiyama, 1998): the chain axis lay perpendicular to both the long axis and the base plane of the crystal. In both methods, the lamellar crystals were formed at high temperature (90°C), as opposed to RCN-II ribbons that were prepared by aqueous regeneration at room temperature. This may explain the apparent lower 'perfection' of RCN-II crystals but, in addition, they also differ in that the chain axis is oriented in-plane. Indeed, it would be interesting to test the crystallization conditions described by Buléon and Chanzy (1978) with the fraction used to prepare the RCN-II sample and see if well-defined lamellar single crystals are obtained.

The ribbon-like RCN-II nanocrystals present a strong analogy with the particles prepared by precipitation of mannan, a linear homopolymer of *β*-(1,4)-*D*-mannosyl residues found as an energy reserve or a cell-wall structural component in plants and algae (Chanzy *et al.*, 1984). Heux *et al.* (2005) precipitated solutions of mannan from ivory nut ($\overline{\mathbf{DP}_n}$ 30) and the seaweed *Acetabularia crenulata* ($\overline{\mathbf{DP}_n}$ 350). The resulting crystals were described as rod-like or ribbon-like depending on the source of mannan, with a width of 7 and 30 nm, respectively, and corresponding to allomorph II. As first shown by Bittiger and Husemann (1972) and confirmed by Heux *et al.* (2005), the mannan chains lie perpendicular to the long axis of the particles. The crooked aspect of the ribbons of mannan from *A. crenulata* is very similar to that of our RCN-II nanocrystals. However, in the former case, chain folding was believed to be involved.

Considering the irregular aspect of the ribbons prepared by regenerating solutions of short-chain cellulose and mannan at room temperature, two different linear polysaccharides in which the sugar units are connected by *β*-(1,4) bonds, one is tempted to describe this crystallization as 'imperfect'. However, nanocrystals with a specific molecular organization, a high crystallinity and a fairly well defined width are obtained. The ribbons axially grow along the $[\mathbf{1\bar{1}0}]_{\mathbf{II}}$ direction by hydrophobic stacking of cellulose sheets containing antiparallel chains.

Due to specific organization of cellulose chains in RCN-II nanocrystals, a large number of reducing ends are exposed at the surface which could be used for chemical modification and grafting of functional groups to impart original properties such as stimuli-responsiveness and develop new applications (*e.g.*, biosensing, bioimaging agents, *etc*).

5. CONCLUSIONS

The three types of CNC prepared by sulfuric acid hydrolysis exhibit different morphologies and crystalline structures. When the acid hydrolysis conditions are set-up in such a way that the crystalline domains in the initial wood pulp and mercerized celluloses (WP and MWP, respectively) are preserved (60 wt% H_2SO_4, 45°C, 50 min), the resulting nanocrystals retain the fibrillar nature of the parent fibers (*i.e.*, the chain axis is parallel to the long axis of the acicular particles) and their initial allomorphic type (I for WP and II for the MWP). In both cases, the particles are mostly made of a few laterally-bound elementary crystallites. The unit nanocrystals in CNCs from mercerized cellulose (MCN-II) are shorter but broader than those prepared from cellulose I fibers (CN-I). If harsher conditions are used (64 wt% H_2SO_4, 40°C, 20 min), resulting in the depolymerisation and dissolution of native cellulose, the short chains ($\overline{DP_v}$ 17) recrystallize into Cel-II ribbons upon regeneration in water at room temperature. In these somewhat tortuous ribbons, the chain axis would lie perpendicular to the long axis of the nanocrystal and parallel to its basal plane. In addition, these nanoribbons are very similar in shape and molecular orientation to mannan II nanocrystals prepared by recrystallization of mannan, a linear polymer of β-(1,4)-D-mannosyl residues, suggesting that this mode of crystallization may be a feature of short-chain linear β-(1,4)-linked polysaccharides.

Although similar ribbons of recrystallized cellulose II have been reported by other authors, it is the first time that a morphological and structural description is proposed. By comparison with the fibrillar nanocrystals prepared by acid hydrolysis of native or mercerized cellulose fibers, the unique molecular and crystal structure of the nanoribbons implies that a higher number of reducing chain ends are located at the particle surface, which may be important for subsequent chemical modification and specific potential applications, *e.g.* biosensing and bioimaging agents.

6. REFERENCES

Atalla, R. H., & VanderHart, D. L. (1984). Native cellulose: a composite of two distinct crystalline forms, *Science*, *223*, 283–284.

Atkins, E. D. T., Blackwell, J., & Litt., M. H. (1979). Texture of cellulose crystallized from hydrazine. *Polymer, 20*, 145–147.

Bendahou, A., Habibi, Y., Kaddami, H., & Dufresne, A. (2009). Physico-chemical characterization of palm from *Phoenix dactylifera* – L, preparation of cellulose whiskers and natural rubber-based nanocomposites. *Journal of Biobased Materials and Bioenergy, 3*, 81–90.

Bittiger, H., & Husemann, E. (1972). Crystal morphology of precipitated mannan. *Polymer Letters, 10*, 367–371.

Brito, B. S., Pereira, F. V., Putaux, J-L., & Jean, B. (2012). Preparation, morphology and structure of cellulose nanocrystals from bamboo fibers. *Cellulose, 19*, 1527–1536.

Buléon, A., & Chanzy, H. (1978). Single crystals of cellulose II. *Journal of Polymer Science, 16*, 833–839.

Chanzy, H. D., & Roche, E. J. (1976). Fibrous transformation of *Valonia* cellulose I into cellulose II. *Applied Polymer Symposium, 28*, 701–711.

Chanzy, H. D., Grosrenaud, A., Vuong, R. & Mackie, W. (1984). The crystalline polymorphism of mannan in plant cell walls and after recrystallisation. *Planta, 161*, 320–329.

Chauve, G., Fraschini, C., & Jean, B. (2013). Separation of cellulose nanocrystals. In "Handbook of Green Materials: Processing Technologies, Properties and Applications", Oksman, K., Mathew, A. P., Bismark, A., Rojas, O. & Sain, M. eds., World Scientific Publishing Co., 73–87.

Cranston, E. D., & Gray, D. G. (2008). Birefringence in spin-coated films containing cellulose nanocrystals. *Colloids and Surfaces A: Physicochemical and Engineering Aspects, 325*, 44–51.

Dhar, P., Tarafder, D., Kumar, A., & Katiyar, V. (2015). Effect of cellulose nanocrystal polymorphs on mechanical, barrier and thermal properties of poly(lactic acid) based bionanocomposites. *Royal Society of Chemistry Advances, 5*, 60426–60440.

dos Santos, R. M., Flauzino Neto, W. P., Silvério, H. A., Martins, D. F., Dantas, N. O., & Pasquini, D. (2013). Cellulose nanocrystals from pineapple leaf, a new approach for the reuse of this agro-waste. *Industrial Crops and Products, 50*, 707–714.

Dufresne, A. (2012). Nanocellulose: From nature to high-performance tailored materials. Berlin/Boston: de Gruyter.

Eichhorn, S. J. (2011). Cellulose nanowhiskers: promising materials for advanced applications. *Soft Matter, 7*, 303–315.

Elazzouzi-Hafraoui, S., Nishiyama, Y., Putaux, J-L., Heux, L., Dubreuil, F., & Rochas, C. (2008). The shape and size distribution of crystalline nanoparticles prepared by acid hydrolysis of native cellulose. *Biomacromolecules, 9,* 57–65.

French, A. D. (2014). Idealized powder diffraction patterns for cellulose polymorphs. *Cellulose, 21,* 885–896.

Gardner, K. H., & Blackwell, J. (1974). The structure of native cellulose. *Biopolymers, 13,* 1975–2001.

Gupta, P. K., Uniyal, V., & Naithani, S. (2013). Polymorphic transformation of cellulose I to cellulose II by alkali pretreatment and urea as an additive. *Carbohydrate Polymers, 94,* 843–849.

Habibi, Y., Lucia, L. A., & Rojas, O. J. (2010). Cellulose nanocrystals: chemistry, self-assembly and applications. *Chemical Reviews, 110*, 3479–3500.

Han, J., Zhou, C., French, A. D., Han, G., & Wu, Q. (2013). Characterization of cellulose II nanoparticles regenerated from 1-butyl-3-methylimidazolium chloride. *Carbohydrate Polymers, 94*, 773–781.

Helbert, W., & Sugiyama, J. (1998). High-resolution electron microscopy on cellulose II and α-chitin single crystals. *Cellulose, 5*, 113–122.

Henrique, M. A., Flauzino Neto, W. P., Silvério, H. A., Martins, D. F., Gurgel, L. V. A., Barud, H. S., de Morais, L. C., & Pasquini, D. (2015). Kinetic study of the thermal decomposition of cellulose nanocrystals with different polymorphs, cellulose I and II, extracted from different sources and using different types of acids. *Industrial Crops and Products, 76,* 128–140.

Heux, L., Chauve, G., & Bonini, C. (2000). Nonflocculating and chiral-nematic self-ordering of cellulose microcrystals suspensions in nonpolar solvents. *Langmuir, 16*, 8210-8212.

Heux, L., Hägglund, P., Putaux, J-L., & Chanzy, H. (2005). Structural aspects in semi-crystalline samples from the mannan II family. *Biomacromolecules, 6*, 324–332.

Hirota, M., Tamura, N., Saito, T., & Isogai, A. (2012). Cellulose II nanoelements prepared from fully mercerized, partially mercerized and regenerated celluloses by 4-acetamido-TEMPO/NaClO/$NaClO_2$ oxidation. *Cellulose, 19*, 435–442.

Hu, T. Q., Hashaikeh, R., & Berry, R. N. (2014). Isolation of a novel, crystalline cellulose material from the spent liquor of cellulose nanocrystals (CNCs). *Cellulose, 21,* 3217–3229.

Isogai, A., & Usuda, M. (1991). Preparation of low-molecular weight celluloses using

phosphoric acid. *Mokuzai Gakkaishi, 37*, 339–344.

Jin, E., Guo, J., Yang, F., Zhu, Y., Song, J., Jin, Y., & Rojas, O. J. (2016). On the polymorphic and morphological changes of cellulose nanocrystals (CNC-I) upon mercerization and conversion to CNC-II. *Carbohydrate Polymers, 143*, 327–335.

Kim, N., Imai, T., Wada, M., & Sugiyama, J. (2006). Molecular directionality in cellulose polymorphs. *Biomacromolecules, 7*, 274–280.

Klug, H. P., & Alexander, L. E. (1974). X-ray diffraction procedures for polycrystalline and amorphous materials. John Wiley & Sons, New York.

Kolpak, F. J., & Blackwell, J. (1976). Determination of the structure of cellulose II. *Macromolecules, 9*, 273–278.

Kumar, V., Reus-Medina, M. D. L. L., & Yang, D. (2002). Preparation, characterization, and tabletting properties of a new cellulose-based pharmaceutical aid. *International Journal of Pharmaceutics, 235*, 129–140.

Langan, P., Nishiyama, Y., & Chanzy, H. (2001). X-ray structure of mercerized cellulose II at 1 angstrom resolution. *Biomacromolecules*, *2*, 410–416.

Langan, P., Sukumar, N., Nishiyama, Y., & Chanzy, H. (2005). Synchrotron X-ray structures of cellulose Iβ and regenerated cellulose II at ambient temperature and 100 K. *Cellulose, 12*, 551–562.

Lin, N., & Dufresne, A. (2014). Surface chemistry, morphological analysis and properties of cellulose nanocrystals with gradiented sulfation degrees. *Nanoscale, 6*, 5384–5393.

Liu, Y. P., & Hu H. (2008). X-ray diffraction study of bamboo fibers treated with NaOH. *Fibers and Polymers, 9*, 735–739.

Marchessault, R. H, Morehead, F. F, & Walter, N. M. (1959). Liquid crystal systems from fibrillar polysaccharides. *Nature, 184*, 632–633.

Mariano, M., El Kissi, N., & Dufresne, A. (2014). Cellulose nanocrystals and related nanocomposites: Review of some properties and challenges. *Journal of Polymer Science B*, 52, 791–806.

Martins, D. F., de Souza, A. B., Henrique, M. A., Silvério, H. A., Flauzino Neto, W. P., & Pasquini, D. (2015). The influence of the cellulose hydrolysis process on the structure of cellulose nanocrystals extracted from capim mombaça (*Panicum maximum*). *Industrial Crops and Products, 65*, 496–505.

Martins, M. A., Forato, L. A., Mattoso, L. H. C., & Colnago, L. A. (2006). A solid state ^{13}C high resolution NMR study of raw and chemically treated sisal fibers. *Carbohydrate Polymers, 64*, 127–133.

Medronho, B., & Lindman, B. (2015). Brief overview on cellulose dissolution/regeneration interactions and mechanisms. *Advances in Colloid and Interface Science, 222*, 502–508.

Moon, R. J., Martini, A., Nairn, J., Simonsen, J., & Youngblood, J. (2011). Cellulose nanomaterials review: structure, properties and nanocomposites. *Chemical Society Reviews, 40*, 3941–3994.

Mukherjee, S. M., & Woods, H. J. (1953). X-ray and electron microscope studies of the degradation of cellulose by sulphuric acid. *Biochimica et Biophysica Acta, 10*, 499−511.

Nishiyama, Y., Johnson, G. P., French, A. D., Forsyth, V. T., & Langan, P. (2008). Neutron crystallography, molecular dynamics, and quantum mechanics studies of the nature of hydrogen bonding in cellulose Iβ. *Biomacromolecules, 9*, 3133–3140.

Nishiyama, Y., Kuga, S., & Okano, T. (2000). Mechanism of mercerization revealed by X-ray diffraction. *Journal of Wood Science, 46*, 452–457.

Novo, L. P., Bras, J., García, A., Belgacem, N., & Curvelo, A. A. S. (2015). Subcritical water: A method for green production of cellulose nanocrystals. *ACS Sustainable Chemistry & Engineering, 3*, 2839−2846.

Oh, S. Y., Yoo, D., Shin Y., Kim, H. C., Kim, H. Y., Chung, Y. S., Park, W. H., & Youk, J. H. (2005). Crystalline structure analysis of cellulose treated with sodium hydroxide and carbon dioxide by means of X-ray diffraction and FTIR spectroscopy. *Carbohydrate Research*, 340, 2376–2391.

Okano, T., & Sarko, A. (1985). Mercerization of cellulose. II. Alkali-cellulose intermediates and a possible mercerization mechanism. *Journal of Applied Polymer Science, 30*, 325–332.

Park, S., Baker, J. O., Himmel, M. E., Parilla, P. A., & Johnson, D. K. (2010). Cellulose crystallinity index: Measurement techniques and their impact on interpreting cellulase performance. *Biotechnology for Biofuels, 3*, 1–10.

Park, S., Johnson, D. K., Ishizawa, C. I., Parilla, P. A., & Davis, M. F. (2009). Measuring the crystallinity index of cellulose by solid state ^{13}C nuclear magnetic resonance. *Cellulose, 16*, 641−647.

Roman, M., & Winter, W. T. (2004). Effect of sulfate groups from sulfuric acid hydrolysis on the thermal degradation behavior of bacterial cellulose. *Biomacromolecules, 5*, 1671–1677.

Sacui, I. A., Nieuwendaal, R. C., Burnett, D. J., Stranick, S. J., Jorfi, M., Weder, C., Foster, E. J., Olsson, R. T., & Gilman, J. W. (2014). Comparison of the properties of cellulose nanocrystals and cellulose nanofibrils isolated from bacteria, tunicate, and wood processed using acid, enzymatic, mechanical, and oxidative methods. *Applied Materials & Interfaces, 6*, 6127–6138.

Sasaki, M., Adschiri, T., & Arai, K. (2003). Production of cellulose II from native cellulose by near- and supercritical water solubilisation. *Journal of Agricultural and Food Chemistry, 51*, 5376–5381.

Scandinavian Pulp Paper and Board (SCAN). Standard test viscosity of cellulose in cupriethylenediamine solution (CED), Stockholm, 1980. NORMA SCAN C 15:62.

Sèbe G., Ham-Pichavant, F., Ibarboure, E., Koffi, A. L. C., & Tingaut, P. (2012). Supramolecular structure characterization of cellulose II nanowhiskers produced by acid hydrolysis of cellulose I substrates. *Biomacromolecules, 13*, 570–578.

Sharma, P. R., Rajamohananb, P. R., & Varma, A. J. (2014). Supramolecular transitions in native cellulose-I during progressive oxidation reaction leading to quasi-spherical nanoparticles of 6-carboxycellulose. *Carbohydrate Polymers, 113*, 615–623.

Sharma, S., Nair, S. S., Zhang, Z., Ragauskas, A.J., & Deng, Y. (2015). Characterization of micro fibrillation process of cellulose and mercerized cellulose pulp. *RSC Advances, 5*, 63111–63122.

Technical Association of the Pulp and Paper Industry (TAPPI). Standard test viscosity of pulp (capillary viscometer method). Atlanta, 1999. NORMA TAPPI T 230 om-99.

Tonoli, G. H. D., Teixeira, E. M., Corrêa, A. C., Marconcini, J. M., Caixeta, L. A., da Silva M. A. P., & Mattoso L. H. C. (2012). Cellulose micro/nanofibres from *Eucalyptus* kraft pulp: preparation and properties. *Carbohydrate Polymers, 89*, 80–88.

Wada, M., Nishiyama, Y., Chanzy, H., Forsyth, T., & Langan, P. (2008). The structure of celluloses. *Powder Diffraction, 23*, 92–95.

Warwicker J. O. 1967. Effect of chemical reagents on the fine structure of cellulose. Part IV. Action of caustic soda on the fine structure of cotton and ramie. *Journal of Polymer Science A1, 5*, 2579–2593.

Yue, Y., Han, G., & Wy, Q. (2013). Transitional properties of cotton fibers from cellulose

I to cellulose II structure. *BioResources, 8*, 6460–6471.

Yue, Y., Zhou, C., French, A. D., Xia, G., Han, G., Wang, Q., & Wu, Q. (2012). Comparative properties of cellulose nano-crystals from native and mercerized cotton fibers. *Cellulose, 19*, 1173–1187.

Zuluaga, R., Putaux, J-L., Cruz, J., Vélez, J., Mondragon, I., & Gañán, P. (2009). Cellulose microfibrils from banana rachis: Effect of alkaline treatments on structural and morphological features. *Carbohydrate Polymers, 76*, 51–59.

7. APPENDIX A

Supplementary data associated with chapter II.

Birefringence analysis. Vials containing aliquots of 0.15 wt% CNC suspensions were photographed while being placed between crossed polarizers and agitated using a magnetic stirrer.

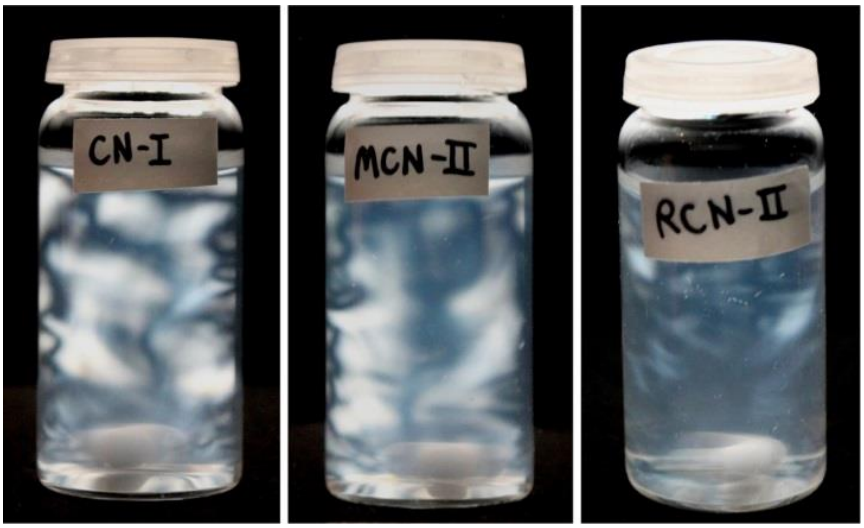

Figure S1 – Shear-induced birefringence for 0.15 wt% aqueous suspensions of cellulose nanocrystals under stirring, visualized between crossed polars.

Atomic force microscopy (AFM). AFM measurements of the CNC thickness were performed on a Shimadzu SPM-9600 instrument. Drops of *c.a.* 0.005 wt% aqueous nanocrystal suspension were left to dry on freshly cleaved mica substrates. 512 × 512-pixel images were recorded at room conditions in the non-contact mode with a scan rate of 1 Hz using Si tips with a curvature radius of less than 10 nm, a spring constant of 42 $N.m^{-1}$ and a resonance frequency of 300 kHz. The images were processed using the VectorScan software. For each sample, about 100 nanoparticles were randomly selected to determine their average thickness.

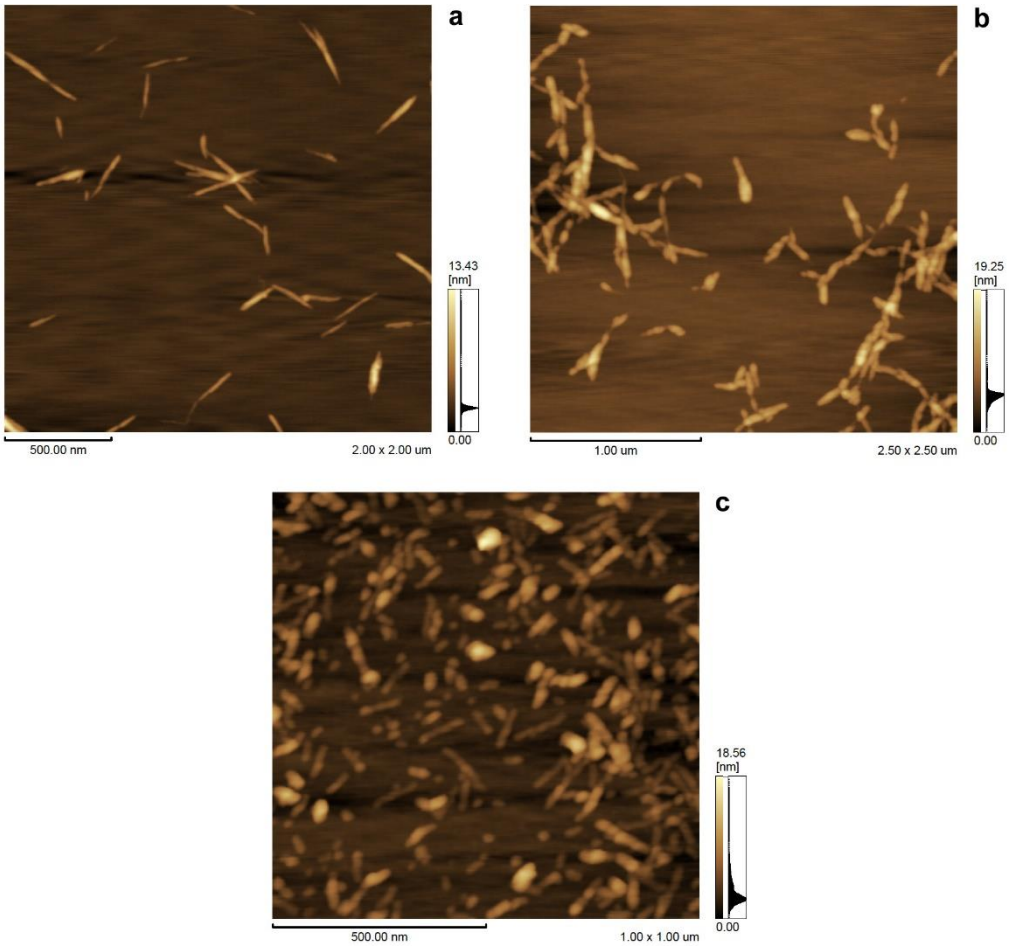

Figure S2 – Tapping mode AFM images of CN-I (a), MCN-II (b) and RCN-II (c) nanoparticles.

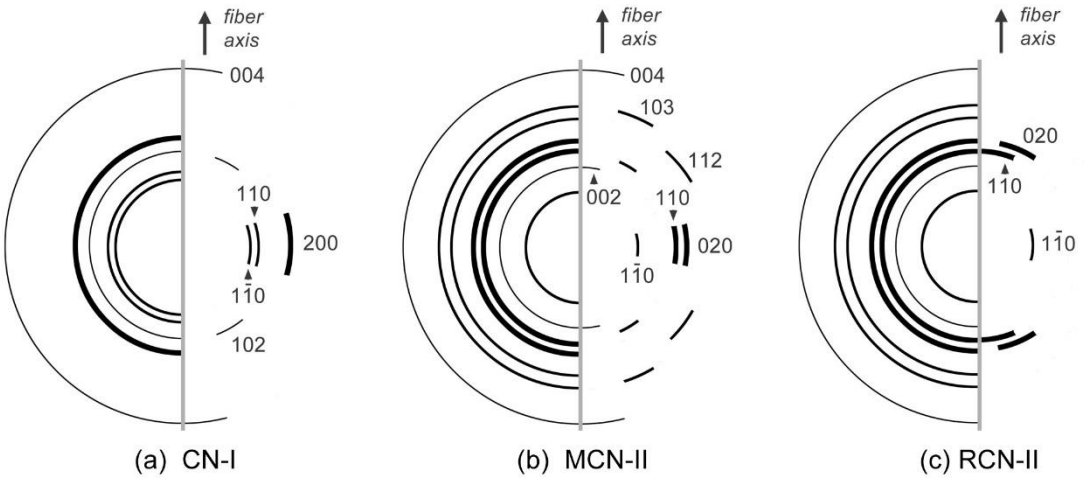

Figure S3 – Schematized XRD patterns of the three CNC samples. The left and right halves are powder and fiber patterns, respectively. The fiber axis is vertical. The indices of cellulose Iβ (CN-I) and cellulose II (MCN-II and RCN-II) of the main reflections are indicated.

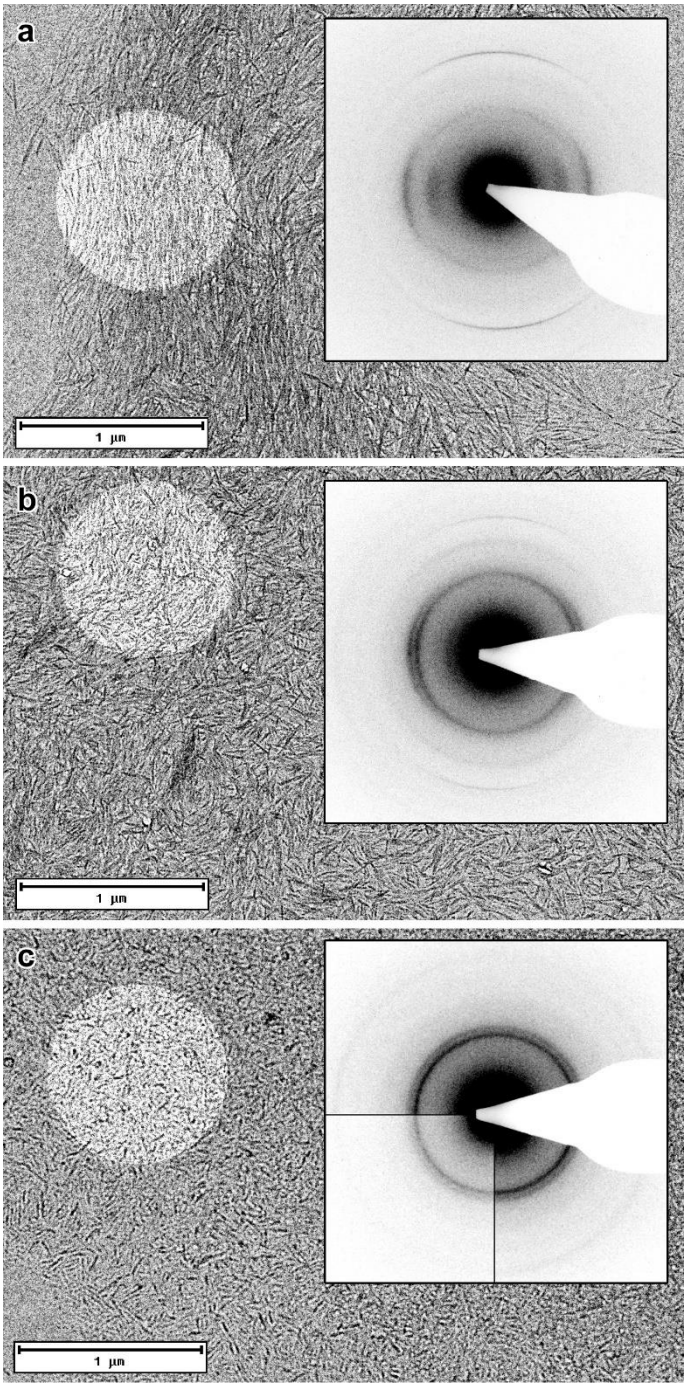

Figure S4 – TEM images of unstained preparations for CN-I (a), MCN-II (b) and RCN-II (c) nanoparticles. Insets: corresponding selected area electron diffraction patterns recorded at low temperature. The position of the selected area aperture is indicated in the image. In c, the lower left quarter of the electron diffraction pattern was recorded with a shorter exposure time in order to show that the 110_{II} reflection, closer to the transmitted beam, was absent.

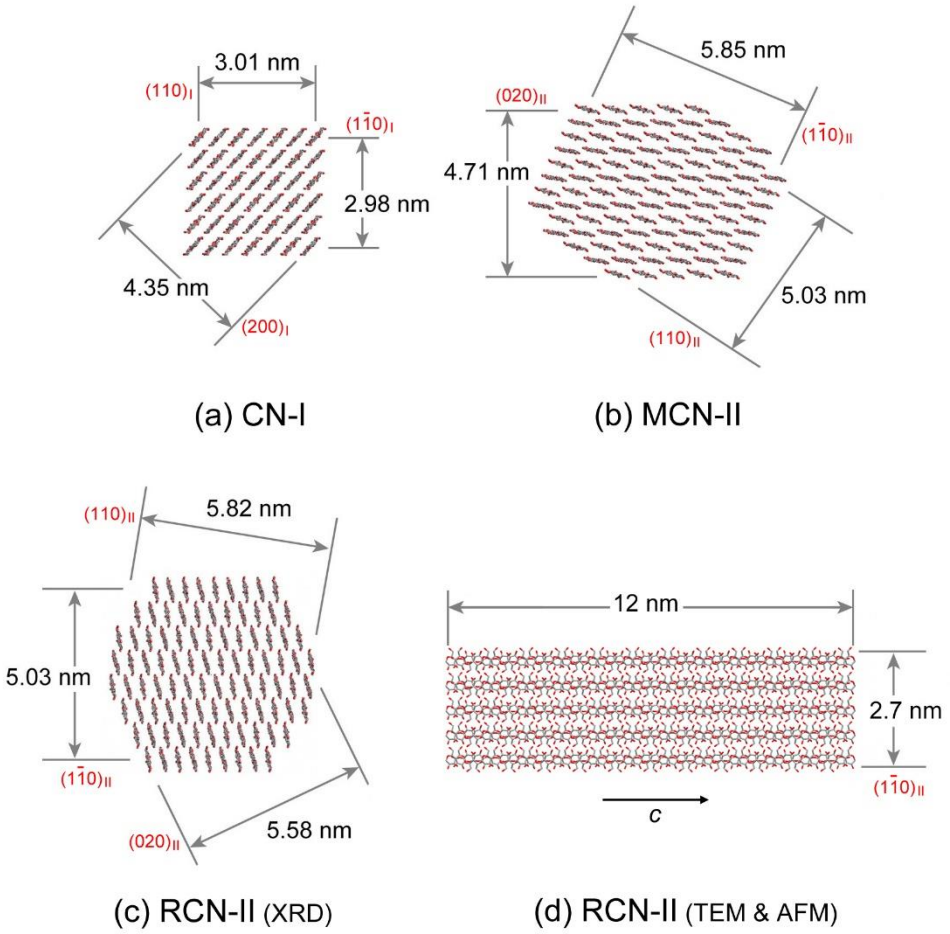

Figure S5 – Proposed models for the cross-sections of the elementary crystallites of CN-I (a), MCN-II (b) and RCN-II (c,d) CNCs. In a, b and c, the dimensions have been deduced from the analysis of the peak broadening in the XRD profiles of films. The cellulose chains are viewed along the *c*-axis the crystal lattice of cellulose I (a) and II (b,c). The dimensions D_{hkl} and indices are the values listed in Table 4, not those that would correspond to an integer numbers of crystallographic planes. In d, the dimensions are those estimated from TEM and AFM images of the ribbon-like particles. Note that the model deduced from XRD data of RCN-II crystallites is twice as thick as the one that was estimated from TEM and AFM images. The reason for this discrepancy is not known yet.

CHAPTER III

Mechanical properties of natural rubber nanocomposites reinforced with high aspect ratio cellulose nanocrystals isolated from soy hulls

This chapter is based on paper "*Mechanical properties of natural rubber nanocomposites reinforced with high aspect ratio cellulose nanocrystals isolated from soy hulls*", published in 2016 in Carbohydrate Polymers, 153, 143-152.

CONTENT CHAPTER III

ABSTRACT 115
1. INTRODUCTION 116
2. EXPERIMENTAL 118
2.1. Materials 118
2.2. Extraction of cellulose nanocrystals 118
2.3. Preparation of CNC-reinforced NR nanocomposites 119
2.4. Characterization 119
2.4.1. Elemental analysis 119
2.4.2. Zeta-Potential 119
2.4.3. Wide-angle X-ray scattering 120
2.4.4. Transmission electron microscopy 120
2.4.5. Atomic force microscopy 121
2.4.6. Scanning electron microscopy 121
2.4.7. Fourier transform infrared spectroscopy 121
2.4.8. Dynamic mechanical analysis 122
2.4.9. Tensile tests 122
2.4.10. Thermogravimetric analysis 122
3. RESULTS AND DISCUSSION 122
3.1. Extraction of cellulose nanocrystals 122
3.2. Characterization of CNC/NR nanocomposites 126
4. CONCLUSIONS 134
5. REFERENCES 135

ABSTRACT

Cellulose nanocrystals (CNCs) were isolated from soy hulls by sulfuric acid hydrolysis. The resulting CNCs were characterized using TEM, AFM, WAXS, elemental analysis and TGA. The CNCs have a high crystallinity, specific surface area and aspect ratio. The aspect ratio (around 100) is the largest ever reported in the literature for a plant cellulose source. These CNCs were used as a reinforcing phase to prepare nanocomposite films by casting/evaporation using natural rubber as matrix. The mechanical properties were studied in both the linear and non-linear ranges. The reinforcing effect was higher than the one observed for CNCs extracted from other sources. It may be assigned not only to the high aspect ratio of these CNCs but also to the stiffness of the percolating nanoparticle network formed within the polymer matrix. Moreover, the sedimentation of CNCs during the evaporation step was found to play a crucial role on the mechanical properties.

Keywords: cellulose nanocrystals, soy hulls, agro-industrial residue, natural rubber, aspect ratio, nanocomposites.

1. INTRODUCTION

Nanocomposites are reported to be the materials of 21st century in view of possessing property combinations that are not found in conventional composites. Their potential is so striking that they are useful in areas ranging from packaging to biomedical applications. In the meantime, there is a growing worldwide interest in the development of bio-based products and innovative process technologies that can decrease the dependence on fossil fuels and move towards sustainable materials. Thus, bio-based nanocomposites potentially represent the next generation of advanced materials. In this context, cellulose nanocrystals (CNCs) have been highlighted, especially as filler in the field of polymer nanocomposites, since they offer a unique combination of unusual physicochemical properties and environmental appeal (Eichhorn, 2011).

CNCs are isolated by preferentially acid-hydrolyzing the amorphous regions of cellulose fibers, releasing the more resistant crystalline nanosized domains. Large specific surface area, high strength and modulus, high aspect ratio, low density, reactive hydroxyl groups that can facilitate grafting chemical species to tailor the surface properties, biocompatibility and biodegradability are some specific useful features of CNCs which make them promising nanoparticles. Moreover, they are derived from cellulose, the most abundant renewable natural polymer available on Earth, therefore low cost (Dufresne, 2012; Habibi et al., 2010; Mariano et al., 2014; Moon et al., 2011).

The incorporation of CNCs in polymer matrices generally leads to polymer-based nanocomposite materials with higher mechanical and barrier properties than the neat polymer or conventional composites. Among various factors that influence the efficiency of the reinforcing effect of CNCs, their intrinsic characteristics, including crystallinity and aspect ratio, play a key role (Dufresne, 2012; Favier et al., 1995; Mariano et al., 2014). It is also well-known that these characteristics depend on the source of the original cellulose, on the extraction method and its conditions (including pretreatment). However, it is widely accepted that the raw starting material is the most important factor (Beck-Candanedo et al., 2005; Dufresne, 2012; Elazzouzi-Hafraoui et al., 2008). The reinforcement capability of CNCs is therefore directly linked to the source of cellulose as well as its biosynthesis. Thus, the optimization of the extraction procedure and further characterization of CNCs from different sources of cellulose are crucial for an efficient exploitation of these sources, allowing the selection of the appropriate source (*i.e.* with targeted morphology) to suit specific end user applications (Brinchi et al., 2013).

CNCs have been isolated from many kinds of cellulose sources, *e.g.* from higher plants (da Silva et al., 2015) and algae (Revol, 1982), sea animals, such as tunicates (Sacui et al., 2014), and bacteria (George et al., 2011). In practice, for most studies, researchers have shown preferences to commercial MCC, filter paper, bleached wood pulp or related products, owing to their purity and availability in laboratories. Tunicin has also been a favored source of CNC due to larger dimensions, and high crystallinity and aspect ratio. However, its widespread use is restricted by the high cost of harvesting and limited availability (Brinchi et al., 2013; Klemm et al., 2011).

Valorization of low-cost crops and agricultural wastes is an important topic. Soy is one of the main crops in the world, and represents a significant agricultural commodity in the Brazilian economy. Brazil is the second largest producer of soybeans, accounting for about 30% of the global production (CONAB, 2015). The seed coat of soybeans, also known as soy hulls, is a by-product of the soybean processing industry. Soy hulls constitute about 2 to 8% of the whole seed and contain about 50% of cellulose. Most of the approximately $5.7 \cdot 10^9$ kg of soy hulls produced in Brazil each year are sold to animal feed formulators as low value product or are simply left to waste (Flauzino Neto et al., 2013; Ipharraguerre & Clark, 2003; Rosa et al., 2015). Therefore, additional product outlets need to be identified to create higher value-added products from this agro-industrial waste, which is available in huge quantities all over the world. In addition, the use of this underutilized biomass residue allows a significant reduction both in the volume of waste accumulated in the environment, as in the extraction of raw materials. Thus, an efficient use of this residue may contribute to the sustainable societal development, minimizing the environmental impact and reducing production costs.

Natural rubber (NR) is a high molecular weight polymer extracted from the sap of rubber trees, mainly consisting of *cis*-1,4-polyisoprene units. It is an elastomer of great economic importance. Either alone or in combination with other materials, NR is widely used in many applications and products, such as tires, condoms, adhesives, *etc*. This biopolymer is available in the form of a colloidal system, known as NR latex, in which rubber particles are dispersed in aqueous medium (Mariano et al., 2016; Rippel & Galembeck, 2009).

NR is a perfect matrix to be used as a model system to study the effect of filler reinforcement, owing to its high flexibility and low stiffness. Its properties can be tailored by the addition of reinforcing fillers of various surface chemistries and aggregate size/aspect ratios to suit the targeted application. Silica and carbon black are common

reinforcing agents in the rubber industry, but the processing of these fillers results in high energy consumption and environmental pollution. CNC is thus a potential alternative which can overcome the previously mentioned shortcomings and partially replace the fillers traditionally used in the rubber industry. CNCs are available as aqueous suspensions. Hence, they can be easily used in processing routes involving their mixing with NR suspensions. Furthermore, the use of bio-nanoparticles, such as CNCs, in NR enables the development of bio-based and green nanocomposites (Mariano et al., 2016). CNCs extracted from different sources have already been studied as nanoreinforcement in NR-based nanocomposites, including CNCs isolated from capim dourado (Siqueira et al., 2010a), rachis of palm date tree (Bendahou et al., 2009), sugarcane bagasse (Pasquini et al., 2010; Bras et al., 2010), sisal (Siqueira et al., 2011), and bamboo (Visakh et al., 2012).

To our knowledge, so far, little results have been reported in the literature on the isolation of CNCs from soy hulls or their use in nanocomposites (Flauzino Neto et al., 2013, Silvério et al., 2014). In this study, we isolated and characterized CNCs prepared from soy hulls by acid hydrolysis treatment. These nanoparticles were used as reinforcing agent in a NR matrix to prepare nanocomposite films by casting/evaporation at different loading levels. The effect of CNC on the structure, as well as thermal and mechanical properties of NR, was investigated.

2. EXPERIMENTAL

2.1. Materials

The soy hulls were kindly supplied by Algar Agro S.A. Company (Uberlândia, Brazil). The natural rubber (NR) latex was kindly received from Centrotrade Deutschland GmbH (Eschborn, Germany). It contained spherical particles with an average diameter around 300 nm and its solid content was about 60 wt%.

2.2. Extraction of cellulose nanocrystals

First the soy hulls were chemically treated to remove non-cellulosic components, as described in our previous report (Flauzino Neto et al., 2013). After this purification process, the soy hulls contained a low amount of lignin and a high amount of cellulose (85 ± 4% cellulose, 11 ± 4% hemicelluloses and 3.7 ± 0.3% lignin). The CNCs were isolated from these purified soy hulls fibers by acid hydrolysis using milder conditions compared to those described in Flauzino Neto et al. (2013). These purified soy hulls fibers

were ground in a blender and passed through a 35-mesh sieve. The hydrolysis was performed at 45°C for 30 min under vigorous stirring, using 20 mL of 60 wt% H_2SO_4 per gram of fiber. These milder hydrolysis conditions were chosen in order to avoid as much as possible the hydrolysis of crystalline cellulose domains. Immediately after hydrolysis, the material was diluted 10-fold with cold deionized water to stop the hydrolysis reaction, and washed by centrifugation at 10,000 rpm and at 10°C for 15 min to remove the excess acid. The precipitate was then dialyzed against deionized water to remove non-reactive sulfate groups, salts and soluble sugars, until a neutral pH was reached. The dialyzed suspension was ultrasonicated for 15 min in an ice bath (Branson sonifier 250 - maximum power of 200 W - operating at a duty cycle of 50% and output of 40%), filtered over a small-pore fritted glass filter and stored in a refrigerator. Some drops of sodium hypochlorite were added to avoid any bacterial growth. The resulting nanocrystals will be referred to as CNC_{SH} (CNCs isolated from soy hulls) in the following.

2.3. Preparation of CNC-reinforced NR nanocomposites

The films were prepared by reinforcing NR with CNC_{SH} at loading level ranging from 0 to 5 wt% (dry basis) by casting/evaporation. The NR latex and the CNC aqueous suspension were first mixed in various proportions (depending on filler content), stirred for 1h using a magnetic stirrer, and then this mixture was cast in aluminum petri dishes and stored at 45°C overnight in an air-circulating oven. The nanocomposite films and neat NR film were stored in hermetic vacuum bags before testing. The final mass for all films was about 1.5 g and their thickness ranged from 0.3 to 0.4 mm. These films were labeled according to the filler content. For instance, NR5% corresponds to the nanocomposite film reinforced with 5 wt% CNC_{SH}.

2.4. Characterization

2.4.1. Elemental analysis

The content of carbon, hydrogen, nitrogen and sulfur were determined with an Element Analyzer (Perkin-Elmer Series II, CHNS/O Analyzer 2400) using freeze-dried CNCs. The oxygen content was determined by the difference.

2.4.2. Zeta-Potential

The zeta-potential ζ of CNC suspension with concentration around 0.01 wt% was analyzed with an equipment model DTS0230 from Malvern Instruments. To avoid the

effect of ionic strength and pH during measurements, the CNC suspension was diluted in an aqueous standard solution with pH 7, ionic strength 5 mmol and 200 µS.cm^{-1} conductivity. This solution was prepared by adding diluted NaOH solution and solid NaCl into deionized water.

2.4.3. Wide-angle X-ray scattering (WAXS)

The WAXS data were collected in reflection mode using a PANalitycal X'pert MPD diffractometer with a PW3373 generator operating at 45 kV and 40 mA in Bragg-Brentano geometry. Freeze-dried CNC powder sample was pressed into flat disks and attached to the slide using double-sided adhesive tape. The specimen was X-rayed at room temperature in 2θ range from 6 to 56° using a fixed time mode with a step interval of 0.067° and Cu Kα radiation (λ = 0.1542 nm). The X-ray scattering data was analyzed as described below.

The baseline-corrected diffraction profile was deconvoluted into peaks and halos referring to the crystalline and amorphous regions, respectively. Deconvolution was obtained using the Pseudo-Voigt 2 peak function from Origin® 7.0 software, which is shown in Equation (11), and it was evaluated according to the traditional two-phase cellulose model that describes cellulose as containing both crystalline and amorphous regions.

$$y = y_0 + A\left[m_u \frac{2}{\pi}\frac{w_L}{4(x-x_c)^2+w_L^2} + (1-m_u)\frac{\sqrt{4ln2}}{\sqrt{\pi}w_G} e^{(-4ln2/w_G^2)(x-x_c)^2}\right] \quad (11)$$

where w_L and w_G are the width at half maximum for Lorentz and Gauss components of the above equation, respectively, A is the area and m_u is the profile shape factor.

Considering this model, the crystallinity index (CI) of the sample was calculated from diffraction patterns by using Equation (12):

$$\mathrm{CI} = 100 \times \left(\frac{A_c}{A_c+A_a}\right) \quad (12)$$

where A_c and A_a are the areas under the crystalline peaks and the amorphous halo, respectively, determined after deconvolution.

2.4.4. Transmission electron microscopy (TEM)

A drop of dilute (*c.a.* 0.001 wt%) CNC suspension was deposited onto glow-discharged copper grids coated with carbon support film. The specimen was negatively

stained with 2 wt% uranyl acetate and observed with a Philips CM200 (FEI) transmission electron microscope operating at 200 kV. Images were recorded on a TVIPS TemCam F216 camera. The width and length of over 100 particles randomly selected were measured from the TEM images by using ImageJ software. For each particle, one measurement for the length and two measurements for the width were performed.

2.4.5. Atomic force microscopy (AFM)

AFM observations were performed on Shimadzu SPM-9600 equipment to evaluate the morphology of CNC. A drop of a diluted nanocrystal aqueous suspension (*c.a.* 0.005 wt%) was deposited onto a freshly cleaved mica substrate and then air-dried. AFM images were obtained under ambient conditions in the non-contact mode with a scan rate of 1 Hz using Si tips with a curvature radius of less than 10 nm, spring constant of 42 $N.m^{-1}$ and resonance frequency of 300 kHz. Images were scanned with 512 x 512-pixel resolution for the purpose of detecting the fine structures. VectorScan software (software for Shimadzu's SPM-9600) was used for the image processing. Assuming a rectangular cross-section and twisted ribbon geometry, the height values were measured to describe the possibly axisymmetric structure of the CNC sample. These height values are not subject to peak/tip broadening artifacts caused by sample tip convolution (Beck-Candanedo et al., 2005; Elazzouzi-Hafraoui et al., 2008). Over 35 nanoparticles were randomly selected to determine their average thickness. For each particle, the height at two locations along the nanoparticle was recorded.

2.4.6. Scanning electron microscopy (SEM)

Pieces of nanocomposite films were frozen in liquid nitrogen and fractured. After drying, the films were coated with Au/Pd and observed in secondary electron mode in a Quanta 250 FEI microscope operating at 10 kV.

2.4.7. Fourier transform infrared spectroscopy (FTIR)

FTIR spectra were recorded with Perkin-Elmer Spectrum One equipment in the range of 600-4000 cm^{-1} with a resolution of 4 cm^{-1} and a total of 16 scans for each sample. All analyses were carried out in the attenuated total reflection (ATR) mode. This analysis was done on the upper and lower faces of the films and freeze-dried CNC powder.

2.4.8. Dynamic mechanical analysis (DMA)

The viscoelastic behavior of the nanocomposites and neat NR film was evaluated on ARES G2 rheometer (TA Instruments, USA) device using film rectangular tension geometry. The measurements were carried out at a constant frequency of 1 Hz, strain amplitude of 0.08%, ramping temperature from -90 to 40°C at 3°C.min^{-1} and loaded at a starting gap height of 10 mm. The dimensions of the rectangular specimens were about 30 mm in length, 5 mm in width, and 0.3–0.4 mm in thickness, which were measured before each analysis.

2.4.9. Tensile tests

The tensile behavior of NR and nanocomposite films was analyzed using Instron 5965 universal testing machine with a 5 kN load cell. The experiments were performed at room temperature with a crosshead speed of 0.10 mm.s^{-1}. The samples were prepared by cutting 30 mm × 5 mm film strips. The distance between the jaws was 15 mm, whereas the thickness was measured before each measurement. Before analysis, the samples were conditioned at 23°C and controlled relative humidity (50% RH) for 7 days. The data were averaged over at least three specimens.

2.4.10. Thermogravimetric analysis (TGA)

Thermal degradation of the CNC sample, neat NR film and nanocomposites produced with 5 wt% of CNC content (NR5%) were monitored on PerkinElmer STA 6000 - Simultaneous Thermal Analyzer device. The analysis conditions were a nitrogen atmosphere with flow rate of 50 mL·min^{-1}, heating rate of 10°C·min^{-1}, temperature range of 30–600°C, sample mass about 10 mg, and alumina pans. The onset degradation temperature (T_{onset}) was defined as the intersection of the tangents drawn from the thermogravimetric curve, one before inflection caused by the degradation and another from 5 wt% degradation after inflection.

3. RESULTS AND DISCUSSION

3.1. Extraction of cellulose nanocrystals

The yield of CNCs with respect to the initial amount of dried soy hulls was 26.9 wt% and based on the initial cellulose content the yield corresponded to 55.8 wt%. Assuming that CNCs could be extracted by acid hydrolysis without any damage or modification of their original crystalline structure and morphology, then the yield should

correspond to the proportion of crystalline domains within of cellulosic fibers for a given raw material. However, this value is only indicative since the actual yield strongly depends on the preparation conditions and post-treatment (*e.g.* filtration, which inevitably induces loss of material inherent to this process and also by mass transfer) (Dufresne, 2012). Taking into account that yield values ranging from 3 to 59 wt% with respect to the cellulose content have been reported in the literature (Dufresne, 2012), the yield value of 55.8 wt% observed for CNC_{SH} can be considered as a high value suggesting that the initial soy hull cellulose fiber contains a high amount of crystalline domains.

The zeta-potential ζ of the nanoparticles in suspension was -32.4 ± 4.2 $mV \cdot cm^{-1}$. This negative value is ascribed to the insertion of charged sulfate ester groups onto the surface of the CNC induced by the sulfuric acid treatment and it indicates that the hydrolysis conditions used led to a colloidal dispersion of CNC_{SH} in water electrostatically stabilized by repulsive forces (Figure 35a). According to the results from elemental analysis the sulfur content and the surface charge were 1.13 wt% and 352 mmol $SO_4^-.kg^{-1}$, respectively. These values are similar with those in other reports, where CNCs were extracted from different sources (Henrique et al., 2015; Teixeira et al., 2010).

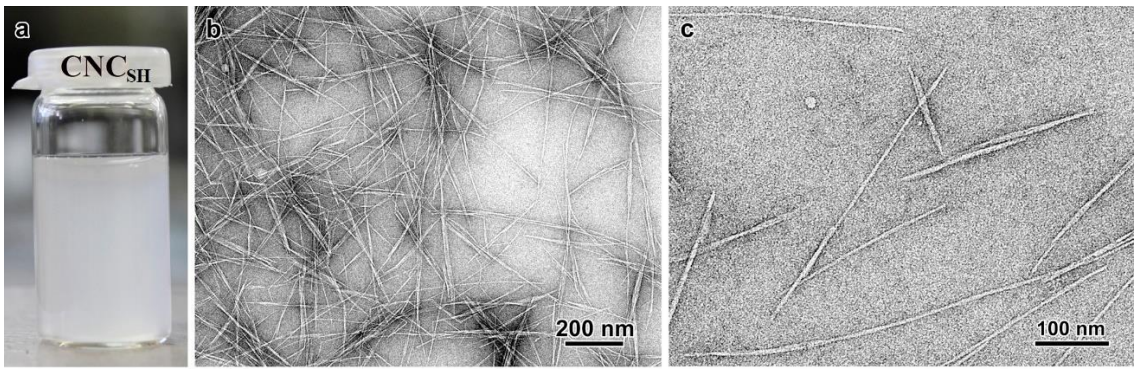

Figure 35 – (a) Picture of CNC_{SH} (a) colloidal suspension. (b,c) Transmission electron micrographs of corresponding negatively stained CNC_{SH}.

The WAXS profile of CNC_{SH} is shown in Figure 36a. As can be seen the diffraction profile is a typical pattern of cellulose I allomorph. It contains peaks at 2θ = 15, 17, 23° corresponding to $1\bar{1}0_I$, 110_I and 200_I reflections, respectively (French & Cintrón, 2013; French, 2014). The CI value calculated as described in the experimental section was 80.4%. The CI for CNC prepared from different cellulose sources ranges between 46% and 96% and significantly depends on the measurement method and data treatment (Dufresne, 2012; Park et al., 2010). Therefore, the CI obtained for CNC_{SH} is within the upper range of values.

The determination of CNC dimensions is complicated due to specific limitations of the different analytical methods used. On the one hand, in the case of TEM images for unstained CNC, the main drawbacks are limited contrast and sample damage from the electron beam. On the other hand, the tip/sample broadening represents the main limitation for AFM, resulting in an overestimation of CNC dimensions. Thus, both TEM and AFM were performed in order to have a detailed characterization of the dimensions of the individual crystallites. Thus, TEM images of negatively stained preparations were recorded in order to measure the length and width of the particle with a better precision, while AFM images allowed measuring the CNC thickness. Moreover, aggregation, bundling, network formation and overlapping of individual CNCs also can make accurate dimension measurements difficult with both techniques (Flauzino Neto et al., 2013; Kvien et al., 2005; Sacui et al., 2014).

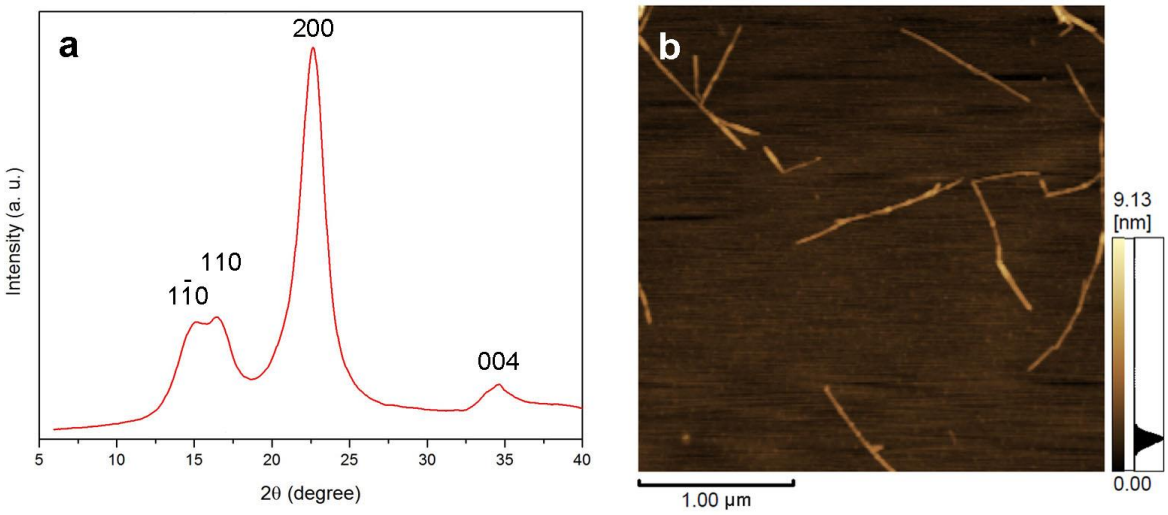

Figure 36 – (a) Wide-angle X-ray diffraction profile of CNC_{SH}. The peak indexes are those of cellulose Iβ. (b) Atomic force microscopy image of CNC_{SH} nanocrystals.

TEM micrographs for CNC_{SH} are shown in Figures 35b-c. These images show individual nanocrystals and some aggregates (*i.e.* particles constituted of few laterally bound elementary crystallites). These aggregates may exist even in suspension, but when the dispersing medium is removed during sample preparation, bundles of CNC can be even more numerous than individual rods (Elazzouzi-Hafraoui et al., 2008). As seen in TEM images, CNC_{SH} displayed typical well-defined rod-like nanosized elements (Figure 35b-c). The CNC_{SH} dimensions, *i.e.* average length $\bar{\mathbf{L}}$, width $\bar{\mathbf{D}}$, and aspect ratio $\bar{\mathbf{L}}/\bar{\boldsymbol{D}}$, obtained from several TEM images were 503 ± 155 nm, 4.9 ± 1.1 nm, and 103, respectively. Figure 36b shows AFM image recorded from CNC_{SH}. Similarly to TEM,

individual and aggregated particles can be seen. The rod-like nanoparticles have an average thickness $\bar{\mathbf{H}}$ of 2.5 ± 0.8 nm.

The extraction process used resulted in longer nanocrystals when compared to those reported by Flauzino Neto et al. (2013) ($\bar{L}$ = 120 ± 40 nm). This was expected, since the stronger acid conditions used in that work partially destroyed part of the crystalline domains and even solubilize them, as shown and reported by Flauzino Neto et al. (2013). However no significant difference in $\bar{D}$ and also in $\bar{H}$ among these CNCs could be detected, if the standard deviation of each value is taken into account.

As the average thickness measured by AFM (2.5 nm) is smaller than width determined from TEM images (4.9 nm), considering a rectangular cross section seems to be reasonable. In addition, from the average dimensions measured from the microscopy images, assuming a rectangular cross-section model for the nanocrystal and density of 1.6 $g \cdot cm^{-3}$ for crystalline cellulose, the specific surface area of CNC_{SH} was estimated to be 747 $m^2 \cdot g^{-1}$ from geometrical considerations. This value is higher than data reported for nanocrystals extracted from tunicin (Dufresne, 2000) and sisal (Siqueira et al., 2010b), 170 and 533 $m^2 \cdot g^{-1}$, respectively. The high specific surface area found for CNCs extracted from soy hulls is related to the high aspect ratio as well as small width, allowing a larger surface-to-volume ratio which can improve the interfacial contact surface for fiber-polymer nanocomposite systems and surface reactivity.

The aspect ratio $\bar{L}/\bar{D}$ of CNC is a crucial parameter with remarkable influence on the mechanical and barrier performances when incorporating it into a polymeric matrix. A higher aspect ratio can provide higher reinforcement effect compared to nanofiller with lower aspect ratio (Dufresne, 2012; Sacui et al., 2014). The aspect ratio found for CNC_{SH} was around 103. It is clearly seen that CNC_{SH} does not consist of partially hydrolyzed microfibril since it displays the classical rod-like morphology of CNC. To our knowledge, so far, the aspect ratio found for CNC_{SH} is the largest ever found in the literature for any cellulose source. This $\bar{L}/\bar{D}$ value is rather high compared to the one reported for CNC extracted from other sources such as capim dourado (~67) (Siqueira et al., 2010a), rachis of the date palm tree (~43) (Bendahou et al., 2009), sisal (~60) (Garcia de Rodriguez et al., 2006), *Posidonia oceanica* leaves (~75) (Bettaieb et al., 2015) or cotton (~10-14) (Teixeira et al., 2010). Furthermore, it has been reported that for aspect ratio values higher than 100, the Young's modulus reaches a plateau corresponding to the maximum point

of reinforcement (Eichhorn et al., 2010), so it means that CNC_{SH} has a very high reinforcing capability.

From these results, the hydrolysis protocol used in this study appears to be the most adapted method to extract CNC from soy hulls fibers compared to that reported by Flauzino Neto et al. (2013), since it has preserved the native structure of crystalline domains of the raw material and gave rise to nanoparticles with desired morphology to be used as reinforcing filler.

3.2. Characterization of CNC/NR nanocomposites

It is well-know that the mechanical properties of CNC-based polymer nanocomposites markedly depend on the filler dispersibility and compatibility of CNC with the matrix. One of the issues with CNC is its strong tendency to aggregate because of the high density of hydroxyl groups on its surface (highly polar and hydrophilic). It makes dispersion of CNC very difficult in polymer matrices, especially those that are non-polar or hydrophobic. The CNC aggregates can act as stress concentrator, resulting in poor performance of the nanocomposite. Thus, CNC aggregates should be avoided for effective reinforcement. Therefore, an in-depth understanding of the mechanical behavior of CNC-based nanocomposites requires detailed information about their morphology.

In this way, FTIR and SEM analyses were performed to evaluate the CNC distribution and dispersion within the NR matrix. The FTIR spectra for NR matrix and for the nanocomposite film reinforced with 5 wt% CNC_{SH} (NR5%) are presented in Figure 37. For the nanocomposite two spectra were recorded, one corresponding to the upper face and the other corresponding to the lower face (in contact with the petri dish during water evaporation). It can be seen that all spectra display the characteristics absorption peaks and bands assigned to NR. The peaks at 834 cm^{-1} and 3036 cm^{-1} are related to =C–H bending and =C–H stretching, respectively, the peak at 1447 cm^{-1} is linked to C–H bending and the series of bands between 2820 and 3000 cm^{-1} correspond to C–H stretching (Mariano et al., 2016; Zhang et al., 2013). In addition to these typical peaks associated to NR, a new prominent peak appears at 1059 cm^{-1} for the lower face of the composite film. It corresponds to C–O stretching and C–H rock vibrations of cellulose (Alemdar & Sain, 2008). It indicates that the lower face of the film is richer in CNC compared to the upper face. All spectra recorded for nanocomposites (not shown) displayed similar effect. It indicates that a probable gradient of CNC concentration exists within the thickness of the film due to a possible sedimentation during film processing by

casting/evaporation. Although rarely mentioned, this phenomenon was already evidenced by SEM, WAXS and DMA (Dufresne et al., 1997). Nevertheless, the visual appearance (Figures 38a and 38d) was similar for both neat and CNC-reinforced films. The possibility of sedimentation of the nanoparticles depends mainly on the viscosity of the medium. Therefore, sedimentation could be avoided, or at least limited, by using more concentrated suspensions. However, it would be in turn more difficult to mix two too concentrated suspensions. This sedimentation phenomenon can also result from the inherent incompatibility and insufficient molecular scale interaction between CNC and NR, which may restrict the overall performance of the nanocomposite material.

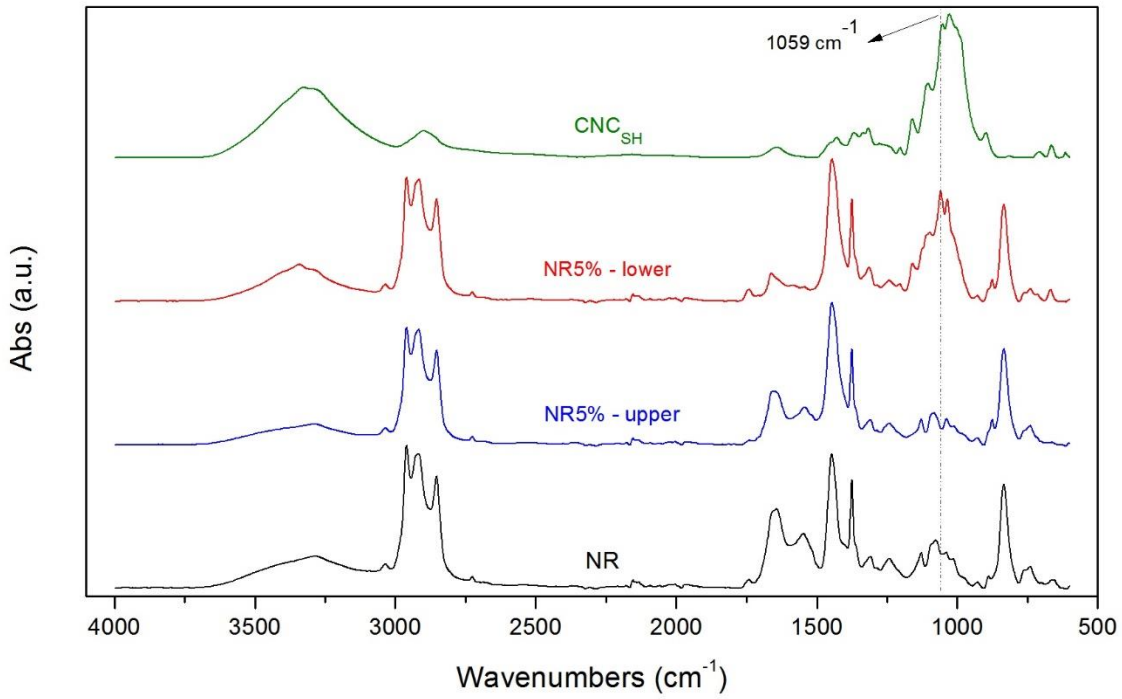

Figure 37 – Fourier transform infrared spectra for CNC_{SH}, neat NR matrix, and upper and lower faces of the nanocomposite film filled with 5 wt% of CNC_{SH} (NR5%).

SEM images of the cross-section for the neat NR film and NR5% nanocomposite film are presented in Figures 38b-c and 38e-f, respectively. A smooth and uniform morphology is observed for unfilled NR, whereas the CNC/NR nanocomposite gives the impression of being composed of two layers, one rougher phase and another smoother phase. They possibly correspond to the lower CNC-rich face and upper NR-rich face, respectively. Nevertheless, it was not possible to observe the presence of microscale CNC aggregates, even for 5 wt% CNC content, with the magnification utilized.

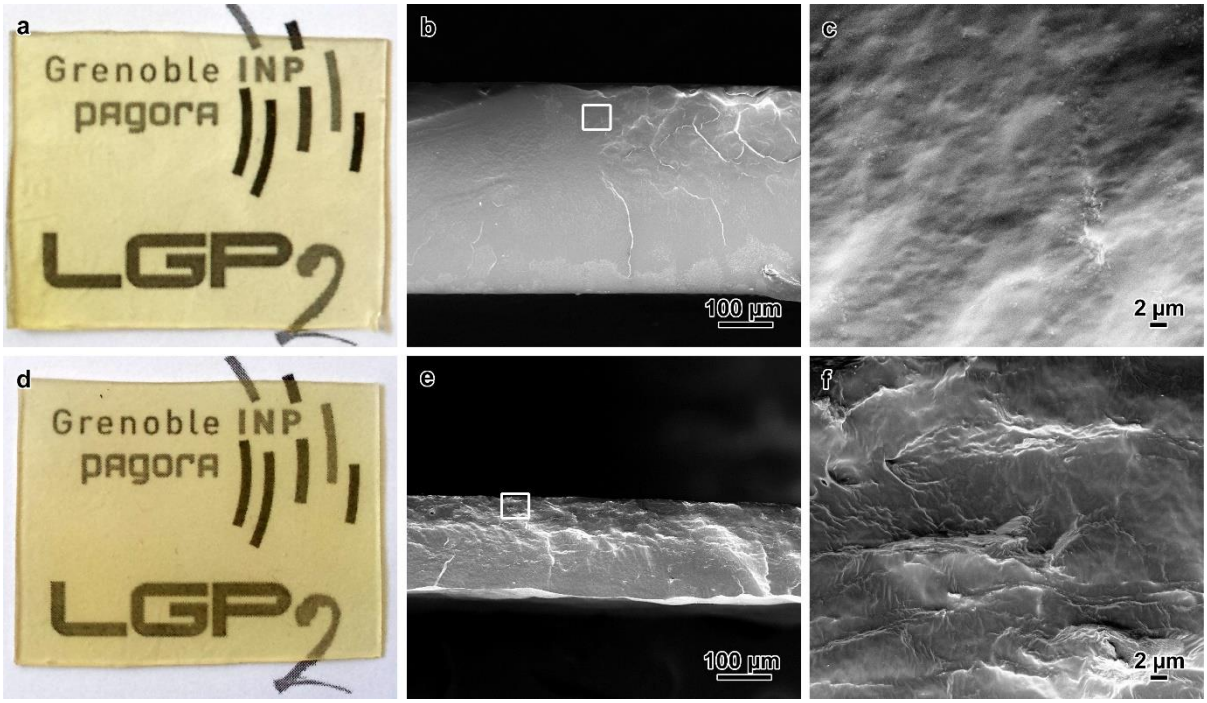

Figure 38 – Appearance of neat NR film (a-c) and NR5% nanocomposite film (d-f). (b,c) and (e,f) are secondary electron SEM images of the cross-section of fractured films. (c) and (f) are higher magnification images of the regions delimited by the white rectangles in (b) and (e), respectively. The upper part in these SEM images corresponds to the lower face of the films (in contact with the petri dish during water evaporation).

The viscoelastic behavior of the films was analyzed in the linear range using DMA. Figures 39a and 39b show the isochronal evolution at 1Hz of the logarithm of the tensile storage modulus (*log E'*) and tangent of the loss angle (*tan δ*), measured as a function of temperature, for the neat NR film and nanocomposite films with different loading levels (1, 2.5 and 5 wt%) of CNC_{SH}. The temperature corresponding to the maximum of tan δ (associated to T_g of the NR matrix) and storage modulus value at 25°C are reported in Table 5.

The *log E'* curve corresponding to the unfilled (or neat) NR matrix is typical of a fully amorphous high molecular weight thermoplastic behavior. For temperatures below the glass transition temperature (T_g), the storage modulus of NR slightly decreases with temperature but remains roughly constant around 1.9 GPa. Then, around -60°C a sharp drop in *log E'* over three decades is observed, corresponding to an energy dissipation effect owing to the increased molecular mobility associated with the glass-rubber transition. Finally, at higher temperatures the NR matrix is in the rubbery state, and the modulus reaches a plateau around 1 MPa due to the cohesion provided by macromolecular entanglements. The broad temperature range from -35 to 40°C of the rubbery state is

ascribed to the high molecular weight of the polymer, resulting in a highly entangled state of the macromolecules.

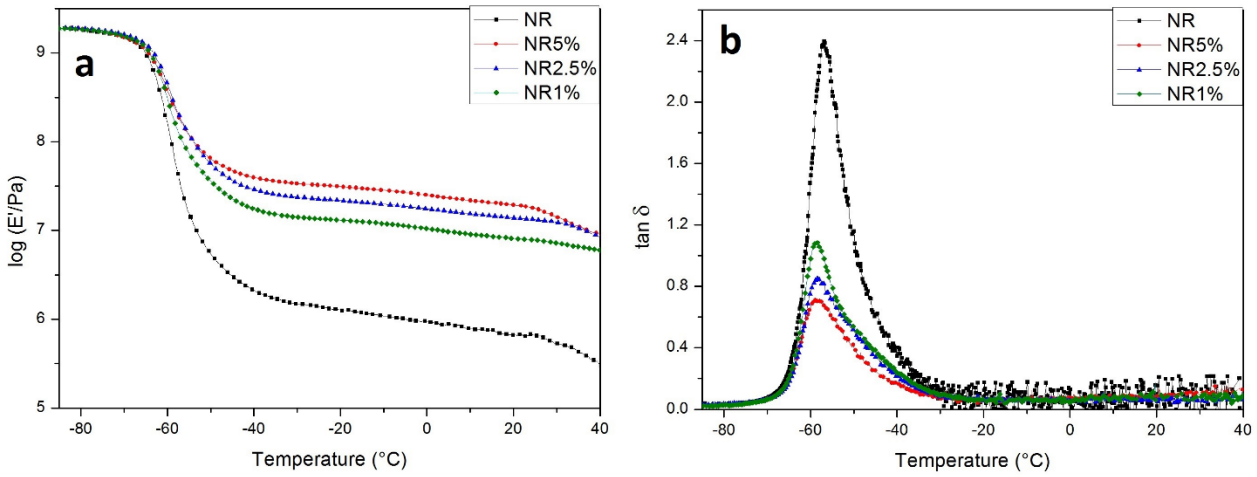

Figure 39 – DMA data obtained for the neat NR film and nanocomposites films with 1, 2.5 and 5 wt% CNC_{SH} as filler. (a) Logarithm of the tensile storage modulus (*log E'*), and (b) loss tangent (*tan δ*) of the films as a function of temperature.

Table 5. Main relaxation temperature (T_α), tensile storage modulus ($E'_{25°C}$) estimated at 25°C, Young's modulus (E), yield stress (σ_y), yields strain (ε_y), strength (σ_B), strain at break (ε_B) and toughness (T) for the neat NR film and nanocomposite films reinforced with CNC_{SH}.

Sample	T_α (°C)	$E'_{25°C}$ (MPa)	E (MPa)	σ_y (MPa)	ε_y (%)	σ_B (MPa)	ε_B (%)	T ($J.m^{-3}.10^4$)
NR	-56.8	0.6	0.6 ± 0.1	0.19 ± 0.04	31 ± 3	0.59 ± 0.08	611 ± 71	278 ± 43
NR1%	-58.6	7.7	1.9 ± 0.3	0.27 ± 0.01	17 ± 2	0.89 ± 0.04	396 ± 21	280 ± 4
NR2.5%	-58.5	13.5	3.7 ± 0.1	0.34 ± 0.02	12 ± 1	1.11 ± 0.13	485 ± 35	399 ± 44
NR5%	-58.4	17.6	18.1 ± 2.8	0.54 ± 0.05	6 ± 1	3.03 ± 0.11	552 ± 9	1074 ± 62

In the glassy state the molecular motions are largely restricted to vibrations and short range rotational motions that limit the strain imposed by the applied stress resulting in a high modulus value of the material. Hence, in this temperature range it is expected that the difference between the modulus of the host matrix and the reinforcing phase is not high enough to generate a significant reinforcing effect. Therefore, to overcome the experimental error due to sample dimension measurements at room temperature at which the material is soft, the modulus value of the nanocomposite films has been normalized to the glassy modulus of the NR matrix. Above T_g a higher improvement of E' is observed by increasing the CNC_{SH} content. For instance, the relaxed modulus at room temperature

(25°C) for nanocomposite films containing 1 and 5 wt% of CNC_{SH} (Table 6) is about 12 and 28 times higher, respectively, than the soft rubbery matrix.

Table 6. Comparison of the relative rubbery storage tensile modulus at 25°C ($E'_{25°CR}$) determined by DMA for NR reinforced with CNC of different origins.

Cellulose source	L/D	CNC content (wt%)	$E'_{25°CR}$ (MPa)	Reference
Soy hulls	103	1	12.02	This study
		2.5	20.70	
		5	27.55	
Capim dourado	67	2.5	7.88*	(Siqueira et al., 2010a)
		10	154*	
Rachis of date palm tree	43	2.5	4.89	(Bendahou et al., 2009)
		5	12.56	
		10	209	
		15	402	
Sugarcane bagasse	13	2.5	1.48*	(Bras et al., 2010)
		7.5	2.36*	
	76	2	4.45	(Pasquini et al., 2010)
		5	15.18	
		7	18.68	
		10	69.95	

*Values estimated from the graphs provided in their studies by digital image processing using ImageJ software.

The mechanical loss factor, *tan δ*, often called damping is the ratio of loss modulus to storage modulus. It is a measure of the energy dissipated in a material under cyclic load, expressed in terms of the recoverable energy, and represents the mechanical damping or internal friction in a viscoelastic system. The curve of *tan δ* exhibits a peak located in the temperature range of the glass transition of NR. This relaxation process, labelled α, is related to the anelastic manifestation of the glass-rubber transition of the polymer and involves cooperative motions of long chain sequences. As shown in Table 5 the temperature at the maximum of the *tan δ* peak was slightly shifted to lower temperatures (less than 2°C) when adding CNC. It is not an indication of a decrease in the T_g value of NR but it is associated to the decrease of the modulus drop displayed in the concomitant relaxation process (well-known mechanical coupling effect). A reduction in the magnitude of the *tan δ* peak upon filler addition was also observed. This can be ascribed to (i) a decrease of the matrix material amount, responsible for damping properties, *viz.* a decrease in the number of mobile units participating to the relaxation

phenomenon, (ii) a possible restriction of NR chains' movement at the filler/matrix interface; and (iii) the decrease of the magnitude of the modulus drop associated with T_g.

It is well-known that the mechanical percolation approach is highly relevant to describe the mechanical behavior of CNC-based nanocomposites when prepared by casting/evaporation. This mechanism suggests the formation of a stiff continuous network of nanocrystals linked through hydrogen bonding, which should lead to an unusual and outstanding reinforcing effect. Furthermore, this phenomenon is expected to occur only above a critical volume fraction of filler phase, defined as the percolation threshold, which in turn depends on the aspect ratio of the nanoparticle and therefore on the origin of cellulose. The filler percolation threshold was calculated from the aspect ratio found by microscopic observations and assuming a density of 1.6 and 0.9 $g \cdot cm^{-3}$ for crystalline cellulose and NR matrix, respectively. The values found for CNC_{SH} was around 0.7 vol%, corresponding to 1.2 wt%. Therefore, it is worth noting that only the nanocomposites films NR2.5% and NR5% should show a percolation effect, in which the filler loading used was high enough for the formation of a rigid CNC network. Previous studies showed that alteration in the mechanical properties could be observed even below the percolation threshold of CNC (Bendahou et al., 2010; Bras et al., 2010). Then, no spectacular improvement of the modulus is observed when reaching the percolation threshold. The main reason is probably related to the almost inevitable sedimentation phenomenon of the nanofiller during the evaporation step leading to a layered material, the lower CNC-rich layer providing high modulus value. For higher CNC contents, sedimentation is expected to be less significant because of the increase in the viscosity of the medium.

The performance of CNC extracted from soy hulls as reinforcing elements in NR matrix was compared to data reported for CNC isolated from different sources (rachis of date palm tree, capim dourado and sugar cane bagasse). Table 6 shows the relative values of the rubbery storage tensile modulus at 25°C corresponding to the ratio of this property of the nanocomposite divided by the one of the unfilled NR matrix. It is worth noting that for each system the NR matrix was unvulcanized. For the same filler content, soy hulls nanocrystals (CNC_{SH}) have the highest reinforcing capability compared to other systems. It is ascribed to the higher aspect ratio of CNC_{SH} that results in a lower filler content to reach percolation, but also to the higher stiffness of the percolating high aspect ratio nanoparticle network, as suggested in a previous study (Bras et al., 2011). So, these results confirm the importance of the CNC aspect ratio for the reinforcing effect.

Tensile tests show that NR based samples exhibit a nonlinear mechanical behavior typical of amorphous polymer at T > T_g (Figure 40). The stress-strain curves obtained for nanocomposites were clearly different from that of neat NR, showing the influence of CNC on the mechanical behavior of the film. The mechanical properties derived from these experiments are listed in Table 5. The material clearly becomes stiffer with an increase in tensile modulus, yield stress and strength when adding CNC. This behavior is possibly related to the restriction of polymer chain mobility in the vicinity of CNC.

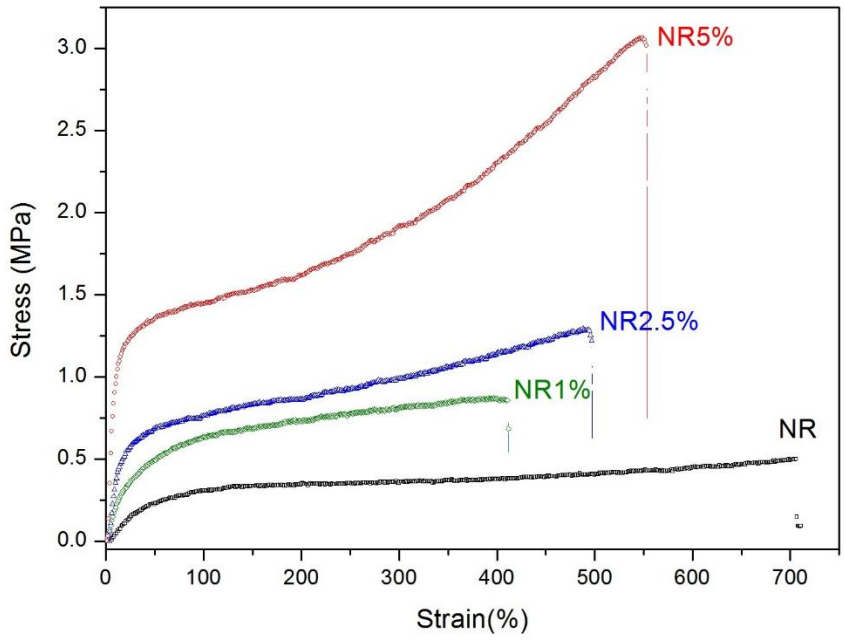

Figure 40 – Representative stress-strain curves obtained from tensile tests for neat NR film and nanocomposites films filled with 1, 2.5 and 5 wt% CNC_{SH}.

Considering the elongation at break, it significantly decreases when adding 1 wt% CNC_{SH} compared to neat NR but increases for higher CNC_{SH} contents. Similar behavior was also reported when increasing the CNC content from 7.5 to 10 wt% in a previous study (Bras et al., 2010). This unexpected behavior is probably ascribed to the distribution and dispersion of CNC within the polymeric matrix, and sedimentation of the nanofiller during the evaporation step and resulting layered structure. It should induce stress concentration that progressively attenuates for higher CNC contents because of the higher viscosity of the processing medium that could limit the sedimentation of the nanofiller. The same behavior is observed for the ductility (area under the stress-strain curve) of the material (Table 5) as a result of increased stiffness and high elongation at break values.

In addition, taking into account that the samples were conditioned at 50% RH for 7 days before tensile tests, another explanation could be ascribed to the increased moisture sensitivity of the films upon increasing the hydrophilic filler content and potential plasticizing role of water. The plasticizer leads to less restriction of molecular chain slipping on the CNC surface, and hence an increase in elongation at break and ductility could result. The effect of the plasticizer to decrease the stiffness is probably less important than the effect of homogeneity of the filler within the polymeric matrix. These materials show therefore a good compromise between strength and ductility, *i.e.* the material withstands both higher stresses and higher strains.

It is also important to point out that only the nanocomposite films with CNC contents higher than the percolation threshold displayed enhancement of toughness compared to the NR matrix (as can be seen in Table 5). Since the toughness is reported to be the ability of a material to absorb energy and plastically deform before fracturing, the increase of toughness should be directly linked to the formation of the percolating network, which can better distribute the applied stress than when there is no percolating network. Comparing the relative mechanical properties obtained from tensile tests with results obtained for Capim dourado CNC reinforced NR (Siqueira et al., 2010a), slightly lower improvement was found in the present work. For instance at loading level of 5 wt%, the relative modulus and strength for NR composites reinforced with CNC extracted from Capim dourado were 32.7 and 5.67, respectively, whereas for NR filled with soy hulls CNC (CNC_{SH}) it was 28.7 and 5.13, respectively. Carefully looking at the experimental conditions under which the tensile tests were performed, it is possible to understand this behavior. In this previous study (Siqueira et al., 2010a), a higher cross-head speed (10 $mm.min^{-1}$) was used compared to our experiments (6 $mm.min^{-1}$) and dry samples were tested. Furthermore, several other factors may have significant influence on stress-strain results, such as diameter of NR latex particles, NR molecular weight, temperature of film formation, drying-time, *etc*. Moreover, much lower elongation at break values were reported in this previous study.

The broad range of NR applications is strongly dependent of its thermal properties. An early degradation may cause worsening in the mechanical properties and gas release (Mariano et al., 2016). The weight-loss curves recorded by TGA analysis are shown in Figure 41. The onset degradation temperature (T_{onset}) estimated from the weight-loss curves as described in experimental section were about 268, 295 and 272°C for CNC_{SH}, neat NR matrix and nanocomposite film NR5%, respectively. The lower T_{onset} of

soy hulls nanocrystals than usually seen for cellulose, reported to be around 315°C by (Morán et al., 2008), is related to the presence of sulfate groups on the nanocrystals surface, since as it was observed in earlier studies the sulfate groups have a catalytic effect on the reaction of thermal degradation of cellulose (Roman and Winter, 2004). The thermal decomposition of rubber shows a slight weight loss below 200°C that can be attributed to the vaporization of water and NH_3 (used as NR stabilizer), followed by a major mass-loss in the temperature range 250–450°C, which is related to volatilization and pyrolysis (Mariano et al., 2016). Both films of neat NR and nanocomposite NR5% followed almost the same thermal degradation behavior. Although NR5% nanocomposite showed lower T_{onset} than rubber, which could be related to the lower T_{onset} of CNC_{SH} compared to that of pure NR. Thus, compared to that of neat NR film, the thermal stability of nanocomposite was retained even at 5 wt% CNC. These results obtained are consistent with other reports in the literature (Bras et al., 2010).

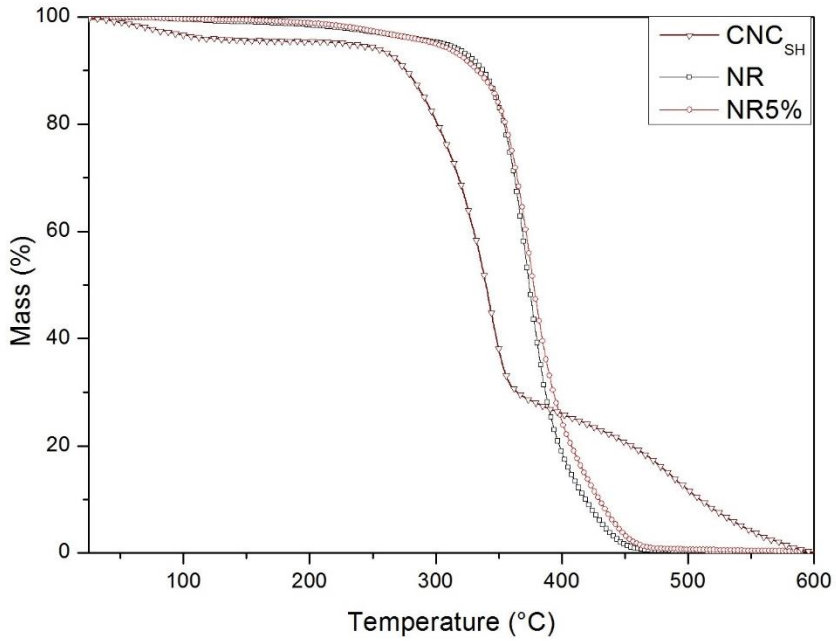

Figure 41 – TGA weight-loss curves obtained of CNC_{SH}, neat NR matrix and NR5% nanocomposite film.

4. CONCLUSIONS

The present work shows that soy hull is an interesting source of raw material for the production of CNC, due to the characteristics of the obtained nanocrystals associated with low lignin content and wide availability of this agro-industrial residue. In the meantime, the reuse of this agro-industrial residue goes towards sustainable development and environment-friendly materials. To tailor the dimensions of CNC and take full

advantage of this source, special care needs to be paid to the extraction process and its conditions. A milder acid hydrolysis is preferable to improve the extraction yield, preserve the crystallinity of native cellulose and obtain high aspect ratio CNC. As expected, a high reinforcing effect is observed even at low filler contents when using this nanofiller to prepare nanocomposites with a natural rubber (NR) matrix by casting/evaporation. For instance, by adding only 2.5 wt% CNC, the storage tensile modulus at 25°C of the nanocomposite was about 21 times higher than that of the neat NR matrix. Both the high aspect ratio of the CNC and sedimentation due to the processing technique are involved in the good mechanical results. Indeed, if sedimentation occurs, then a multilayered film results and the CNC content in the lowest layers is higher than the average CNC content. It means that CNC mechanical percolation can occur in the lowest layers for an average CNC content which is lower than the percolation threshold. Since, the system can be considered as constituted of parallel layers in the direction of the mechanical solicitation (tensile mode), then these CNC-rich layers can support a higher stress leading to a higher modulus value. Moreover, if high aspect ratio CNC is used, then percolation can occur in the lowest layers for lower average CNC contents. An important contribution of this work is to highlight the importance of the sedimentation of CNC during the evaporation step on the mechanical properties of the nanocomposites which is rarely mentioned in the literature.

5. REFERENCES

Alemdar, A., & Sain, M. (2008). Isolation and characterization of nanofibers from agricultural residues - wheat straw and soy hulls. *Bioresource Technology, 99*, 1664-1671.

Beck-Candanedo, S., Roman, M., & Gray, D. G. (2005). Effect of reaction conditions on the properties and behavior of wood cellulose nanocrystal suspensions *Biomacromolecules, 6*, 1048-1054.

Bendahou, A., Habibi, Y., Kaddami, H., & Dufresne, A. (2009). Physico-chemical characterization of palm from Phoenix dactylifera L., preparation of cellulose whiskers and natural rubber-based nanocomposites. *Journal of Biobased Materials and Bioenergy*, *3*, 81-90.

Bendahou, A., Kaddami, H., & Dufresne, A. (2010). Investigation on the effect of cellulosic nanoparticles morphology on the properties of natural rubber based nanocomposites. *European Polymer Journal*, *46*, 609-620.

Bettaieb, F., Khiari, R., Dufresne, A., Mhenni, M. F., & Belgacem, M. N. (2015). Mechanical and thermal properties of *Posidonia oceanica* cellulose nanocrystal reinforced polymer. *Carbohydrate Polymers*, *123*, 99-104.

Bras, J., Hassan, M. L., Bruzesse, C., Hassan, E. A., El-Wakil, N. A., & Dufresne, A. (2010). Mechanical, barrier, and biodegradability properties of bagasse cellulose whiskers reinforced natural rubber nanocomposites. *Industrial Crops and Products*, *32*, 627-633.

Bras, J., Viet, D., Bruzzese, C., & Dufresne, A. (2011). Correlation between stiffness of sheets prepared from cellulose whiskers and nanoparticles dimensions. *Carbohydrate Polymers*, *84*, 211-215.

Brinchi, L., Cotana, F., Fortunati, E., & Kenny, J. M. (2013). Production of nanocrystalline cellulose from lignocellulosic biomass: Technology and applications. *Carbohydrate Polymers*, *94*, 154-169.

da Silva, I. S. V., Flauzino Neto, W. P., Silvério, H. A., Pasquini, D., Andrade, M. Z., & Otaguro, H. (2015). Mechanical, thermal and barrier properties of pectin/cellulose nanocrystal nanocomposite films and their effect on the storability of strawberries (*Fragaria ananassa*). *Polymers for Advanced Technologies*, doi: 10.1002/pat.3734.

CONAB. Companhia Nacional de Abastecimento. (2015). Monitoring of the Brazilian grain hasvest 2015/2016. Available online http://www.conab.gov.br (accessed 20 August 2016).

Dufresne, A., Cavaillé, J. Y., & Helbert, W. (1997). Thermoplastic nanocomposites filled with wheat straw cellulose whiskers. Part II: effect of processing and modeling. *Polymer Composites*, *18*, 198-210.

Dufresne, A. (2000). Dynamic mechanical analysis of the interphase in bacterial polyester/ cellulose whiskers natural composites. *Composite Interfaces*, *7*, 53-67.

Dufresne, A. (2012). *Nanocellulose: From nature to high-performance tailored materials*. de Gruyter, Berlin/Boston.

Eichhorn, S. J. (2011). Cellulose nanowhiskers: promising materials for advanced applications. *Soft Matter*, *7*, 303-315.

Eichhorn, S. J., Dufresne, A., Aranguren, M., Marcovich, N. E., Capadona, J. R., Rowan, S. J., Weder, C., Thielemans, W., Roman, M., Renneckar, S., Gindl, W., Veigel, S., Yano, H., Abe, K., Nogi, M., Nakagaito, A. N., Mangalam, A., Simonsen, J., Benight, A. S., Bismarck, A., Berglund, L. A., & Peijs, T. (2010). Review: Current

international research into cellulose nanofibres and nanocomposites. *Journal of Materials Science, 45*, 1-33.

Elazzouzi-Hafraoui, S., Nishiyama, Y., Putaux, J-L., Heux, L., Dubreuil, F., & Rochas, C. (2008). The shape and size distribution of crystalline nanoparticles prepared by acid hydrolysis of native cellulose. *Biomacromolecules, 9*, 57-65.

Favier, V., Chanzy, H., & Cavaillé, J.-Y. (1995). Polymer nanocomposites reinforced by cellulose whiskers. *Macromolecules, 28*, 6365-6367.

Flauzino Neto, W. P., Silvério, H. A., Dantas, N. O., & Pasquini, D. (2013). Extraction and characterization of cellulose nanocrystals from agro-industrial residue-soy hulls. *Industrial Crops and Products, 42*, 480-488.

French, A. D., & Cintrón, M. S. (2013). Cellulose polymorphy, crystallite size and the Segal crystallinity index. *Cellulose, 20*, 583-588.

French, A. D. (2014). Idealized powder diffraction patterns for cellulose polymorphs. *Cellulose, 21*, 885-896.

Garcia de Rodriguez, N. L., Thielemans, W., & Dufresne, A. (2006). Sisal cellulose whiskers reinforced polyvinyl acetate nanocomposites. *Cellulose, 13*, 261-270.

George, J., Ramana, K. V., Bawa, A. S., & Siddaramaiah. (2011). Bacterial cellulose nanocrystals exhibiting high thermal stability and their polymer nanocomposites. *International Jounal of Biological Macromolecules, 48*, 50-57.

Habibi, Y., Lucia, L. A., & Rojas, O. J. (2010). Cellulose nanocrystals: chemistry, self-assembly and applications. *Chemical Reviews, 110*, 3479-3500.

Henrique, M. A., Flauzino Neto, W. P., Silvério, H. A., Martins, D. F., Gurgel, L. V. A., Barud, H. S., de Morais, L. C., & Pasquini, D. (2015). Kinetic study of the thermal decomposition of cellulose nanocrystals with different polymorphs, cellulose I and II, extracted from different sources and using different types of acids. *Industrial Crops and Products, 76*, 128-140.

Ipharraguerre, I. R., & Clark, J. H. (2003). Soyhulls as an alternative feed for lactating dairy cows: A review. *Journal Dairy Science, 86*, 1052-1073.

Klemm, D., Kramer, F., Moritz, S., Lindström, T., Ankerfors, M., & Gray, D. (2011). Nanocelluloses: A new family of nature-based materials. *Angewandte Chemie International Edition, 50*, 5438-5466.

Kvien, I., Tanem, B.S., & Oksman, K. (2005). Characterization of cellulose whiskers and their nanocomposites by atomic force and electron microscopy. *Biomacromolecules, 6*, 3160-3165.

Mariano, M., El Kissi, N., & Dufresne, A. (2014). Cellulose nanocrystals and related nanocomposites: Review of some properties and challenges. *Journal of Polymer Science B, 52*, 791-806.

Mariano, M., El Kissi, N. El., & Dufresne, A. (2016). Cellulose nanocrystal reinforced oxidized natural rubber nanocomposites. *Carbohydrate Polymers, 137*, 174-183.

Moon, R. J., Martini, A., Nairn, J., Simonsen, J., & Youngblood, J. (2011). Cellulose nanomaterials review: structure, properties and nanocomposites. *Chemical Society Reviews, 40*, 3941-3994.

Morán, J. I., Alvarez, V. A., Cyras, V. P., & Vázquez, A. (2008). Extraction of cellulose and preparation of nanocellulose from sisal fibers. *Cellulose, 15*, 149-159.

Park, S., Baker, J. O., Himmel, M. E., Parilla, P. A., & Johnson, D. K. (2010). Cellulose crystallinity index: Measurement techniques and their impact on interpreting cellulase performance. *Biotechnology for Biofuels, 3*, 1-10.

Pasquini, D., Teixeira, E. M., Curvelo, A. A. S., Belgacem, M. N., & Dufresne, A. (2010). Extraction of starch nanocrystals and cellulose whiskers from cassava bagasse and their applications as reinforcing agent in natural rubber. *Industrial Crops and Products, 32*, 486-490.

Revol, J. F. (1982). On the cross-sectional shape of cellulose crystallites in *Valonia ventricosa*. *Carbohydrate Polymers*, *2*, 123–-134.

Rippel, M. M., & Galembeck, F. (2009). Nanostructures and adhesion in natural rubber: New era for a classic. *Journal of the Brazilian Chemical Society, 20*, 1024-1030.

Roman, M., & Winter, W. T. (2004). Effect of sulfate groups from sulfuric acid hydrolysis on the thermal degradation behavior of bacterial cellulose. *Biomacromolecules, 5*, 1671-1677.

Rosa, J. R., Silva, I. S. V., Lima, C. S. M., & Pasquini, D. (2015). Production of polyols and new biphasic mono-component materials from soy hulls by oxypropylation. *Industrial Crops and Products, 72*,152-158.

Sacui, I. A., Nieuwendaal, R. C., Burnett, D. J., Stranick, S. J., Jorfi, M., Weder, C., Foster, E. J., Olsson, R. T., & Gilman, J. W. (2014). Comparison of the properties of cellulose nanocrystals and cellulose nanofibrils isolated from bacteria, tunicate, and wood processed using acid, enzymatic, mechanical, and oxidative methods. *ACS Applied Materials & Interfaces, 6*, 6127-6138.

Silvério, H. A., Flauzino Neto, W. P., Silva I. S. V., Rosa, J. R., Assunção, R. M. N., Barud, H. S., Ribeiro, S. J. L., & Pasquini, D. (2014). Mechanical, thermal, and

barrier properties of methylcellulose/cellulose nanocrystals nanocomposites. *Polímeros*, *24*, 683-688.

Siqueira, G., Abdillahi, H., Bras, J., & Dufresne, A. (2010a). High reinforcing capability cellulose nanocrystals extracted from *Syngonanthus nitens* (Capim dourado). *Cellulose*, *17*, 289-298.

Siqueira, G., Bras, J., & Dufresne, A. (2010b). New process of chemical grafting of cellulose nanoparticles with a long chain isocyanate. *Langmuir*, *26*, 402-411.

Siqueira, G., Tapin-Lingua, S., Bras, J., da Silva Perez, D., & Dufresne, A. (2011). Mechanical properties of natural rubber nanocomposites reinforced with cellulosic nanoparticles obtained from enzymatic and acid hydrolysis of sisal fibers. *Cellulose*, *18*, 57-65.

Teixeira, E. M., Corrêa, A. C., Manzoli, A., Leite, F. L., Oliveira, C. R., & Mattoso, L. H. C. (2010). Cellulose nanofibers from white and naturally colored cotton fibers. *Cellulose*, *17*, 595-606.

Visakh, P. M., Thomas, S., Oksman, K., & Mathew, A. P. (2012). Crosslinked natural rubber nanocomposites reinforced with cellulose whiskers isolated from bamboo waste: Processing and mechanical/thermal properties. *Composites Part A*, *43*, 735-741.

Zhang, C., Huang, Y., Luo, C., Jiang, L., & Dan., Y. (2013). Enhanced ductility of polylactide materials: Reactive blending with pre-hot sheared natural rubber. *Journal of Polymer Research*, *20*, 121.

GENERAL CONCLUSIONS AND FUTURE PERSPECTIVES

This doctoral dissertation introduced two independent studies on CNC with different focuses. The study presented in chapter II was focused on the morphological and molecular structure of nanocrystals consisting of cellulose type II polymorph, which were prepared by means of two distinct processes, namely mercerization and regeneration. In particular, the nanoribbons obtained by regeneration process have proved to be very interesting, since the unique molecular and crystal structure found implies that a higher number of reducing chain ends are located at the particle surface, which may be important for subsequent chemical surface modification and specific potential applications. On the other hand, these regenerated nanocrystals do not look promising materials to be applied as reinforcement element because of their low aspect ratio. Indeed, further characterization of these regenerated cellulose nanoparticles is required to evaluate their applicative potential as, for instance, excipient in tablets for drug release, biosensing and bioimaging agents, or as a constituents in nanocomposite materials. This study has shed some light on the understanding of crystalline morphology and structure of cellulose nanoparticles formed by regeneration process using sulfuric acid. Moreover, it should be emphasized that, unlike the conventional top-down deconstructing strategies such as acid hydrolysis, the regeneration process can be considered as a bottom-up approach to produce cellulose nanoparticles. This type of approach could perhaps allow producing cellulose nanostructures more homogenous in size, with better long-range ordering (less defects) and desired morphology. But, much more studies are required to explore this hypothesis.

The research work presented in chapter III was focused on mechanical properties of natural rubber nanocomposites reinforced with high aspect ratio CNCs extracted fom soy hulls. The processing technique utilized was casting/evaporation. This study showed that soy hull is an interesting source of raw material for the production of CNC, due to the characteristics of the extracted nanocrystals (high crystallinity, specific surface area and aspect ratio) associated with low lignin content and wide availability of this agro-industial residue. This study demonstrated that to tailor the dimensions of CNC and take full advantage of any cellulose source, special care needs to be paid to the extraction process and its conditions. This way, mainly considering applications where a high aspect ratio is essential, the hydrolysis process should be carried out using milder conditions to improve the extraction yield and avoid as much as possible the destruction of crystalline cellulose domains. Regarding the mechanical performance observed for the

nanocomposites, the higher reported reinforcing effect compared to the one observed for CNCs extracted from other sources may be assigned to the high aspect ratio of these CNCs and the stiffness of the percolating nanoparticle network formed within the polymer matrix. Moreover, the sedimentation of CNCs during the evaporation step was found to play a crucial role on the mechanical properties. Thus, this work not only emphasized the influence of the CNC's aspect ratio on the mechanical properties of polymer/CNC nanocomposites but also highlighted the importance of the sedimentation of CNC during the evaporation step on these mechanical properties, which is rarely mentioned in the literature. Indeed, it could be interesting to perform other microscopic analysis towards a more in-depth understanding of the mechanical properties of this system. However, it is a real challenge considering the natural rubber sensibility to the electron beam used in most of microscopy techniques.